WASM: Minerals, Energy and Chemical Engineering

Metal-Organic Framework (MOF) derived Catalysts for Efficient Syngas Conversion to Oxygenates

Fuping Li
0000-0003-0086-5437

This thesis is presented for the Degree of
Doctor of Philosophy
of
Curtin University

November 2020

Declaration

To the best of my knowledge and belief this thesis contains no material previously published by any other person except where due acknowledgment has been made.

This thesis contains no material which has been accepted for the award of any other degree or diploma in any university.

Signature: Fuping Li ……...

Date: 16/11/2020 ……..

To my beloved family

Abstract

The Fischer-Tropsch technology is a promising solution to address the growing energy crisis and environmental concerns. Through this process, syngas can be converted to value-added fuels and platform chemicals. Among all the products, dimethyl ether (DME) and higher alcohols ($C_{2+}OH$) are two typical examples with particular research enthusiasm because of their versatile applications and environmentally benign properties. It is acknowledged that an efficient catalyst for oxygenates production requires high activity, selectivity and stability. Although tremendous efforts have been devoted on catalyst exploration, none of these catalysts are sufficiently active and selective for the industrial implementation. Metal-organic frameworks (MOFs), consisting of metal ions and organic ligands, have been considered as promising templates to design efficient catalysts for heterogeneous catalysis, owing to their unique structure and tunable microenvironment. Therefore, the purpose of this study is to explore the MOFs-derived catalysts for selective conversion of syngas to DME and higher alcohols.

In the first part of my thesis, we successfully fabricated a bifunctional MOF composite by encapsulating a solid acid (STA, $H_4SiW_{12}O_{40}$) in the internal pore structure of Zr-MOF (UiO-66) and depositing Cu on the external surface. The prepared Cu/STA-UiO composite retained the original morphology and porosity of pure UiO-66 and presented bifunctional properties in DME synthesis from syngas. Tested under 290 °C and 30 bar, the Cu/STA-UiO exhibited a high selectivity (69.6%) towards DME and excellent DME production rate (10.2 mmol/g_{Cu}.h) as well as exceptional stability.

The second part of my thesis is to investigate a MOF mediated synthesis strategy in preparation highly active Cu/ZnO catalyst. Bimetallic MOFs CuZn-BTC with different Cu/Zn ratios were developed by one-pot synthesis method and annealed to prepare

Cu/ZnO materials. Different calcination procedures and temperatures were investigated. Our results highlighted the significance of two-step annealing of MOF templates in preparing well-defined Cu/ZnO catalysts. Mixed with γ-Al_2O_3, the prepared CZ-350/A (calcined in air at 350 ºC) outperformed its counterpart with DME selectivity of 70% and lower deterioration rate.

Lastly, we manufactured Co/Co_6Mo_6C@C nanocages by direct pyrolysis of a Co-MOF (ZIF-67) composite. A Mo-containing polyoxometalate (PTA, $H_3PMo_{12}O_{40}$) was trapped in the pores of ZIF-67 by one-pot synthesis method to get the PZIF precursors. During carbonization under 600 ºC in N_2 atmosphere, Mo atoms reacts with adjacent Co and C to generate a noble-metal like bimetallic carbide Co_6Mo_6C, while extra Co is reduced to be metallic Co^0. The prepared Co/Co_6Mo_6C@C composite favorable activity and selectivity for higher alcohols synthesis from syngas, which is attributed to enhanced synergistic effect between C-C chain growth and CO insertion derived from the close affinity of active Co^0 sites and Co_6Mo_6C sites.

In summary, this thesis provides a series of highly selective catalyst prepared by using MOFs as template and highlights the advantages of MOFs-derived catalysts for oxygenates synthesis from syngas. Additionally, the finding in this study paves new way for rational design of multifunctional catalysts in heterogeneous catalysis.

Acknowledgements

Firstly, I would like to express my deepest and most sincere thanks to my supervisor Prof. Shaomin Liu, for offering me this precious opportunity to pursue my study in his group and for his instructive guidance, persistent support and inspiration during my PhD research. His encouragement and invaluable advice have helped me get through many problems during this journey. He is very kind, patient and professional. The discussions on my research topic were always enthusiastic and fruitful. During the past three years, I have learned a lot from him, especially his serious attitude towards research and this will inspire me to pursue a meaning career in the future.

Equally, I am grateful to my co-supervisor, Dr Gia Hung Pham, for his generous help and professional suggestions on my experiments. His dedication and commitment work have had great influence on my career. I owe special thanks to Dr Min Ao, who helped me so much for my lab work. She is very patient and supportive. Without her help and accompany, my study cannot be completed smoothly. I am also very grateful to Prof. Jian Liu and Dr. Jaka Sunarso for their professional help and advice on my writing skills.

I would also like to thank my thesis committee chairperson, Prof. Zongping Shao, for his valuable advice and assistance throughout this study. I would like to extend my gratitude to Prof. Shaobin Wang and Prof. Sanping Jiang for their kind help and suggestions on my research topic. Special thanks also go to Dr Lihong Liu for her great assistance for both my research and my life.

I would like to offer my sincere thanks to my colleagues and friends, Zhangfeng Shen, Jiaquan Li, Zhengxin Yao, Xiaojie Li, Kai Wang, Qiaoran Liu, Jinxiu Cao, Changya Deng, Xiu Liu, Mingyang Li, Ning Han, Nabil Majd Alawi, Minh Hoang Nguyen,

Wenran Gao, Suiboon Liaw, Xujun Chen and many others. Thank you very much for all your help and support during my PhD study. My life would be boring and tough without you!

Here, I would also like express my gratitude to all the Curtin Chemical Engineering lab technicians, Mr Jason Wright, Mr Andrew Chan, Ms Melina Miralles, Dr. Roshanak Doroushi, Mr Xiao Hua, Ms Jennifer Wang and Mr Araya Abera for their professional help and technical support in the lab. My special appreciations also go to staff from Curtin John de Laeter Centre, Ms Veronica Avery, Mr Jean-Pierre Veder, Ms Elaine Miller, Ms Kelly Merigot and Dr Aaron Dodd for their help with the XRD/XPS/TEM/SEM measurements.

I also sincerely acknowledge the financial support from the Curtin International Postgraduate Research Scholarship that have made my PhD study possible.

Last but not the least, I would like to express my deepest gratitude to my beloved parents, my sister and my boyfriend Jie Zou. Their unconditional support and love encourage me reach so far. I love you all.

List of Publications

Publications by the author:

1. **Fuping Li**, Min Ao, Gia Hung Pham, Jaka Sunarso, Yanping Chen, Jian Liu, Kai Wang and Shaomin Liu. “Cu/ZnO Catalysts Derived from Bimetallic Metal–Organic Framework for Dimethyl Ether Synthesis from Syngas with Enhanced Selectivity and Stability.” ***Small*** 2020, 16(14), 1906276.
2. **Fuping Li**, Min Ao, Gia Hung Pham, Yun Jin, Minh Hoang Nguyen, Nabil Majd Alawi, Moses O. Tade, and Shaomin Liu. "A novel UiO-66 encapsulated 12-silicotungstic acid catalyst for dimethyl ether synthesis from syngas." ***Catalysis Today*** 2020, 355, 3-9.

Manuscript in Preparation:

1. **Fuping Li**, Min Ao, Kai Wang, Jiaquan Li and Shaomin Liu. “Manufacture of $Co/Co_6Mo_6C@C$ nanoreactors from polyoxometalate encapsulated ZIF-67 for Higher Alcohols Synthesis”. **Composites Part B: Engineering**, under review.
2. **Fuping Li**, Shaomin Liu. MOF-derived Robust catalysts: new opportunities for heterogenous conversion of C1chemicals. **To be submitted**.

Table of Contents

Chapter 1 Introduction

1.1 Background and Motive

The tremendous consumption of nonrenewable petroleum-based fossil fuels is bringing in energy crisis and environmental pollution with the rapid growth in global industrialization and population expansion.[1, 2] As a result, it is imperative and of significant importance to seek alternative energy sources to power the world or to produce fuels and chemicals for sustainable development in coming decades.[3, 4] Methane has been considered to be a very promising alternative energy resource and is attracting worldwide academic and industrial interest, owing to its abundant resources, vigorous production and cleaner output than the non-renewable petroleum counterpart.[5]

Methane is the major constituent of natural gas or landfill gas usually in remote locations and cannot be used directly. Due to the low-energy content per unit volume, it is difficult to justify economically transporting natural gas from the wellheads to the consumers, which requires expensive infrastructure and causes environmental concerns from leaking. Gas-to-Liquids (GTL) technology opens up new opportunities to chemically convert methane to more valuable fuels or chemicals. In this process, methane is firstly transformed into synthesis gas (or syngas), a mixture of carbon monoxide and hydrogen. Then the syngas is catalyzed to produce liquid fuels or chemicals through the well-established Fischer-Tropsch (F-T) synthesis. In fact, syngas economy has been seen as the core technology of C1 chemistry.[6] Syngas can be produced from a variety of sources including natural gas, coal, biomass and even organic waste.[7] Moreover, the F-T synthesis has shown versatile potential to convert syngas into a wide range of value-added hydrocarbons (*e.g.* gasolines, diesel and olefins) and organic oxygenates (e.g. methanol, ethers, higher alcohols) by using

various reaction conditions and catalyst systems. With the anticipated depletion of liquid petroleum and the soaring price of crude oil, the conversion of syngas to liquid feedstock or fuels will become more and more important.

Since the discovery of F-T process in the 1920s, most research efforts have been focused on the production of hydrocarbons and methanol. However, the hydrocarbon products usually need further treatment such as cracking to convert into more useful products, while methanol cannot promise considerable economic profit due to the relatively low price. Consequently, the research interest has now been shifted towards the production of higher oxygenates, *e.g.* dimethyl ether (DME) and higher alcohols (HA). DME is the simplest ether derived from methanol dehydration process. As a clean fuel in the 21st century, DME can partially replace diesel or liquefied petroleum gas (LPG) owing to high cetane number and environmentally benign combustion performance. Higher alcohols containing 2 or more carbon atoms can also be used directly as the transportation fuels or gasoline additives. Moreover, both DME and HA can be used as important feedstock for more valuable products. Currently, the effective synthesis of DME and HA is one of the hot research areas in the energy chemistry.

The direct DME and higher alcohols synthesis from syngas involve tandem reactions. Therefore, both processes require bifunctionality of catalysts to boost each reaction involved. The synergistic effect and the affinity between different functional groups are vital for manufacturing active and selective catalysts in syngas-to-DME process and higher alcohol synthesis. Copper-, cobalt-, molybdenum-based catalysts are widely used for oxygenates production. However, catalysts obtained from traditional perpetration methods suffer from unavoidable sintering issue, random dispersion, as well as low synergism between active sites, resulting in low activity and stability. Thus, a great effort is still required to develop novel catalysts with enhanced activity and selectivity.

Metal-organic framework, the assembly of metal ions and organic linkers, is supposed

to be a promising platform to update the traditional catalysts due to their well-defined structures, high porosity and easy-tailored composition and morphology.[8, 9] The abundant internal pores and channels along with the broad external surface can facilitate the mass diffusion during the reactions and confine/support functional groups to prepare active composites. Moreover, MOF mediated synthesis can fabricate porous metal or metal oxide, carbon materials, and their hybrids. Most importantly, uniform element distribution and close affinity of cooperative active centers are expected in the MOF microenvironment. To our best knowledge, limited reports have focused on the application of MOF-derived catalyst for oxygenates production from syngas.

1.2 Scope and Objectives

Therefore, this PhD thesis aims to develop novel MOF-based bifunctional catalysts with high activity and selectivity for oxygenates synthesis from syngas. In addition, this thesis also dedicates to providing insights on the formation of active centers and the synergistic effect of MOF-derived catalyst on catalytic performance. The specific objectives of this study are listed below:

- To summarize the current research status of organic oxygenates synthesis from syngas and the recent progress of MOF-derived catalysts for heterogeneous catalysis;
- To develop the Zr-MOF based composite as bifunctional catalyst for DME synthesis and investigate the structural properties and catalytic performance;
- To fabricate the well-defined Cu/ZnO catalyst via pyrolysis of bimetallic CuZn-MOF and evaluate the effect of pyrolysis process on the catalytic performance for DME synthesis;
- To conduct investigation into Co-MOF derived catalysts with different Co/Mo ratios for HAS and explore the plausible reaction mechanism.

1.3 Thesis Outline

This thesis contains 7 chapters (including this current chapter) according to the specific objectives as listed above. Each chapter is outlined below:

- **Chapter 1** provides the background and objectives of the current research.
- **Chapter 2** presents an up-to-date literature review on the synthesis of dimethyl ether and higher alcohols, the catalyst development for DME and higher alcohols, the synthesis strategies of MOFs-based materials and the corresponding applications in solid-gas phase catalysis.
- **Chapter 3** provides an overview of the research methodology adopted to achieve the research objectives and stepwise sample preparation, catalyst evaluations and the analytical techniques applied.
- **Chapter 4** presents the explorations of MOF composites as bifunctional catalyst for DME synthesis from syngas. A Zr-MOF (UiO-66) is used to host solid acid in the pore structure and support Cu species on the surface. The catalyst structural properties, morphology and catalytic performance are investigated.
- **Chapter 5** provides the applications of bimetallic MOF derived Cu/ZnO catalyst for DME production. A CuZn-MOF is developed through one-pot solvent thermal treatment. The effect of pyrolysis procedures and temperatures on the resultant catalysts are evaluated.
- **Chapter 6** examines the performance of MOF composite derived Co/Co_6Mo_6C@C for higher alcohols synthesis. The effect of catalyst composition is studied, and the catalytic mechanism is explored.
- **Chapter 7** summarize the major finding in this study and gives recommendations for future work in this area.

References

1. Saravanan, K.; Ham, H.; Tsubaki, N.; Bae, J. W., Recent progress for direct synthesis of dimethyl ether from syngas on the heterogeneous bifunctional hybrid catalysts. *Appl. Catal. B-Environ.* **2017,** *217*, 494-522.

2. Azizi, Z.; Rezaeimanesh, M.; Tohidian, T.; Rahimpour, M. R., Dimethyl ether: A review of technologies and production challenges. *Chem Eng Process* **2014,** *82*, 150-172.

3. Álvarez, A.; Bansode, A.; Urakawa, A.; Bavykina, A. V.; Wezendonk, T. A.; Makkee, M.; Gascon, J.; Kapteijn, F., Challenges in the greener production of formates/formic acid, methanol, and DME by heterogeneously catalyzed CO_2 hydrogenation processes. *Chem. Rev.* **2017,** *117* (14), 9804-9838.

4. Luk, H. T.; Mondelli, C.; Ferré, D. C.; Stewart, J. A.; Pérez-Ramírez, J., Status and prospects in higher alcohols synthesis from syngas. *Chem. Soc. Rev.* **2017,** *46* (5), 1358-1426.

5. Ao, M.; Pham, G. H.; Sunarso, J.; Tade, M. O.; Liu, S., Active Centers of Catalysts for Higher Alcohol Synthesis from Syngas: A Review. *ACS Catal.* **2018,** *8* (8), 7025-7050.

6. Kasipandi, S.; Bae, J. W., Recent Advances in Direct Synthesis of Value-Added Aromatic Chemicals from Syngas by Cascade Reactions over Bifunctional Catalysts. *Adv. Mater.* **2019**, 1803390.

7. Ni, Y.; Liu, Y.; Chen, Z.; Yang, M.; Liu, H.; He, Y.; Fu, Y.; Zhu, W.; Liu, Z., Realizing and Recognizing Syngas-to-olefins Reaction via a Dual-bed Catalyst. *ACS Catal.* **2018**.

8. Kirchon, A.; Feng, L.; Drake, H. F.; Joseph, E. A.; Zhou, H.-C., From fundamentals to applications: a toolbox for robust and multifunctional MOF materials. *Chem. Soc. Rev.* **2018**.

9. Wang, C.; Liu, X.; Demir, N. K.; Chen, J. P.; Li, K., Applications of water stable metal–organic frameworks. *Chem. Soc. Rev.* **2016,** *45* (18), 5107-5134.

Chapter 2 Literature Review

2.1 Introduction

With industrialization proceeding, the tremendous consumption of nonrenewable petroleum-based fossil fuels has caused energy shortage and severe air pollution. It has been predicted that the nonrenewable energy resources can only sustain for several centuries.[1] The utilization of fossil fuels is also known to be a key contributor to greenhouse gas emission which is responsible for global warming. Toxic chemicals, *e.g.* NO_x and SO_x, generated from vehicle exhaust further accelerate the environmental deterioration. To maintain a clean environment for our future generation, the society should be shifted from petroleum dependence to other more renewable or sustainable sources.[2, 3] Currently, exploration of alternative energy sources is one of the hot topics to address the global environmental crisis and energy shortage issues.

Syngas, the mixture of CO and H_2, is a key chemical intermediate for the utilization of non-petroleum carbon resources.[4] Syngas can be produced from natural gas, shale gas, coal, biomass, and organic wastes.[5, 6] Through a versatile "Fischer-Tropsch synthesis (FTS)" process, syngas can be transformed into valuable chemicals such as hydrocarbons (gasoline, diesel fuel, light olefins, and aromatics) and oxygenates (alcohols and ether).[7-9] In particular, the oxygenates, especially dimethyl ether (DME) and higher alcohols (HA) have received considerable interest owing to their superior combustion performance, clean output and vast applications to produce industrial goods.

The objective of this chapter is to provide the basic knowledge of catalyst development of higher oxygenates production from syngas. This review starts with a brief introduction of synthesis method and mechanisms in the DME and higher alcohols

production (section 2.2), then moves on to the discussion of the active centers for DME and higher alcohols (section 2.3). In addition, the application of metal-organic framework (MOF) based materials for potential utilization in heterogeneous catalysis is also reviewed, beginning with the brief introduction of MOF, modification strategies for MOFs and their applications in solid-gas phase processes (section 2.4). Finally, the last section describes the potential of MOFs based catalyst for DME and HA formation from syngas (section 2.5).

2.2 Oxygenates synthesis from syngas

2.2.1 DME synthesis

As the simplest ether, DME only possesses C-O and C-H bonds.[10] In spite of high volatility, DME is easily handled with less safety concerns due to its non-carcinogen, non-teratogenic, non-mutagenic and non-toxic merits.[2, 11] The physical and chemical properties of DME are detailed in Table 2-1.

Table 2-1 Physical and chemical properties of DME

Item	Property	Item	Property
Formular	CH_3OCH_3	Heat of Combustion (KJ/mol)	1455
Molecular weight ($g.mol^{-1}$)	46.07	Cetane number	55-60
Density ratio	1.617	Density ($g.cm^{-3}$, 20°C)	0.661
Normal boiling point (°C)	-24.9	Gas viscosity (μPa.s, 20°C)	85.5
Critical temperature (°C)	128.8	Explosion limit (in air %)	3.45 - 26.7
Critical pressure (MPa)	5.32	Vapour pressure (MPa, 20°C)	0.51
Melting point (°C)	-141.5	Autoignition point (°C)	350
Carbon content (wt.%)	52.2	Sulfur content (wt.%)	0

As a clean fuel for 21st century, DME can play an important role in many aspects.[12] It can be used as substitute of diesel fuel and liquefied petroleum gas due to high cetane

number, low soot emission and equivalent engine performance with liquefied petroleum gas (LPG).[13, 14] Due to the zero ozone depletion potential and low greenhouse index (0.2), DME can be used for coolant and aerosol instead of chlorofluorocarbons.[15 16] In addition, DME can be used as the feedstock for lots of important chemicals, for instance, methyl acetate and formaldehyde, and valuable H_2 supply for fuel cells. [17-19]

Two different routes have been reported to produce DME from syngas: indirect synthesis route (or two step synthesis) and direct syngas-to-DME route (or STD process).[20] Normally, three major reactions occur in DME synthesis:

Methanol synthesis reaction: $$CO + 2H_2 \rightarrow CH_3OH \quad (2\text{-}1)$$

Methanol dehydration reaction: $$2CH_3OH \rightarrow CH_3OCH_3 + H_2O \quad (2\text{-}2)$$

Water gas shift reaction (WGSR): $$H_2O + CO \rightarrow H_2 + CO_2 \quad (2\text{-}3)$$

The main difference between both synthesis routes lies in water-gas-shift reaction (WGSR). In indirect process, WGSR (Eq.(2-3)) is not involved and methanol synthesis and dehydration occur in different reactors, with both reactions under equilibrium controlled featured by low CO conversion and DME yield. However, for the direct synthesis method, three reactions occur simultaneously in a single reactor and the intermediate product of one reaction is soon consumed by another reaction. Such synergetic effect suppresses thermodynamic limitation and shifts the equilibrium to DME constantly. The huge economic benefit of direct synthesis of DME has inspired enormous studies worldwide. However, this is still in the laboratory stage.[21]

2.2.2 Higher alcohols synthesis

Apart from DME formation, higher alcohols (or HA), containing 2 or more carbon atoms have also shown great potential as the commodity chemicals owing to their broad range of applications. The linear or branched C_2-C_5 alcohols, namely short-chain

alcohols, can be used directly as the transportation fuel or gasoline additives to enhance to octane number and subsequent engine performance. The long-chain alcohols containing over five carbon atoms are regarded as promising feedstocks to produce primary materials in industrial chemistry, such as detergent, surfactants and lubricants. Considering their versatile properties, HA have demonstrated fabulous potential market and the direct higher alcohols synthesis (HAS) from syngas leaps out of a catalytic route of prominent interest over 30 years.

Generally, the higher alcohols are produced from syngas following the Equation (2-4):

$$2n\ H_2 + n\ CO \rightarrow C_nH_{(2n+1)}OH + (n-1)H_2O \qquad (2\text{-}4)$$

As for the reaction pathways, Xu *et al.* proposed a widely accepted CO insertion mechanism to elucidate the intrinsic chemistry for HA formation.[22] This mechanism involves cascade reactions in terms of CO dissociation, carbon chain growth, CO insertion and stepwise hydrogenation.[23] As interpreted in Figure 2-1, the CO molecules firstly undergo dissociative adsorption to the surface carbon C*, which then react with the surface H* to form the intermediate C_1H_x*. The carbon chain propagation of alkyl species C_nH_z* is implemented via the successive C_1H_x* addition. To form the final alcohols, the non-dissociatively adsorbed CO* molecule inserts into the metal site and react with C_nH_z* to generate the acyl intermediate C_nH_zCO*, which then is hydrogenated to form the C_{n+1} alcohols. It should be noted that the hydrocarbons are also produced simultaneously through the direct hydrogenation of alkyl groups during HA synthesis, which unavoidably impact the selectivity to higher alcohols.

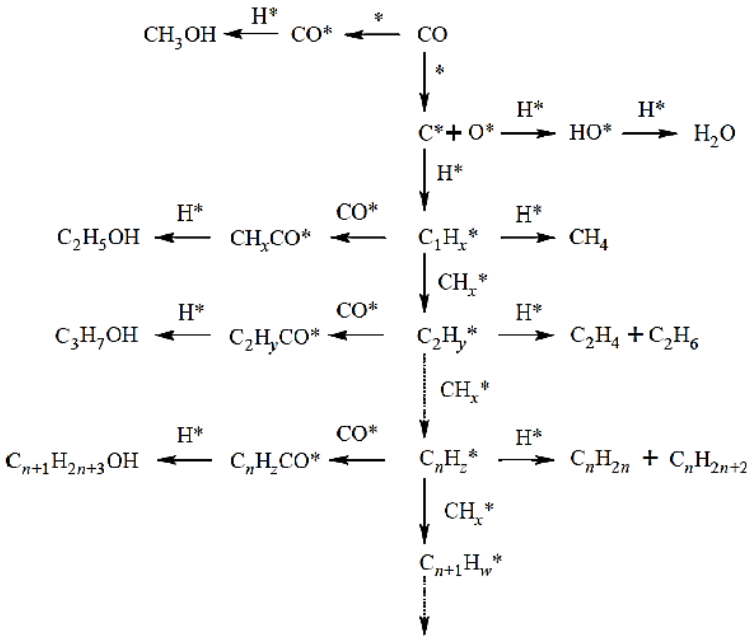

Figure 2-1. Higher alcohol and hydrocarbons formation through CO insertion mechanism. Reprinted with the permission from ref. [22]

Following the above-mentioned mechanism, the higher alcohols synthesis requires the chain growth and CO insertion to occur simultaneously to produce massive alcoholic products. Unfortunately, the active sites for both secondary reactions are usually different. Therefore, the synergetic effect between two different active centers is highly desirable to facilitate the C-C propagation and CO insertion. To date, none effective catalyst system on the syngas-to-higher alcohols process has been sufficiently active and selective to justify the industrial application.

2.3 Active centers for oxygenates

2.3.1 Active centers for DME

For STD process, the key to get high DME yield is to develop catalyst with high activity for all three involved reactions. Since methanol synthesis catalyst is always

functional for WGSR, the catalyst used in the STD process must be bifunctional not only for methanol synthesis catalyst but also for methanol dehydration catalyst.

2.3.1.1 Methanol synthesis catalyst

Copper based catalyst in a typical composition of CuO-ZnO have been widely used for methanol synthesis.[24, 25] Strong synergetic effect between copper and ZnO has been well known to facilitate formation of the active sites. Cu^0 particles in Cu-ZnO interface can improve the methanol synthesis rates.[25] Other metal oxides (Al_2O_3, MgO, ZrO_2, *etc*.) are also effective promoters for Cu-ZnO catalysts since they can modify the structural properties of active sites. For example, ZrO_2 can alter the outer-shell electrons of Cu and improve the catalyst reducibility.[26] The addition of Al can form $Cu_2Zn_4Al_2(OH)_{16}CO_3.4H_2O$ hydrotalcite and consequently increase the dispersion of copper. [27]

However, the active site of Cu-based catalyst is still not clear. It is well recognized that Cu^0 is the active site functioning for methanol synthesis, but not Cu^+ or Cu^{2+}, which has been proved by many researchers.[20, 28, 29] Whereas in some circumstances, Cu^+ also plays an important role, because the non-dissociate adsorption of CO on Cu^+ is much stronger than metallic copper particles. [20, 30] The molecular adsorption of CO facilitates methanol synthesis, while dissociate adsorption favors hydrocarbons and coke formation. It seems that the ratio of Cu^+/Cu^0 plays the crucial role in methanol synthesis.[31]

2.3.1.2 Methanol dehydration catalyst

The solid acid catalysts for DME synthesis mainly include γ-Al_2O_3, zeolite, amorphous SiO_2-Al_2O_3 and heteropolyacid.[32] Among these catalysts, γ-Al_2O_3 and zeolite are typical examples being most widely used.

γ-Al_2O_3 has been applied to DME synthesis by many researchers.[24, 33-35] Its low-cost and good stability makes itself a reasonable option for methanol dehydration.[36] However, the disadvantage associated with its weak acidity and strong hydrophilicity

limit its performance on DME synthesis.[37] Besides, its high performance can only be observed when temperature is over 300°C, thus restricting its collaboration with Cu-based methanol synthesis catalyst on one step DME synthesis due to the severe copper sintering behavior. Many promoters, such as Ta_2O_5, SiO_2, TiO_2, and phosphate have been employed to improve the acidity of γ-Al_2O_3.[38-41] In addition to the acidity adjustment, morphology modification, η-Al_2O_3 for instance, has been proved a facile way to improve DME yield. Despite higher calcination temperature, η-Al_2O_3 results in higher stability in DME synthesis than γ-Al_2O_3.[42] Ordered mesoporous γ-Al_2O_3 is a promising methanol dehydration catalyst as well as catalyst support due to its acidic characteristics, large pore size and high thermal stability.[43] The mesoporous Cu/γ-Al_2O_3 catalysts can be prepared via solution combustion[44] and evaporation induced self-assembly method.[45] Cu-Al-O crystallite network was formed after reduction, thus small copper particles (around 6 nm) were well surrounded by alumina, facilitating methanol consumption once it was formed.[45] Due to the unique crystallite network, a CO conversion of 72% and DME selectivity of 69% was achieved at 50 bar and 310℃ without serious copper sintering. [45]

Zeolite with excellent shape selectivity and thermal stability has been used on DME synthesis extensively. The typical zeolite is ZSM-5, which possesses larger BET surface area (400~500 m^2/g), alterable acidity and broad Si/Al ratio.[46-49] However, the Bronsted acidity of ZSM-5 is quite strong for DME formation and thus leads to coking. Co, Na modified ZSM-5 shows better stability and DME yield than pure ZSM-5 due to increased weak acid sites and lower proportion of strong acid sites. [35, 50] Microporous zeolite, Y, BEA , MCM-22, Ferrierite and Mordenite , for instance, have also been effective for methanol dehydration to form DME.[51-56] SAPO-n zeolites (n=5,11,18,34) have also been evaluated for DME synthesis either in direct or indirect methods.[57, 58] Mesoporous and hierarchical zeolites also attract much attention due to their moderate pore channels, which facilitate efficient diffusion of reactant and product molecule. Wei *et al.* employed alkaline treatment method to develop mesoporosity and macroporosity in ZSM-5 via desilication with NaOH solution, and

found that methanol conversion was higher than pure ZSM-5.[59] SBA-15 zeolite, as a mesoporous silica, can be modified by Al or Zr to increase its acidity for methanol dehydration.[60-62]

2.3.2 Active centers for higher alcohols

Extensive studies on catalytic conversion of syngas to higher alcohols using various catalysts have been performed on various catalytic systems in terms of monometallic or heterometallic catalysts, and many active metals including Cu, Fe, Co, Mo and Rh have shown good activity for this reaction. This part briefly reviews the exploration of active centers for HAS.

2.3.2.1 Monometallic catalyst for HAS

Generally, the monometallic catalyst system is not appealing because the HAS process requires dual active sites for separate reactions. Nevertheless, some transition metal elements (i.e. Mo, Rh, Co and Fe) can exhibit different oxidation states under HAS conditions, thus providing the opportunities to form bifunctionalities. Xiang *et al.* observed the active Mo^{0-2+} - Mo^{4+} pair formation over K promoted β-Mo_2C catalyst, where Mo^{0-2+} promotes the C-O bond cleavage and C-C chain growth and Mo^{4+} is mainly for CO insertion step.[63] The formation of Mo^{0-2+} - Mo^{4+} interfacial pair in the monometallic Mo catalysts facilitates the migration of C_nH_z* species from Mo^{0-2+} site to Mo^{4+} site. Similarly, Rh monometallic catalysts are also reported to induce adjacent Rh^{n+}/Rh^0 species with Rh^0 for CO dissociation and CH_x* formation and Rh^{n+} for CH_xCO* formation through CO insertion and subsequent hydrogenation to produce higher oxygenates.[64] Pei *et al*. prepared Co-Co_2C catalyst free of any promoter or support for HAS. The characterization results and density functional theory calculations verified the significance of Co/Co_2C interface for alcohols formation.[65] The metallic Co^0 is active for CO dissociative adsorption and C-C propagation, whereas the noble-metal-like Co_2C is mainly responsible for CO no dissociative

adsorption and subsequent CO insertion into the linear alkyl intermediate to produce higher alpha-alcohols. Such a reaction pathway is also validated by other reports.[66] The Fe monometallic catalysts of Fe/Al_2O_3 and Fe_2O_3/Al_2O_3 were also reported to follow the CO insertion mechanism. However, the active centers in such catalyst system is still not clear.[67]

Although several modification routes have been investigated to improve the catalytic performance of monometallic catalysts in HAS, the resultant CO conversion and yield for higher alcohols are still insufficient for commercial considerations. This is mainly because the monometallic catalyst systems fail in the accurate control of the dual active sites formation and the balance between separate functional component for different steps, which is of great importance for HAS.

2.3.2.2 Heterometallic catalyst for HAS

The heterometallic catalysts, composed of different active metal elements, are pormising catalyst candidates for HAS owing to tunable compostion and nature of active centers. The binary catalysts (i.e. Cu-Co, Co-Mo and Cu-Fe) and multimetallic catalysts (i.e. Cu-Co-Mo, Zn-Cr-Mo and Cu-Fe-Mo) have exhibited exceptional activity toward HA formations with enhanced stability. Moreover, the combinations of various metal elements would induce novel active sites around the interface for selective higher alcohols formation. Thus, the heterometallic catalysts for HAS have been drawing considerable research attention and the nature of active centers behind the activity are deeply digged.

Liakakou *et al.* synthesized a series of K-NiMo/AC catalysts by stepwise incipient impregnation of activated carbon with the metal precursors.[68] The combination of Ni and Mo rendered the formation of β-$NiMoO_4$ phase which is of weak acidity and improved reducibility. The above-mentioned catalyst achieved a space time yield to oxygenates of 141.5 $mg/g_{catalyst}/h$ under HAS conditions, owing to the enhanced CO

affinity and activation on the Ni-O-Mo sites. The Mo-based binary catalysts (eg. Mo-Co, Mo-Fe and Mo-Ni) would induce the formation of noble-metal-like bimetallic carbide for HAS. Wang *et al.* investigated the Fe modified K-β-Mo_2C catalyst for HAS.[69] The newly formed Fe_3Mo_3C is mainly responsible for CO insertion, while Fe_3C provided the active centers for carbon chain growth. Co and Ni are also capable to generate the Co_3Mo_3C and Ni_6Mo_6C carbide when used as promoters for K-Mo_2C catalyst, which play the similar roles as Fe_3Mo_3C.[70, 71] Recently, Cu-Fe binary catalysts are found to be highly active for higher alcohols synthesis from syngas. To elucidate the synergistic interaction between copper and Hagg iron carbide, Lu *et al.* prepared three-dimensionally ordered microporous (3DOM) Cu-Fe catalyst for HAS.[72] The Cs-corrected HAADF-STEM clearly reveals the adjacent χ-Fe_5C_2 and Cu^0 sites with extensive interface in the reduced 3DOM Cu-Fe catalyst with χ-Fe_5C_2 primarily for C-O cleavage and chain propagation and Cu^0 sites for CO* generation and insertion into the hydrocarbon intermediate formed on χ-Fe_5C_2 to produce oxygenates. Moreover, the synergistic interaction of Cu^0-χ-Fe_5C_2 provided an electron-rich interface by facile electron transfer from Cu^0 site to the adjacent χ-Fe_5C_2 site, reduced the activation barriers for CO insertion into the CH_x* to C_2 oxygenates and facilitated the CO activation and insertion at the interfacial area. Ma and co-workers immobilized Fe_5C_2 clusters on the surface of Cu nanoparticles by direct thermolysis of CuFeMg-layered double hydroxide ($Cu_xFe_yMg_4$-LDH).[73] The ultrasmall Fe_5C_2 clusters (about 2 nm) located on the Cu^0 surface created a large density of interfacial sites and greatly enhanced the kinetic rate coordination between C-C coupling step and CO insertion step. As a result, the selectivity toward long-chain alcohols were significantly elevated at a surprisingly benign reaction pressure of 1 MPa.

Lin *et al.* reported a multifunctional catalyst CoMn | CuZnAlZr for selective higher oxygenates production from syngas.[74] The CuZnAlZr is higly selective for methanol formation with low CO conversion, while the CoMn catalyst resulted in a higher oxygenates selectivity of 34.4 wt%. However, the solid mixture of CuZnAlZr and CoMn oxide greatly enhanced the higher oxygenates selectivity to 54.5%. For this

bifunctional catalyst system, the Co/Co_2C in the CoMn is regarded as the active sites for higher oxygenate formation. The CuZnAlZr component mainly provides extra active site for CH_xO^* generation as well as the hydrogenation of aldehydes to alcohols. The close proximity of CoMn and CuZnAlZr is proved to be vital for the process of relay reactions to boost the higher oxygenates production and to suppress the C1 formation. A $ZnCrAlO_x$ | KNiMoS-MMO catalyst has also been reported to follow the similar reaction pathway, where KNiMoS-MMO presents active sites for carbon chain growth and CO* insertion and $ZnCrAlO_x$ enhances associative CO adsorption and supply the CH_xO^* intermediates to be inserted in the carbon chains.[75]

2.3.3 Key factors of catalyst architecture for DME and HA synthesis

The aforementioned explorations of active centers for DME and higher alcohols production clearly demonstrate that the rational design of catalysts is of great significance. Both processes require bifunctionality of the prepared catalysts with highly dispersed active centers and close affinity of each component. Generally, there are two predominant factors widely investigated in syngas-to-DME and syngas-to-higher alcohols: synergistic effect and strong metal-support interactions.

Synergistic effect derived from adjacent different kinds of active centers is highlighted in the tandem catalysis reactions. The reaction intermediates can be catalyzed on one active center once it is produced on another active site. As a result, the synergistic effect can shift the reaction to the products of interest via fast elimination of reaction intermediates. For example, the close affinity of Cu-based methanol synthesis catalyst and solid acid catalyst can induce a strong synergistic effect between methanol synthesis step and following dehydration step. Similarly, the synergism between CO dissociation and CO insertion can also improve the selectivity for HAS. To enhance the synergism, it is desirable that the different active sites are homogeneously dispersed in the catalyst with small nanoparticle size to maximum the interfacial area.

Strong metal-support interaction (SMSI) effect, as the name suggested, is derived from the interactions between active centers and the catalyst supports. SMSI effect represents an important feature in heterogeneous catalysis, especially solid-gas phase reactions. Usually, thermostable supports with high surface area and ample internal pores, such as metal oxides of Al_2O_3, MgO and ZnO and porous carbon materials, are extensively applied to improve the distribution of active sites. The SMSI effect of Cu/ZnO results in a partial reduction of Zn^{2+} to $Zn^{(2-\delta)+}$ during the methanol synthesis reaction and generates the new active sites Cu-O-$Zn^{(2-\delta)+}$ which shows exceptional activity towards methanol synthesis. However, the SMSI effect could also manipulate the catalyst properties, e.g. impeding the reduction of metal oxides and therefore reducing the catalytic activity in HAS.

Although tremendous efforts have been devoted, it is still difficult to rationally design efficient catalyst series with enhanced synergistic effect and positive SMSI in the oxygenates synthesis from syngas. The traditional coprecipitation method of metallic catalysts provide the insufficient dispersion of active centers, and thus lead to quick deactivation owing to metal NPs aggregation during the reactions. Moreover, the impregnation of active sites on the porous support brings about uncertainties of the catalyst distribution. Furthermore, the accommodation of different active sites with close affinity remains a big challenge. Consequently, it is imperative to develop new platform to construct novel catalysts with high activity and stability to justify the industrial applications.

2.4 Metal-organic frameworks for solid-gas phase reactions

2.4.1 Introduction of metal-organic framework

Since the first report at the end of last century, a new class of crystalline materials, Metal-Organic Frameworks (MOFs), also known as Porous Coordination Polymers

(PCPs), has been attracting worldwide research interest. MOFs are the assembly of metal ions or clusters coordinating with the organic ligands. The metal ions for MOFs are usually transition metals, such as Cu, Zn, Zr, Co and Fe. The organic linkers can be 2-methylimidazaole (2-MIM), terephthalic acid (1,4-dicarboxybolic acid, also called H_2BDC), or trimesic acid (1,3,5-Benzenetricarboxylic acid, also called H_3BTC). Based on different linking designs of the initial metal cluster formation, the final frameworks can be in one-, two-, or three-dimensional arrangements. Normally, MOFs can be synthesized through hydrothermal or solvent thermal method or using ultrasonic and microwave. To date, thousands of MOFs have been successfully developed and applied extensively for various of research fields, such as gas adsorption, separation, drug delivery, sensing, and catalysis.

The unique structure confers MOFs materials several outstanding properties as described below:

(1) Extremely high porosity and surface area

The high porosity of MOFs is owing to the removal of guest molecules, creating abundant pores and wide-open channels in the framework. The pore size varies with the types of MOFs. For example, ZIF-8, the assembly of Zn and 2-methylimidazole, is a typical microporous MOF, whereas MIL-101, a typical Cr-MOF using H_2BDC as the organic ligand, possesses large amount of mesopores in its structure. Notably, the molecular size of organic linkers also impacts the pore size in the resultant MOFs. MOF-177 developed by Yaghi' s group through reacting Zn nodes with a large linker H_3BTB (1,3,5-tris(4-carboxyphenyl)benzene) was reported to have a giant pore volume of 1.59 $cm^3.g^{-1}$.[76] This MOF can even be used to adsorb C_{60} and dye molecules. It is well acknowledged that the porosity of materials is an important parameter to define the corresponding ability for adsorption, separation and catalysis. Thus, the great variety of MOFs materials with different pore size distribution makes MOF a viable alternative for traditional application.

The high surface area is another typical feature of MOF material. For instance, MOF-5 reported in 1999 has a surface area of 3000 $m^2.g^{-1}$.[77] MOF-210 even reaches the highest level among porous materials with a surface area of 6240 $m^2.g^{-1}$.[78] The large internal surface can ensure efficient adsorption of molecules as well as resident functional groups in the framework, extending the potential applications of MOFs.

(2) Uniform structure

MOFs materials always possess ordered structure with similar particle size. Based on the coordination topology, the formed MOF particles can be octahedral, cubic or rhombic dodecahedral. The uniform structure can rule out the effect of shape heterogeneity on target applications, thus benefit more accurate clarification of reaction mechanism.

(3) Tunable structure and composition

The easy tailoring morphology is an important feature of MOFs for specific applications, especially for structure-sensitive reactions where catalytic activity is strongly dependent on the particular facets. Normally, altering preparation method or adding surfactant such as cetyltrimethylammonium bromide (CTAB) are applied to change the shape of MOF. For example, increasing CTAB content in the mother solution can change ZIF-8 morphology from rhombic dodecahedron to nanocube or nanorod.[79] The as-synthesized mixed-matrix membrane containing ZIF-8 showed significantly different performance for C_3H_6/C_3H_8 separation due to diverse morphologies. It is also reported that the inter-dimensional topotactic phase changes from rhombic dodecahedral ZIF-67 to leaf-like lamella by simply modifying the methanol/water ratio.[80] Moreover, the composition of MOFs can be reconstructed by using another type of ligand or a combination of different types of organic linkers, imparting MOFs more functions to meet the demand for specific applications.

2.4.2 Architecture of MOF based catalyst

Although MOFs have shown more fascinating merits over conventional porous materials like activated carbon and zeolite, they themselves are inert for catalysis processes in most cases due to lack of active sites. As a result, modifications are highly desirable to impart functionalities to the MOFs prior to the real applications.

2.4.2.1 MOF composites

MOF composites are very promising for various reactions. The vast internal structure of MOF can trap a variety of functional groups, such as metal nanoparticles (NPs). Generally, metal NPs/MOF composites can be achieved through direct reduction of metal precursors with a MOF template or encapsulation of pre-synthesized metal NPs in MOFs.[81-83] The latter method, namely encapsulation strategy, is more attractive for developing highly active catalyst. With this strategy, the pre-synthesized metal NPs stabilized by polyvinylpyrrolidone (PVP) can be completely confined within the MOFs via a facile one-pot synthesis method. Furthermore, one can easily tune the size and/or shape of NPs for various applications, as well as isolating the formed NPs within the MOF to avoid particle agglomeration. Huo, Hupp and their co-workers have installed Pt, Au, Ag NPs and nanocubes in the ZIF-8 framework, as shown in Figure 2-2.[81] Especially, the resultant Pt/PVP/ZIF-8 displayed high activity for CO oxidation and n-hexene hydrogenation. It's worth to mention that the PVP stabilized NPs are well surrounded by the ZIF-8 lattice, rather than occupying the ZIF-8 cavities, because of their larger size (2.5-34 nm) than the cavity size of ZIF-8 (11.6 Å).

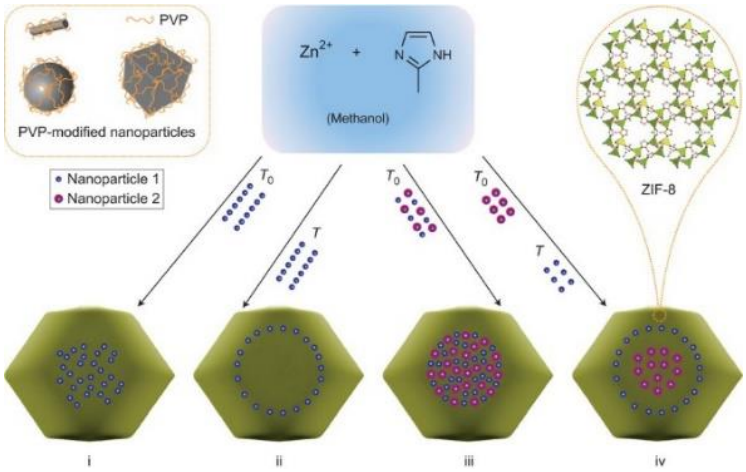

Figure 2-2. Scheme of the controlled encapsulation of nanoparticles in ZIF-8 crystals. The PVP stabilized nanoparticles of various sizes, shapes and compositions can be encapsulated in a well-dispersed fashion in ZIF-8 crystals. The spatial distribution of incorporated nanoparticles within ZIF-8 crystals can also be controlled by their addition sequence (that is, addition at the beginning (T0) or after a certain time (T) during the MOF synthesis). Reprinted with the permission from ref.[81]

Additionally, the incorporation of functional groups like polyoxometalates (POMs) in MOFs has been widely investigated.[84-90] POMs, especially Keggin-type POMs with the composition of $H_nXM_{12}O_{40}$ (X=Si, Ge, P, As; M=W, Mo), are highly active and environmentally benign catalysts for acid-catalyzed reactions and industrial applications owing to their strong Brønsted acidity and tunable redox properties. The molecular size of POMs (about 1 nm) is quite similar to the cavity size of MOFs and larger than the MOF aperture size. Hence, POMs/MOF composites combine the advantages of both components, resolving the poor porosity of POMs and limited activities of MOFs in specific applications. Liu *et al*. reported the synthesis of NENU-n series compounds (POMs@HKUST-1) by adding POMs directly to the feed solutions for HKUST-1.[84] Tested for methanol dehydration to DME, the prepared NENU-1a exhibited an outstanding CO conversion of 60.1% and DME selectivity of nearly 100%, much higher than its traditional counterparts γ-Al_2O_3 or γ-Al_2O_3 supported POM.[86] This is because the HKUST-1 host can ensure homogenous

dispersion of POM molecules in its cavities while remaining high accessibility of all active sites. In addition, Cr-MOFs, such as MIL-101 and MIL-100, are widely used as the scaffolds to encapsulate POMs due to their remarkable porosity and strong acid/basic resistance which are highly desirable for industrial applications including Friedel–Crafts acylation, esterification and acetalization reactions.[91-95] The MIL-101 can load as high as 70 wt% of $H_3PW_{12}O_{40}$ in the formed $H_3PW_{12}O_{40}$@MIL-101 composite while retaining the intact structure and mesoporosity. Wang, Hu and co-workers even used facile solid grinding method to trap three different kinds of POMs ($H_3PW_{12}O_{40}$, $H_4SiW_{12}O_{40}$, $H_3PMo_{12}O_{40}$) in well-defined ZIF-8 cages.[96] These materials showed excellent controlled release of methylene blue and anti-cancer agent 5-fluorouracil.

2.4.2.2 Hetero-bimetallic MOFs

Doping another type of metal node in a MOF is an effective approach to improve the performance of MOFs in a variety of applications. The rational design of bimetallic MOFs lies in the fact that metal element A and B can both coordinate with the organic linkers in a single MOF crystal rather than forming the mixtures of A-MOF and B-MOF. For example, 2,5-dioxido-1,4-benzenedicarboxylate (H_4DOBDC) can coordinate with different kinds of metal centers including Mg^{2+}, Ni^{2+} and Co^{2+} to form MOF-74. Wang *et al.* reported the synthesis of Ni_xMg_{1-x}-MOF-74 for CO_2 photoreduction to formate ($HCOO^-$).[97] The aqueous solution containing Ni and Mg precursors with different Ni/Mg ratios and H_4DOBDC underwent hydrothermal treatment at 175 °C for 12 hours. Characterization data show Ni and Mg can be homogeneously dispersed in the pure phase of MOF-74. The prepared $Ni_{0.75}Mg_{0.25}$-MOF-74 produced more $HCOO^-$ than the monometallic Ni-MOF-74 and Mg-MOF-74, owing to the enhanced CO_2 adsorption capacity. Qiu *et al.* also developed a series of NiCo-MOF-74 with different Ni/Co ratios.[98] It should be noted that different metal ions have distinct coordination ability with the same ligand. For instance, it is more likely for Zn^{2+} to coordinate with 2-methylimidazole than Co^{2+}. As a result, the Co/Zn

ratio in the final Co/ZIF-8 is much lower than the value used for bimetallic MOF synthesis.[99] Similar phenomena have also been observed in the synthesis of NiCo-MOF-74, NiMg-MOF-74 and CuZn-BTC coordination polymers.[98, 100-102]

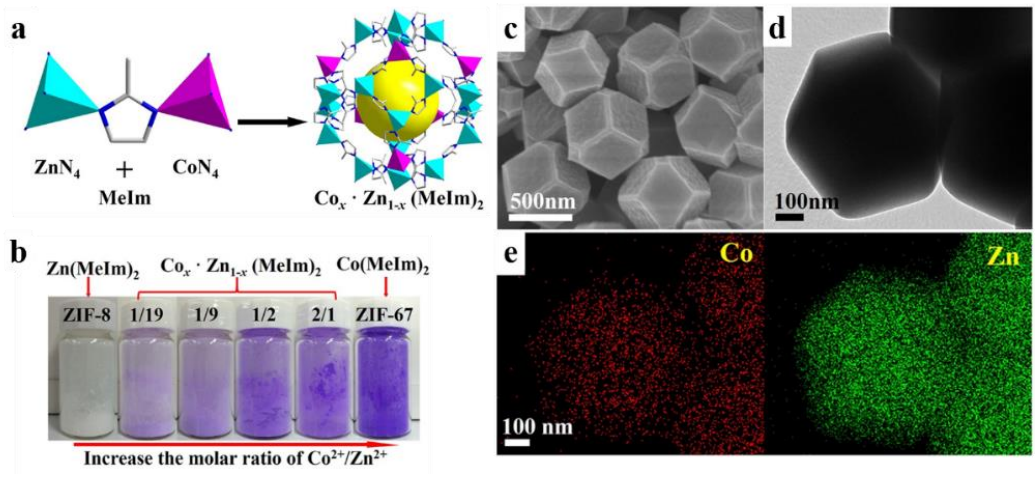

Figure 2-3. (**a**) Schematic illustration of the crystal structure of the bimetallic ZIFs ($Co_x{\cdot}Zn_{1-x}(MeIm)_2$). (**b**) Photograph of ZIF-8, ZIF-67 and the bimetallic ZIF ($Co_x{\cdot}Zn_{1-x}(MeIm)_2$) crystals. The initial molar ratios of Co^{2+}/Zn^{2+} for the synthesis of each bimetallic ZIF is shown on top of the bottles in the form of an irreducible fraction. (**c**) TEM image, (**d**) elemental mapping and (**e**) SEM image of the $Co_{0.1}{\cdot}Zn_{0.9}(MeIm)_2$. Reprinted with the permission from ref.[99]

2.4.2.3 MOF pyrolysis derivates

Recently, MOFs have been widely studied as an emerging kind of templates or precursors to obtain novel catalysts owing to their fascinating topologies and tunable structure and composition. The thermal treatment of MOFs is expected to generate metal oxides upon annealing in air. Moreover, carbon-metal/metal oxide hybrids and porous carbon materials can be fabricated under inert atmosphere because of the abundant content of carbon in the organic linkers. Furthermore, carbonization of some MOFs under inert atmosphere would produce novel metal species (metal carbide and nitride) embedded in the carbon matrix, exerting exceptional catalytic performance.

Since nanoporous metal species are especially appealing because of their broad applications including energy storage and heterogeneous catalysis, the rational design of MOFs-derived catalysts is in the spotlight of research.

Carbon-metal or metal oxide (C-M/MO) hybrids are of great importance in the fields of heterogenous catalysis. Traditionally, the hybrids can be fabricated by direct nucleation, growth, and anchoring of metal oxides on the carbon materials. During the last decade, MOFs have gained wide popularity as the unique templates for preparation of the composites. Apart from forming the carbon matrix, the organic ligands in MOFs also act as reducing agents to reduce the metal ions with redox potential higher than - plays two important roles in the -0.27 V (eg. Co, Ni and Cu) during thermolysis process in N_2.[103] Cu-BTC MOF, also known as HKUST-1 or MOF-199, was applied as the template to fabricate Cu/nanoporous carbon composites.[104-106] Well-defined Cu nanoparticles embedded in the porous carbon matrix was achieved under direct carbonization in N_2 atmosphere at 400-800 °C. Moreover, the resultant Cu@C inherited the original morphology of HKUST-1 with a surface area of up to1025 cm^{-3} g^{-1}.[104] However, higher carbonization temperature will lead to a reduction of surface area and porosity, due to the increasing graphitization degree of formed carbon matrix.[106] The metal carbide can also be realized using the MOF mediated synthesis route. Santos *et al.* developed a facile method to fabricate Fe@C composites with tunable Fe content.[107] They firstly impregnated Basolite F300 (Fe-BTC MOF) with furfuryl alcohol (FA) to modify the Fe/C ratio in the MOF precursor by incipient wetness impregnation, followed by thermolysis under N_2 atmosphere. The obtained Fe@C presented abundant Fe_3C species and high incorporation of homogeneously dispersed active ion phase in the carbon matrix.[107] Li, Zhang and co-workers developed a cage-confinement method to prepare ultrasmall tungsten carbide (ca. 2 nm) encapsulated in porous carbon.[108] They firstly trapped an organic tungsten species ($W(CO)_6$) in a zeolitic metal-zaolate framework (RHO-[$Zn(Meim)_2$], also called MAF-6) through a vapor adsorption treatment to synthesize the $W(CO)_6$ @ MAF-6 composite. The postsynthetic installation method ensures the uniformly dispersion and

isolation of $W(CO)_6$ in the MAF-6 cavities. Therefore, during the heating process under 980 °C and N_2 atmosphere, the well-confined and isolated $W(CO)_6$ molecules in the MAF-6 pore structures was decomposed to form reactive W atoms, which easily bonded with carbon atoms from the MAF-6, inducing the formation of ultrasmall WC without any aggregation.

Although carbon-metal/metal oxides hybrids are quite fascinating in morphology control and porosity, metal oxides, especially mixed metal oxides (MMO) are commonly adopted in most applications, especially for these reaction systems where strong metal-support interaction (SMSI) is vital. The SMSI effect is an important feature in solid-gas phase reactions to define the performance of catalysts. The tunable MOFs microenvironment has offered new opportunities to build porous catalysts with strong SMSI. Yang *et al*. developed IrO_2/CuO by annealing the Ir NPs@Cu-BTC composite directly in air under 500 °C.[109] The formed IrO_2 displayed high dispersion around the CuO particles and stronger interaction between IrO_2 and CuO than its counterpart prepared from conventional impregnation method. However, Cu-BTC underwent complete decomposition at about 350 ˚C and the framework collapsed simultaneously. As a result, the prepared IrO_2/CuO failed to inherit the octahedral morphology of the Cu-BTC precursor. To retain the structural properties of MOFs precursor, Wu *et al.* firstly adopted a two-step pyrolysis protocol.[110] A series of Zn-Co-ZIFs with different Co/Zn ratios were firstly synthesized through co-precipitation of zinc and cobalt precursors in the presence of 2-methylimidazole. The first pyrolysis in N_2 was found to be essential because the generated carbon matrix would prevent total collapse of ZIFs during this process, inducing well-preserved ZIFs framework. The second pyrolysis in air would remove the carbon matrix without jeopardizing the morphology properties. The selected area electron diffraction (SAED) results clearly revealed the incorporation of Zn atoms into the Co_3O_4 lattice, forming polycrystalline texture of $Zn_xCo_{3-x}O_4$. Wang *et al.* developed core-shell ZnO@ Co_3O_4 polyhedrons by a two-step thermolysis of ZIF-8@ZIF-67.[111] The high porosity and order structure derived from the special pyrolysis procedure brought about the superior photocatalytic

activity for CO_2 photoreduction. Following this strategy, Liu *et al.* succeeded in the development of dodecahedral $NiCo_2O_4$ and $NiCo_2S_4$ through calcination of bimetallic NiCo-ZIF.[112]

2.4.3 Applications of MOFs based catalyst for heterogeneous catalysis

2.4.3.1 Fischer-Tropsch synthesis (FTS)

Gascon's group did extensive investigations on the applications of MOF derived catalysts for industrial process, especially FTS.[107, 113-118] They reported the first trial to prepare Fe sites embedded in the porous carbon via the MOF-mediated synthesis (MOFMS) strategy in 2015.[107] The template Fe-MOF Basolite F300 (Fe(BTC), $C_9H_3FeO_6$; BTC = 1,3,5- benzenetricarboxylate), loaded with furfuryl alcohol and potassium promoter, was pyrolyzed under N_2 atmosphere to prepare Fe@C with different Fe to C ratios and K loadings. Through this strategy, very high loading of Fe (25-38 *wt*%) was realized in the prepared Fe@C catalysts together with high specific surface area and nanosized Fe nanoparticles (2.5-3.6 nm) embedded in the porous carbon matrix. More importantly, the high dispersion of Fe NPs in the Fe@C catalysts allowed excellent accessibility of Fe sites to syngas, thus favoring the production of χ-Fe_2C_5 sites, which is the most active phase for FTS. Tested under FTS reaction at 613K, 20 bar and a H_2 to CO ratio of 1, all the four MOF derived catalysts exhibited high CO conversion of 59-72 %, and the activity per gram of Fe (FTY) over 0.6K38-Fe@C reached up to 0.438 mmol g_{Fe}^{-1} s^{-1}, nearly two orders of magnitude more active than the commercial counterpart Ruhrchemie catalyst. Additionally, the Fe phase in prepared Fe@C catalysts can be easily tuned by changing the calcination temperature, as confirmed by in situ and ex-situ experiments.[113] Under pyrolysis temperature near 450 °C, FeO was the dominant phase (73%) in the formed catalyst with 27% of Fe_xC species. When the temperature raised to 600 °C, the Fe@C-600 consisted of 75% Fe^0 and 25% Fe_xC. Upon the exposure of syngas of 5 h under FT conditions, the catalyst pyrolyzed under 450 °C demonstrated 53% of ε'-$Fe_{2.2}C$ and 47% of FeO, whereas the

Fe@C-600 transformed to 67% of χ-Fe_2C_5 and 27% of ε'-$Fe_{2.2}C$. The obtained catalysts Fe@C-400, Fe@C-500 and Fe@C-600 exhibited very high FTS activity with CO conversion of 74%-76% and FTY of 0.31-0.38 mmol g_{Fe}^{-1} s^{-1}. Moreover, the formation of χ-Fe_2C_5 in the Fe@C-600 improved the chain growth probability α and suppressed the CH_4 formation. However, when the annealed temperature reached up to 900 °C, the nature of Fe in the obtained Fe@C-900 completely converted to θ-Fe_3C, which was less active in the FTS conditions.

In addition to Fe-based MOF, Co-based MOFs have also been investigated as the scaffold for the preparation of highly active catalyst for F-T process. To elucidate the effect of pore structure and compositional property, two Co-based MOFs, ZIF-67 with abundant N species and Co-MOF-74 without N, were selected as the template to prepare Co embedded carbon catalyst for F-T reaction.[119] The resultant Co@C catalyst from pyrolysis of Co-MOF-74 exhibited higher activity for long-chain hydrocarbons production and lower deterioration rate than Co@NC derived from ZIF-67. Such a good performance is sourced from the large pore size of Co@C facilitating the mass diffusion of products. The particle size and crystal phase can also be tuned by ethyne assisted reduction of Co-MOF-74 under different temperatures.[120] As the temperature increased from 400 to 600 °C, the formed carbon shell transformed from amorphous state to graphene, and phase of Co^0 changed from *hcp* to *fcc*. Compared with the direct annealing of Co-MOF-74, this approach promised smaller Co^0 particles embedded in the porous graphene matrix and high capability towards long-chain hydrocarbons formation. Additionally, doping Si in the parent MOF, i.e.Co-MOF-71 and ZIF-67, can further tailor the pore texture and phase properties of the final catalysts, significantly altering the performance for F-T reaction.[115, 121]

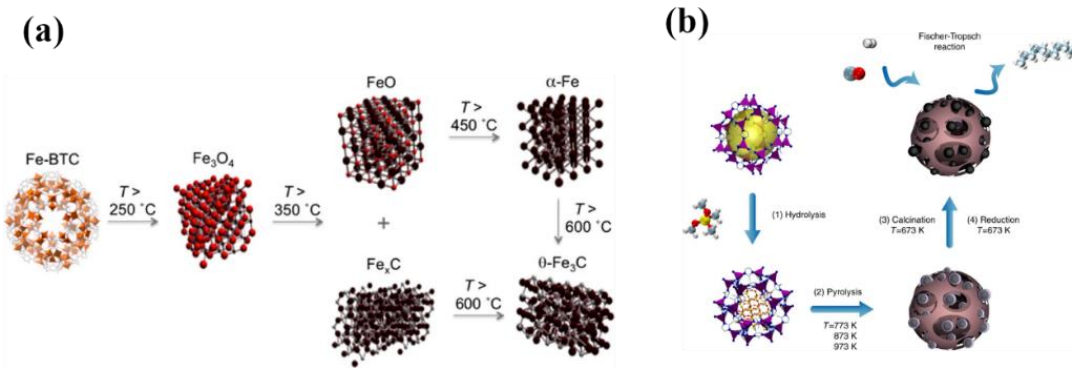

Figure 2-4. **(a)** Phase transformation of formed Fe species during pyrolysis of Fe-BTC MOF to Fe@C. Reprinted with permission from ref.[113] **(b)** Schematic illustration of the synthesis of the Co@SiO_2 catalysts via TMOS impregnation, pyrolysis in N_2 to form Co@C-SiO_2, further calcination of the Co@C-SiO_2 in air for carbon removal and reduction of the Co@SiO_2 in H_2 to produce metallic Co for Fischer–Tropsch synthesis. Reprinted with permission from ref.[115]

2.4.3.2 Alcohol synthesis from CO/CO_2 hydrogenation

The metal SBUs in MOF framework can also promise a valid metal-support interaction for methanol formation. Fischer's group reported the first trial of methanol production from syngas over a Cu loaded MOF-5 with a Zn_4O building block.[122] Prepared by chemical vapor deposition (CVD) method, the as-prepared Cu@MOF-5 with loading performed 70 $umol_{MeOH}g_{cat}^{-1}h^{-1}$ (220 °C), which is comparable to that of Cu/ZnO@MCM-41/48. They further developed a doubly-loaded Cu/ZnO@MOF-5 with higher initial activity of 212 $umol_{MeOH}g_{cat}^{-1}h^{-1}$ (220 °C).[123] However, this material quickly deactivated after several hours, due to the poor thermal resistance of MOF-5 framework.

Apparently, a robust MOF is more favorable to justify an industrial implementation. Zr-MOFs have been widely reported for exceptional thermal and chemical stability.[124] The most popular Zr-MOFs, UiO-66 with BDC linkers and UiO-67 with BPDC linkers, which comprise $Zr_6O_4(OH)_4$ building blocks, can retain intact morphology under up

to 500 °C. Since Cu/ZrO_2 interface is also important for methanol formation, Zr-MOFs open up new opportunities to combine the confinement influence and the SMSI effect between Cu and ZrO_x species. Yaghiand co-workers constructed a core-shell structure MOF catalyst via incorporation of Cu nanoparticles in the UiO-66 framework.[125] Applied to CO_2 hydrogenation, the obtained catalyst gave a high TOF of methanol formation (0.023 s^{-1}) at 200 °C. Wang *et al.* further improved the catalytic performance through anchoring ultrasmall Cu/ZnO_x nanoparticles in the UiO-bpy MOF cavities by *in situ* reduction of preanchored Cu and Zn centers and obtained a space-time-yield of up to 2.59 g_{MeOH} $kg_{Cu}^{-1}h^{-1}$.[126] Both designed catalysts achieved 100 % selectivity to methanol, much higher than the state of art of Cu/ZnO/Al_2O_3. X-ray photoelectron spectroscopy (XPS) probed partial reduction of Zr (IV) to Zr (III) in the spent catalyst, indicative a strong metal-support interaction between Cu and Zr species. These observations confirm that the metal oxide SBUs in the MOF backbones can also render similar SMSI as observed in the bulk ZrO_2.

Application of MOF catalyst for higher alcohols synthesis has been rarely reported. Spivey and co-workers prepared the potassium promoted cobalt-based catalysts from a Co-MOF (ZIF-67) and then tested it for higher oxygenates synthesis.[127] Their results demonstrated that the cobalt oxide skeleton along with the carbon-rich environment via pyrolysis of ZIF-67 gave rise to the increased selectivity to C_{2+} oxygenates due to the highly dispersed Co nanoparticles and formation of Co_2C species. Unfortunately, no well-defined structure could be preserved with direct calcination of ZIF-67 under air in this sample.

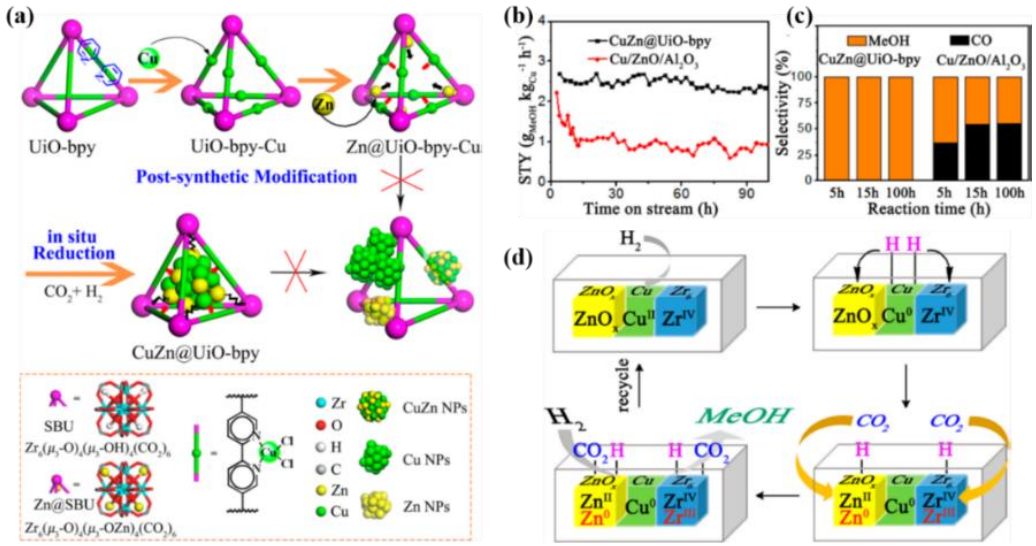

Figure 2-5. **(a)** Preparation of CuZn@UiO-bpy via in Situ Reduction of Post-Synthetically Metalated UiO-bpy: Cu^{2+} ions were coordinated to the bpy groups, while Zn^{2+} ions were attached to the SBUs. **(b)** STY of MeOH vs reaction time over a period of 100 h on stream. **(c)** Selectivity of product vs reaction time. **(d)** Schematic showing the encapsulated active sites in MOFs and the functions of the various surface sites in catalytic CO_2 hydrogenation. Reprinted with permission from ref. [126]

2.4.3.3 CO oxidation reaction

CO in automotive exhaust gas and H_2 stream for polymer fuel cells brings both environmental problems and industrial impediment. Thus, CO oxidation reaction is of great significance to remove this pollutant. Noble metals, such as Pt, Pd, Au, are found to be exceptionally active for this process. To minimize the cost, the metal nanoparticles are usually dispersed on a support material with high surface area. MOFs proved to be a very promising candidate as the catalyst support, as the high porosity and surface area can enhance the exposure of active sites to CO molecules. Xu *et al.* reported the first application of ZIF-8 supported Au nanoparticles (NPs) for CO oxidation.[128] By a facile solid grinding method, monodispersed Au NPs in the crystalline structure of ZIF-8 was achieved, exhibiting nearly 100 % conversion of CO

under 300 °C. Notably, the pore structure of different MOFs would affect the gas diffusion rate and the consequent catalytic performance. For example, UiO-66 has larger pore aperture (6 Å) than ZIF-8 (3.4 Å). When both MOFs were applied to accommodate the Pt NPs, the Pt/UiO-66 composite demonstrated higher CO conversion than Pt/ZIF-8 at 180 °C.[82] Cr-MOF (MIL-101), the mesoporous MOF with hierarchical pore structure, can be used to accommodate Pd-Cu bimetallic NPs of 2-3 nm for efficient CO conversion.[129] Yaghi's group successfully anchored single Cu atoms to the defect site in UiO-66.[130] Although Cu is believed to have inferior performance than noble metal element, this catalyst still exhibited high activity and stability for CO oxidation, owing to the atomically dispersed Cu sites in the well-defined structure of UiO-66. Noteworthy that the incorporation of metal NPs in MOF requires high thermal stability of the chosen MOFs material. Thus, it is very important to choose the right MOFs as the support for this process.

Compared with the encapsulation method, the MOF mediated synthesis route is more versatile, especially for developing active non-noble metal catalyst. Li *et al*. developed nanosized Co_3O_4 catalyst through pyrolysis of Co impregnated ZIF-8 and removal of ZnO, and applied this catalyst for CO oxidation under H_2-rich atmosphere.[131] Compared with the direct thermolysis of Co-MOF, this method immobilizes Co in the pores of ZIF-8 and prevents the cobalt migration or aggregation during pyrolysis process, resulting in excellent catalyst distribution for subsequent outstanding catalytic activity and stability. HKUST-1 is also a good candidate as the matrix to prepare copper-based catalyst.[132, 133] A novel CuO/CeO_2 catalyst prepared by pyrolysis of Ce impregnated HKUST-1 outperformed its counterpart synthesized through loading Cu ions on the CeO_2 support.[132] This is because the HKUST-1 can well separate the metal ions, suppress the particle accretion, and enhance the interactions between CuO and CeO_2, all of which are indispensable factors for high catalytic activity.

2.4.3.4 Methanol synthesis from methane oxidation

The direct conversion of methane to value-added products is a very appealing route due to the abundant reserves of natural gas, coal and shale gas. Particularly, methanol synthesis from methane oxidation process has been attractive in recent years. Currently, methanol is massively produced through two separate processes; methane is firstly converted to syngas and then syngas undergoes hydrogenation to produce methanol. The direct conversion of methane to methanol is thus of great economic potential.

A Cu modulated NU-1000 (Zr-MOF) was investigated to catalyze methane conversion to methanol. The copper sites were firmly immobilized in the NU-1000 structure by bridging two ZrO_2 nodes to form a Cu-hydroxide-like structure.[134] Applied for methane oxidation, this catalyst displayed a carbon selectivity of 45-60% to methanol, elucidating the potential of MOF-based catalyst for this reaction. A novel enzyme-like catalyst was also successfully developed *via* installing biologically relevant imidazole ligands in the porous structure of MOF-808 and subsequent metalation to incorporate Cu-O complexes in the framework; the resultant catalyst displayed high selectivity and recyclability towards methanol formation.[135] Similarly, the di-iron clusters confined in the MIL-53(Al, Fe) has also been reported to be active for methane oxidation to methanol with H_2O_2, owing to the formation of isolated Fe-(μ-O)-Fe dimers to efficiently activate the C-H bond in CH_4.[136] Rui *et al*. developed hybrid oxide IrO_2/CuO by annealing of Ir@Cu-BTC composite in air.[109] This catalyst exhibited higher methanol production capability compared to the corresponding counterpart synthesized by conventional impregnation method. The strong interaction between IrO_2 and CuO suppressed the unfavorable IrO_2 particle growth but increased the homogeneity of IrO_2 distribution on CuO, thus providing the synergism for C-H bond cleavage and CH_3-O bond construction.

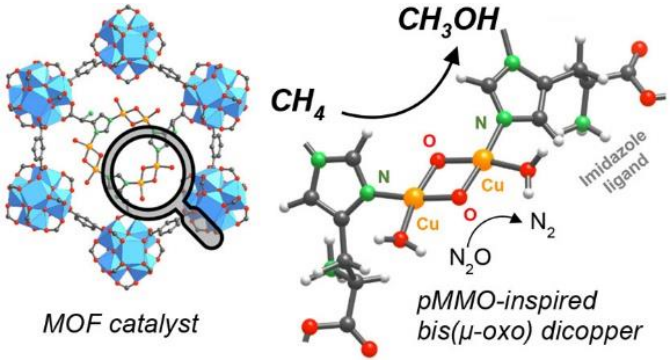

Figure 2-6. Design and synthesis of the catalysts bearing copper–oxygen complexes in MOF-808 for methane oxidation to methanol. Reprinted with permission from ref.[135]

2.5 MOFs-based Catalyst opportunities for oxygenates synthesis from syngas

The issues of rapid diminishing petroleum reserves and the increasing awareness for environmental conservation have triggered the urgent demand in seeking cleaner and more sustainable energy resources. Fischer-Tropsch (F-T) process provides a very promising route to convert methane-rich feedstocks (i.e. natural gas, coal and biomass) into diverse commodity chemicals via the syngas (a mixture of H_2 and CO) intermediate. Among all the F-T products, higher oxygenates, *e.g.* DME and higher alcohols, show great potential as the alternative energy source owing to their vast applications including fuel additives, hydrogen carriers or precursors for major platform chemicals. However, the STD and HAS reactions suffer from low yields and poor selectivity towards the targeted oxygenates, and thus significantly impede their industrial applications. The conventional catalyst preparation strategies cannot obtain the catalyst uniform distribution and fail to provide sufficient proximity of cooperative active sites for the tandem catalysis to produce oxygenates. As a result, it is highly imperative to develop a rational strategy to accurately control the dispersion of active sites and preserve their necessary proximity.

As a new type of porous materials, MOFs have received tremendous research interests for heterogeneous catalysis, especially for solid-gas phase reactions. Firstly, the ample micropores and mesopores inside the framework and the broad outer surface of MOFs can accommodate different types of active centers in a single MOF crystal, which can obtain close affinity with remaining compositional and structural properties. Secondly, the heterometallic MOFs can render well-isolated metal sites by the organic ligands. Thirdly, some MOFs possess metal oxide secondary building units (SBU), such as MOF-5 (Zn-MOF) and UiO-66 (Zr-MOF). These SBUs can give similar SMSI effect with Cu as the traditional ZnO and ZrO_2. Finally, pyrolysis of MOFs can generate active metallic catalysts (metal/metal oxide/metal carbide) ideally with the preserved MOF topologies and porosities. These derivates can show great potential for syngas adsorption and conversion.

2.6 Conclusion

Developing efficient catalysts with high activity, ideal products selectivity as well as excellent stability under moderate reaction conditions is a highly pursued goal for organic oxygenates (DME, higher alcohols, *etc.*) synthesis from syngas. In this chapter, reaction mechanisms and active centers for DME and HAS have been reviewed and assessed to identify the critical factors for effective catalyst development in both processes. This chapter also introduces the novel metal-organic frameworks (MOFs)-based catalysts and their potential application in solid-gas phase reactions. It was found that the improvement of active sites distribution and proximity of different functional groups are vital for enhanced selectivity and yield towards DME and higher alcohols formation. While some progress has been done accordingly, the current catalyst systems are still insufficient to justify the industrial application. Compared with the traditional catalysts, the MOFs-based catalysts are very promising for syngas conversion to DME and higher alcohols. Therefore, systematic experiment processes for the development of novel MOFs-based catalysts are required to improve the

corresponding performance in DME and higher alcohols synthesis. Since there have been very limited reports about MOFs-based catalysts for this process, the objective of this study is to provide a pioneering investigation which can offer guidance on the development of MOFs-derived catalysts for the direct oxygenates production from syngas.

References

1. Saidur, R.; Abdelaziz, E.; Demirbas, A.; Hossain, M.; Mekhilef, S., A review on biomass as a fuel for boilers. *Renew. Sust. Energ. Rev.* **2011,** *15* (5), 2262-2289.

2. Semelsberger, T. A.; Borup, R. L.; Greene, H. L., Dimethyl ether (DME) as an alternative fuel. *J. Power Sources* **2006,** *156* (2), 497-511.

3. Trippe, F.; Fröhling, M.; Schultmann, F.; Stahl, R.; Henrich, E.; Dalai, A., Comprehensive techno-economic assessment of dimethyl ether (DME) synthesis and Fischer–Tropsch synthesis as alternative process steps within biomass-to-liquid production. *Fuel Process. Technol.* **2013,** *106*, 577-586.

4. Zhang, P.; Tan, L.; Yang, G.; Tsubaki, N., One-pass selective conversion of syngas to para-xylene. *Chem. Sci.* **2017,** *8* (12), 7941-7946.

5. Kasipandi, S.; Bae, J. W., Recent Advances in Direct Synthesis of Value-Added Aromatic Chemicals from Syngas by Cascade Reactions over Bifunctional Catalysts. *Adv. Mater.* **2019**, 1803390.

6. Cho, J. M.; Lee, S. R.; Sun, J.; Tsubaki, N.; Jang, E. J.; Bae, J. W., Highly ordered mesoporous Fe_2O_3–ZrO_2 bimetal oxides for an enhanced CO hydrogenation activity to hydrocarbons with their structural stability. *ACS Catal.* **2017,** *7* (9), 5955-5964.

7. Cheng, K.; Zhou, W.; Kang, J.; He, S.; Shi, S.; Zhang, Q.; Pan, Y.; Wen, W.; Wang, Y., Bifunctional catalysts for one-step conversion of syngas into aromatics with excellent selectivity and stability. *Chem* **2017,** *3* (2), 334-347.

8. Zhao, B.; Zhai, P.; Wang, P.; Li, J.; Li, T.; Peng, M.; Zhao, M.; Hu, G.; Yang, Y.; Li, Y.-W., Direct Transformation of Syngas to Aromatics over Na-Zn-Fe_5C_2 and Hierarchical HZSM-5

Tandem Catalysts. *Chem* **2017,** *3* (2), 323-333.

9. Huang, Z.; Wang, S.; Qin, F.; Huang, L.; Yue, Y. H.; Hua, W. M.; Qiao, M. H.; He, H. Y.; Shen, W.; Xu, H. L., Ceria-Zirconia/Zeolite Bifunctional Catalyst for Highly Selective Conversion of Syngas into Aromatics. *Chemcatchem* **2018,** *10* (20), 4519-4524.

10. Sun, J.; Yang, G.; Yoneyama, Y.; Tsubaki, N., Catalysis chemistry of dimethyl ether synthesis. *ACS Catal.* **2014,** *4* (10), 3346-3356.

11. Raoof, F.; Taghizadeh, M.; Eliassi, A.; Yaripour, F., Effects of temperature and feed composition on catalytic dehydration of methanol to dimethyl ether over γ-alumina. *Fuel* **2008,** *87* (13), 2967-2971.

12. Takeishi, K., Dimethyl ether and catalyst development for production from syngas. *Biofuels* **2010,** *1* (1), 217-226.

13. Park, S.; Kim, H.; Choi, B., Effective parameters for DME steam reforming catalysts for the formation of H_2 and CO. *J. Ind. Eng. Chem.* **2010,** *16* (5), 734-740.

14. Wang, Y.; Chen, Y.; Yu, F.; Pan, D.; Fan, B.; Ma, J.; Li, R., One-step synthesis of dimethyl ether from syngas on ordered mesoporous copper incorporated alumina. *J. Energy Chem.* **2016,** *25* (5), 775-781.

15. Good, D.; Francisco, J.; Jain, A.; Wuebbles, D., Lifetimes and global warming potentials for dimethyl ether and for fluorinated ethers: CH_3OCF_3 (E143a), CHF_2OCHF_2 (E134), CHF_2OCF_3 (E125). *J. Geophys. Res.: Atmos.* **1998,** *103* (D21), 28181-28186.

16. Sofianos, A. C.; Scurrell, M. S., Conversion of synthesis gas to dimethyl ether over bifunctional catalytic systems. *Ind. Eng. Chem. Res.* **1991,** *30* (11), 2372-2378.

17. Cheung, P.; Bhan, A.; Sunley, G. J.; Iglesia, E., Selective carbonylation of dimethyl ether to methyl acetate catalyzed by acidic zeolites. *Angew. Chem. Int. Ed.* **2006,** *45* (10), 1617-1620.

18. Liu, H.; Cheung, P.; Iglesia, E., Structure and support effects on the selective oxidation of dimethyl ether to formaldehyde catalyzed by MoO_x domains. *J. Catal.* **2003,** *217* (1), 222-232.

19. Gayubo, A. G.; Vicente, J.; Ereña, J.; Oar-Arteta, L.; Azkoiti, M. J.; Olazar, M.; Bilbao, J., Causes of deactivation of bifunctional catalysts made up of CuO-ZnO-Al_2O_3 and desilicated HZSM-5 zeolite in DME steam reforming. *Appl. Catal. A-Gen.* **2014,** *483*, 76-84.

20. Asthana, S.; Samanta, C.; Bhaumik, A.; Banerjee, B.; Voolapalli, R. K.; Saha, B., Direct

synthesis of dimethyl ether from syngas over Cu-based catalysts: Enhanced selectivity in the presence of MgO. *J. Catal.* **2016,** *334*, 89-101.

21. Hadipour, A.; Sohrabi, M., Synthesis of some bifunctional catalysts and determination of kinetic parameters for direct conversion of syngas to dimethyl ether. *Chem. Eng. J.* **2008,** *137* (2), 294-301.

22. Xiaoding, X.; Doesburg, E. B. M.; Scholten, J. J. F., Synthesis of higher alcohols from syngas - recently patented catalysts and tentative ideas on the mechanism. *Catal. Today* **1987,** *2* (1), 125-170.

23. Ao, M.; Pham, G. H.; Sunarso, J.; Tade, M. O.; Liu, S., Active Centers of Catalysts for Higher Alcohol Synthesis from Syngas: A Review. *ACS Catal.* **2018,** *8* (8), 7025-7050.

24. Garcia-Trenco, A.; White, E. R.; Shaffer, M. S. P.; Williams, C. K., A one-step Cu/ZnO quasi-homogeneous catalyst for DME production from syn-gas. *Catal. Sci. Technol.* **2016,** *6* (12), 4389-4397.

25. Behrens, M.; Studt, F.; Kasatkin, I.; Kühl, S.; Hävecker, M.; Abild-Pedersen, F.; Zander, S.; Girgsdies, F.; Kurr, P.; Kniep, B.-L., The active site of methanol synthesis over $Cu/ZnO/Al_2O_3$ industrial catalysts. *Science* **2012,** *336* (6083), 893-897.

26. Liu, R.-w.; Qin, Z.-z.; Ji, H.-b.; Su, T.-m., Synthesis of dimethyl ether from CO_2 and H_2 using a Cu–Fe–Zr/HZSM-5 catalyst system. *Ind. Eng. Chem. Res.* **2013,** *52* (47), 16648-16655.

27. Flores, J. H.; Solórzano, G.; da Silva, M. I. P., Effect of aluminum on the morphological and textural properties of CuO–ZnO/H-Ferrierite. *Appl. Surf. Sci.* **2008,** *254* (20), 6461-6466.

28. Waller, D.; Stirling, D.; Stone, F. S.; Spencer, M. S., Copper–zinc oxide catalysts. Activity in relation to precursor structure and morphology. *Faraday Discuss. Chem. Soc.* **1989,** *87*, 107-120.

29. Qin, Z. z.; Su, T. m.; Ji, H. b.; Jiang, Y. x.; Liu, R. w.; Chen, J. h., Experimental and theoretical study of the intrinsic kinetics for dimethyl ether synthesis from CO_2 over Cu–Fe–Zr/HZSM-5. *AlChE J.* **2015,** *61* (5), 1613-1627.

30. Sun, K.; Lu, W.; Qiu, F.; Liu, S.; Xu, X., Direct synthesis of DME over bifunctional catalyst: surface properties and catalytic performance. *Appl. Catal. A-Gen.* **2003,** *252* (2), 243-249.

31. Bae, J. W.; Kang, S.-H.; Lee, Y.-J.; Jun, K.-W., Effect of precipitants during the preparation of Cu-ZnO-Al_2O_3/Zr-ferrierite catalyst on the DME synthesis from syngas. *J. Ind. Eng. Chem.*

2009, *15* (4), 566-572.

32. Bayat, A.; Dogu, T., Optimization of CO_2/CO Ratio and Temperature for Dimethyl Ether Synthesis from Syngas over a New Bifunctional Catalyst Pair Containing Heteropolyacid Impregnated Mesoporous Alumina. *Ind. Eng. Chem. Res.* **2016,** *55* (44), 11431-11439.

33. Erena, J.; Garoña, R.; Arandes, J. M.; Aguayo, A. T.; Bilbao, J., Effect of operating conditions on the synthesis of dimethyl ether over a CuO-ZnO-Al_2O_3/NaHZSM-5 bifunctional catalyst. *Catal. Today* **2005,** *107*, 467-473.

34. Ereña, J.; Sierra, I.; Olazar, M.; Gayubo, A. G.; Aguayo, A. T., Deactivation of a CuO− ZnO− Al_2O_3/γ-Al_2O_3 Catalyst in the Synthesis of Dimethyl Ether. *Ind. Eng. Chem. Res.* **2008,** *47* (7), 2238-2247.

35. Aguayo, A. T.; Ereña, J.; Sierra, I.; Olazar, M.; Bilbao, J., Deactivation and regeneration of hybrid catalysts in the single-step synthesis of dimethyl ether from syngas and CO_2. *Catal. Today* **2005,** *106* (1), 265-270.

36. Yang, Q.; Kong, M.; Fan, Z.; Meng, X.; Fei, J.; Xiao, F.-S., Aluminum Fluoride Modified HZSM-5 Zeolite with Superior Performance in Synthesis of Dimethyl Ether from Methanol. *Energy Fuels* **2012,** *26* (7), 4475-4480.

37. Sung, D. M.; Kim, Y. H.; Park, E. D.; Yie, J. E., Role of surface hydrophilicity of alumina in methanol dehydration. *Catal. Commun.* **2012,** *20*, 63-67.

38. Wang, Y. F.; Liu, H. W.; Zhang, H. T.; Ying, W. Y., Ta_2O_5 modified gamma-Al_2O_3 as a methanol dehydration component in the single-step synthesis of dimethyl ether from syngas. *React. Kinet. Mech. Catal.* **2016,** *119* (2), 585-594.

39. Yaripour, F.; Baghaei, F.; Schmidt, I.; Perregaard, J., Catalytic dehydration of methanol to dimethyl ether (DME) over solid-acid catalysts. *Catal. Commun.* **2005,** *6* (2), 147-152.

40. Xu, M.; Lunsford, J. H.; Goodman, D. W.; Bhattacharyya, A., Synthesis of dimethyl ether (DME) from methanol over solid-acid catalysts. *Appl. Catal. A-Gen.* **1997,** *149* (2), 289-301.

41. Yaripour, F.; Mollavali, M.; Jam, S. M.; Atashi, H., Catalytic dehydration of methanol to dimethyl ether catalyzed by aluminum phosphate catalysts. *Energy Fuels* **2009,** *23* (4), 1896-1900.

42. Seo, C. W.; Jung, K. D.; Lee, K. Y.; Yoo, K. S., Influence of structure type of Al_2O_3 on dehydration of methanol for dimethyl ether synthesis. *Ind. Eng. Chem. Res.* **2008,** *47* (17),

6573-6578.

43. Okuhara, T.; Mizuno, N.; Misono, M., Catalysis by heteropoly compounds—recent developments. *Appl. Catal. A-Gen.* **2001,** *222* (1), 63-77.

44. Wang, Y.; Chen, Y. X.; Yu, F.; Pan, D. H.; Fan, B. B.; Ma, J. H.; Li, R. F., One-step synthesis of dimethyl ether from syngas on ordered mesoporous copper incorporated alumina. *J. Energy Chem.* **2016,** *25* (5), 775-781.

45. Jiang, H.; Bongard, H.; Schmidt, W.; Schüth, F., One-pot synthesis of mesoporous Cu–γ-Al_2O_3 as bifunctional catalyst for direct dimethyl ether synthesis. *Microporous Mesoporous Mater.* **2012,** *164*, 3-8.

46. Cai, M.; Palcic, A.; Subramanian, V.; Moldovan, S.; Ersen, O.; Valtchev, V.; Ordomsky, V. V.; Khodakov, A. Y., Direct dimethyl ether synthesis from syngas on copper-zeolite hybrid catalysts with a wide range of zeolite particle sizes. *J. Catal.* **2016,** *338*, 227-238.

47. Dadgar, F.; Myrstad, R.; Pfeifer, P.; Holmen, A.; Venvik, H. J., Catalyst Deactivation During One-Step Dimethyl Ether Synthesis from Synthesis Gas. *Catal. Lett.* **2017,** *147* (4), 865-879.

48. Ramos, F.; de Farias, A. D.; Borges, L. E. P.; Monteiro, J.; Fraga, M. A.; Sousa-Aguiar, E. F.; Appel, L. G., Role of dehydration catalyst acid properties on one-step DME synthesis over physical mixtures. *Catal. Today* **2005,** *101* (1), 39-44.

49. Chen, W.-H.; Lin, B.-J.; Lee, H.-M.; Huang, M.-H., One-step synthesis of dimethyl ether from the gas mixture containing CO_2 with high space velocity. *Appl. Energy* **2012,** *98*, 92-101.

50. García-Trenco, A.; Martínez, A., Direct synthesis of DME from syngas on hybrid CuZnAl/ZSM-5 catalysts: New insights into the role of zeolite acidity. *Appl. Catal. A-Gen.* **2012,** *411*, 170-179.

51. Jin, D.; Zhu, B.; Hou, Z.; Fei, J.; Lou, H.; Zheng, X., Dimethyl ether synthesis via methanol and syngas over rare earth metals modified zeolite Y and dual Cu–Mn–Zn catalysts. *Fuel* **2007,** *86* (17), 2707-2713.

52. Fei, J.; Hou, Z.; Zhu, B.; Lou, H.; Zheng, X., Synthesis of dimethyl ether (DME) on modified HY zeolite and modified HY zeolite-supported Cu–Mn–Zn catalysts. *Appl. Catal. A-Gen.* **2006,** *304*, 49-54.

53. Kochkin, Y. N.; Vlasenko, N. V.; Kasian, N. V.; Shvets, O. V., Effect of the Acidity of

Ca,H-Bea Zeolites on Their Catalytic Characteristics in the Dimethyl Ether Production from Methanol. *Theor. Exp. Chem.* **2015,** *51* (5), 327-332.

54. Mao, D.; Xia, J.; Chen, Q.; Lu, G., Highly effective conversion of syngas to dimethyl ether over the hybrid catalysts containing high-silica HMCM-22 zeolites. *Catal. Commun.* **2009,** *10* (5), 620-624.

55. Prasad, P. S.; Bae, J. W.; Kang, S.-H.; Lee, Y.-J.; Jun, K.-W., Single-step synthesis of DME from syngas on Cu–ZnO–Al_2O_3/zeolite bifunctional catalysts: the superiority of ferrierite over the other zeolites. *Fuel Process. Technol.* **2008,** *89* (12), 1281-1286.

56. Bandiera, J.; Naccache, C., Kinetics of methanol dehydration on dealuminated H-mordenite: Model with acid and basic active centres. *Appl. Catal.* **1991,** *69* (1), 139-148.

57. Yoo, K. S.; Kim, J.-H.; Park, M.-J.; Kim, S.-J.; Joo, O.-S.; Jung, K.-D., Influence of solid acid catalyst on DME production directly from synthesis gas over the admixed catalyst of Cu/ZnO/Al_2O_3 and various SAPO catalysts. *Appl. Catal. A-Gen.* **2007,** *330*, 57-62.

58. Ateka, A.; Sierra, I.; Ereña, J.; Bilbao, J.; Aguayo, A. T., Performance of CuO–ZnO–ZrO_2 and CuO–ZnO–MnO as metallic functions and SAPO-18 as acid function of the catalyst for the synthesis of DME co-feeding CO_2. *Fuel Process. Technol.* **2016,** *152*, 34-45.

59. Wei, Y.; de Jongh, P. E.; Bonati, M. L. M.; Law, D. J.; Sunley, G. J.; de Jong, K. P., Enhanced catalytic performance of zeolite ZSM-5 for conversion of methanol to dimethyl ether by combining alkaline treatment and partial activation. *Appl. Catal. A-Gen.* **2015,** *504*, 211-219.

60. Xu, Y.; Yang, P.; Zhang, H.; Deng, Z., Atomic layer deposition synthesis of alumina-modified SBA-15 and its catalytic reactivity toward methanol dehydration. *Synth. React. Inorg., Met.-Org., Nano-Met. Chem.* **2011,** *41* (8), 1033-1038.

61. Macina, D.; Piwowarska, Z.; Tarach, K.; Góra-Marek, K.; Ryczkowski, J.; Chmielarz, L., Mesoporous silica materials modified with alumina polycations as catalysts for the synthesis of dimethyl ether from methanol. *Mater. Res. Bull.* **2016,** *74*, 425-435.

62. Cruz-Rodríguez, K.; García-Alamilla, R.; Ramos-Galván, C. E.; Paraguay-Delgado, F.; Silva-Rodrigo, R.; Handy, B. E.; Robles-Andrade, S., Zirconium and phosphorous modified SBA-15: texture, enhanced acidity and methanol dehydration activity. *React. Kinet. Mech. Catal.* **2017,** *120* (1), 371-384.

63. Xiang, M.; Li, D.; Qi, H.; Li, W.; Zhong, B.; Sun, Y., Mixed alcohols synthesis from carbon monoxide hydrogenation over potassium promoted β-Mo_2C catalysts. *Catal. Lett.* **2007,** *86* (9), 1298-1303.

64. Liu, Y.; Murata, K.; Inaba, M.; Takahara, I.; Okabe, K. J. C. T., Synthesis of ethanol from syngas over Rh/$Ce_{1-x}Zr_xO_2$ catalysts. *Catal. Today* **2011,** *164* (1), 308-314.

65. Pei, Y.-P.; Liu, J.-X.; Zhao, Y.-H.; Ding, Y.-J.; Liu, T.; Dong, W.-D.; Zhu, H.-J.; Su, H.-Y.; Yan, L.; Li, J.-L., High alcohols synthesis via Fischer–Tropsch reaction at cobalt metal/carbide interface. *ACS Catal.* **2015,** *5* (6), 3620-3624.

66. Zhao, Z.; Lu, W.; Yang, R.; Zhu, H.; Dong, W.; Sun, F.; Jiang, Z.; Lyu, Y.; Liu, T.; Du, H., Insight into the formation of Co@Co_2C catalysts for direct synthesis of higher alcohols and olefins from syngas. *ACS Catal.* **2017,** *8* (1), 228-241.

67. Hindermann, J. P.; Hutchings, G. J.; Kiennemann, A. J. C. R.-s., Mechanistic Aspects of the Formation of Hydrocarbons and Alcohols from CO Hydrogenation. *Catal. Rev. Sci. Eng.* **1993,** *35* (1), 1-127.

68. Liakakou, E.; Heracleous, E.; Triantafyllidis, K.; Lemonidou, A., K-promoted NiMo catalysts supported on activated carbon for the hydrogenation reaction of CO to higher alcohols: Effect of support and active metal. *Appl. Catal. B-Environ.* **2015,** *165*, 296-305.

69. Wang, N.; Fang, K.; Lin, M.; Jiang, D.; Li, D.; Sun, Y. J. C. L., Synthesis of Higher Alcohols from Syngas over Fe/K/β-Mo_2C Catalyst. *Catal. Lett.* **2010,** *136* (1), 9-13.

70. Kiai, R. M.; Nematian, T.; Tavasoli, A.; Karimi, A., Effect of elemental molar ratio on the synthesis of higher alcohols over Co-promoted alkali-modified Mo_2C catalysts supported on CNTs. *J. Energy Chem.* **2015,** *24* (3), 278-284.

71. Zhao, L.; Fang, K.; Jiang, D.; Li, D.; Sun, Y., Sol–gel derived Ni–Mo bimetallic carbide catalysts and their performance for CO hydrogenation. *Catal. Today* **2010,** *158* (3), 490-495.

72. Lu, Y.; Zhang, R.; Cao, B.; Ge, B.; Tao, F. F.; Shan, J.; Nguyen, L.; Bao, Z.; Wu, T.; Pote, J. W., Elucidating the Copper–Hägg Iron Carbide Synergistic Interactions for Selective CO Hydrogenation to Higher Alcohols. *ACS Catal.* **2017,** *7* (8), 5500-5512.

73. Li, Y.; Gao, W.; Peng, M.; Zhang, J.; Sun, J.; Xu, Y.; Hong, S.; Liu, X.; Liu, X.; Wei, M.; Zhang, B.; Ma, D., Interfacial Fe_5C_2-Cu catalysts toward low-pressure syngas conversion to long-chain alcohols. *Nat. Commun.* **2020,** *11* (1), 61.

74. Lin, T.; Qi, X.; Wang, X.; Xia, L.; Wang, C.; Yu, F.; Wang, H.; Li, S.; Zhong, L.; Sun, Y., Direct Production of Higher Oxygenates by Syngas Conversion over a Multifunctional Catalyst. *Angew. Chem. Int. Ed.* **2019,** *58* (14), 4627-4631.

75. Luan, X.; Ren, Z.; Dai, X.; Zhang, X.; Yong, J.; Yang, Y.; Zhao, H.; Cui, M.; Nie, F.; Huang, X., Selective Conversion of Syngas into Higher Alcohols via a Reaction-Coupling Strategy on Multifunctional Relay Catalysts. *ACS Catal.* **2020,** *10* (4), 2419-2430.

76. Chae, H. K.; Siberio-Pérez, D. Y.; Kim, J.; Go, Y.; Eddaoudi, M.; Matzger, A. J.; O'Keeffe, M.; Yaghi, O. M.; Materials, D.; Discovery, G., A route to high surface area, porosity and inclusion of large molecules in crystals. *Nature* **2004,** *427* (6974), 523-527.

77. Li, H.; Eddaoudi, M.; O'Keeffe, M.; Yaghi, O. M., Design and synthesis of an exceptionally stable and highly porous metal-organic framework. *Nature* **1999,** *402* (6759), 276-279.

78. Furukawa, H.; Ko, N.; Go, Y. B.; Aratani, N.; Choi, S. B.; Choi, E.; Yazaydin, A. O.; Snurr, R. Q.; Okeeffe, M.; Kim, J., Ultrahigh Porosity in Metal-Organic Frameworks. *Science* **2010,** *329* (5990), 424-428.

79. Yang, F.; Mu, H.; Wang, C.; Xiang, L.; Yao, K. X.; Liu, L.; Yang, Y.; Han, Y.; Li, Y.; Pan, Y., Morphological Map of ZIF-8 Crystals with Five Distinctive Shapes: Feature of Filler in Mixed-Matrix Membranes on C_3H_6/C_3H_8 Separation. *Chem. Mater.* **2018,** *30* (10), 3467-3473.

80. Li, X.; Li, Z.; Lu, L.; Huang, L.; Xiang, L.; Shen, J.; Liu, S.; Xiao, D.-R., The Solvent Induced Inter-Dimensional Phase Transformations of Cobalt Zeolitic-Imidazolate Frameworks. *Chemistry* **2017,** *23* (44), 10638-10643.

81. Lu, G.; Li, S.; Guo, Z.; Farha, O. K.; Hauser, B. G.; Qi, X.; Wang, Y.; Wang, X.; Han, S.; Liu, X., Imparting functionality to a metal–organic framework material by controlled nanoparticle encapsulation. *Nat. Chem.* **2012,** *4* (4), 310.

82. Zhang, W.; Lu, G.; Cui, C.; Liu, Y.; Li, S.; Yan, W.; Xing, C.; Chi, Y. R.; Yang, Y.; Huo, F., A Family of Metal-Organic Frameworks Exhibiting Size-Selective Catalysis with Encapsulated Noble-Metal Nanoparticles. *Adv. Mater.* **2014,** *26* (24), 4056-4060.

83. Tian, H.; Huang, F.; Zhu, Y.; Liu, S.; Han, Y.; Jaroniec, M.; Yang, Q.; Liu, H.; Lu, G. Q. M.; Liu, J., The Development of Yolk–Shell-Structured Pd&ZnO@Carbon Submicroreactors with High Selectivity and Stability. *Adv. Funct. Mater.* **2018,** *28* (32), 1801737.

84. Sun, C.-Y.; Liu, S.-X.; Liang, D.-D.; Shao, K.-Z.; Ren, Y.-H.; Su, Z.-M., Highly stable

crystalline catalysts based on a microporous metal− organic framework and polyoxometalates. *J. Am. Chem. Soc.* **2009,** *131* (5), 1883-1888.

85. Juan-Alcaniz, J.; Goesten, M.; Martinez-Joaristi, A.; Stavitski, E.; Petukhov, A. V.; Gascon, J.; Kapteijn, F., Live encapsulation of a Keggin polyanion in NH_2-MIL-101 (Al) observed by in situ time resolved X-ray scattering. *Chem. Commun.* **2011,** *47* (30), 8578-8580.

86. Liang, D. D.; Liu, S. X.; Ma, F. J.; Wei, F.; Chen, Y. G., A Crystalline Catalyst Based on a Porous Metal-Organic Framework and 12-Tungstosilicic Acid: Particle Size Control by Hydrothermal Synthesis for the Formation of Dimethyl Ether. *Adv. Synth. Catal.* **2011,** *353* (5), 733-742.

87. Ma, F.-J.; Liu, S.-X.; Sun, C.-Y.; Liang, D.-D.; Ren, G.-J.; Wei, F.; Chen, Y.-G.; Su, Z.-M., A Sodalite-Type Porous Metal−Organic Framework with Polyoxometalate Templates: Adsorption and Decomposition of Dimethyl Methylphosphonate. *J. Am. Chem. Soc.* **2011,** *133* (12), 4178-4181.

88. Bromberg, L.; Diao, Y.; Wu, H.; Speakman, S. A.; Hatton, T. A., Chromium (III) terephthalate metal organic framework (MIL-101): HF-free synthesis, structure, polyoxometalate composites, and catalytic properties. *Chem. Mater.* **2012,** *24* (9), 1664-1675.

89. Juan-Alcañiz, J.; Gascon, J.; Kapteijn, F., Metal–organic frameworks as scaffolds for the encapsulation of active species: state of the art and future perspectives. *J. Mater. Chem.* **2012,** *22* (20), 10102-10118.

90. Sabyrov, K.; Jiang, J.; Yaghi, O. M.; Somorjai, G. A., Hydroisomerization of n-Hexane Using Acidified Metal–Organic Framework and Platinum Nanoparticles. *J. Am. Chem. Soc.* **2017,** *139* (36), 12382-12385.

91. Khder, A. E. R. S.; Hassan, H. M. A.; El-Shall, M. S., Metal-organic frameworks with high tungstophosphoric acid loading as heterogeneous acid catalysts. *Appl. Catal. A-Gen.* **2014,** *487*, 110-118.

92. Zang, Y.; Shi, J.; Zhao, X.; Kong, L.; Zhang, F.; Zhong, Y., Highly stable chromium (III) terephthalate metal organic framework (MIL-101) encapsulated 12-tungstophosphoric heteropolyacid as a water-tolerant solid catalyst for hydrolysis and esterification. *React. Kinet. Mech. Catal.* **2013,** *109* (1), 77-89.

93. Ribeiro, S.; Granadeiro, C. M.; Silva, P.; Paz, F. A. A.; de Biani, F. F.; Cunha-Silva, L.;

Balula, S. S., An efficient oxidative desulfurization process using terbium-polyoxometalate@ MIL-101 (Cr). *Catal. Sci. Technol.* **2013,** *3* (9), 2404-2414.

94. Hu, X.; Lu, Y.; Dai, F.; Liu, C.; Liu, Y., Host–guest synthesis and encapsulation of phosphotungstic acid in MIL-101 via "bottle around ship": An effective catalyst for oxidative desulfurization. *Microporous Mesoporous Mater.* **2013,** *170*, 36-44.

95. Granadeiro, C. M.; Barbosa, A. D. S.; Silva, P.; Paz, F. A. A.; Saini, V. K.; Pires, J.; de Castro, B.; Balula, S. S.; Cunha-Silva, L., Monovacant polyoxometalates incorporated into MIL-101(Cr): novel heterogeneous catalysts for liquid phase oxidation. *Appl. Catal. A-Gen.* **2013,** *453*, 316-326.

96. Li, R.; Ren, X.; Zhao, J.; Feng, X.; Jiang, X.; Fan, X.; Lin, Z.; Li, X.; Hu, C.; Wang, B., Polyoxometallates trapped in a zeolitic imidazolate framework leading to high uptake and selectivity of bioactive molecules. *J. Mater. Chem. A* **2014,** *2* (7), 2168-2173.

97. Guo, S.-H.; Qi, X.-J.; Zhou, H.-M.; Zhou, J.; Wang, X.-H.; Dong, M.; Zhao, X.; Sun, C.-Y.; Wang, X.-L.; Su, Z.-M., A bimetallic-MOF catalyst for efficient CO_2 photoreduction from simulated flue gas to value-added formate. *J. Mater. Chem. A* **2020,** *8* (23), 11712-11718.

98. Chen, S.; Xue, M.; Li, Y.; Pan, Y.; Zhu, L.; Qiu, S., Rational design and synthesis of $Ni_xCo_{3-x}O_4$ nanoparticles derived from multivariate MOF-74 for supercapacitors. *J. Mater. Chem. A* **2015,** *3* (40), 20145-20152.

99. Tang, J.; Salunkhe, R. R.; Zhang, H.; Malgras, V.; Ahamad, T.; Alshehri, S. M.; Kobayashi, N.; Tominaka, S.; Ide, Y.; Kim, J. H.; Yamauchi, Y., Bimetallic Metal-Organic Frameworks for Controlled Catalytic Graphitization of Nanoporous Carbons. *Sci. Rep.* **2016,** *6* (1), 30295.

100. Li, H.; Liang, M.; Sun, W.; Wang, Y., Bimetal–Organic Framework: One-Step Homogenous Formation and its Derived Mesoporous Ternary Metal Oxide Nanorod for High-Capacity, High-Rate, and Long-Cycle-Life Lithium Storage. *Adv. Funct. Mater.* **2016,** *26* (7), 1098-1103.

101. Zhang, J.; An, B.; Hong, Y.; Meng, Y.; Hu, X.; Wang, C.; Lin, J.; Lin, W.; Wang, Y., Pyrolysis of metal–organic frameworks to hierarchical porous Cu/Zn-nanoparticle@ carbon materials for efficient CO_2 hydrogenation. *Mater. Chem. Front.* **2017,** *1* (11), 2405-2409.

102. Zheng, L.; Li, X.; Du, W.; Shi, D.; Ning, W.; Lu, X.; Hou, Z., Metal-organic framework derived Cu/ZnO catalysts for continuous hydrogenolysis of glycerol. *Appl. Catal. B-Environ.*

2017, *203*, 146-153.

103. Das, R.; Pachfule, P.; Banerjee, R.; Poddar, P., Metal and metal oxide nanoparticle synthesis from metal organic frameworks (MOFs): finding the border of metal and metal oxides. *Nanoscale* **2012,** *4* (2), 591-599.

104. Raoof, J.-B.; Hosseini, S. R.; Ojani, R.; Mandegarzad, S., MOF-derived Cu/nanoporous carbon composite and its application for electro-catalysis of hydrogen evolution reaction. *Energy* **2015,** *90*, 1075-1081.

105. Tan, H.; Ma, C.; Gao, L.; Li, Q.; Song, Y.; Xu, F.; Wang, T.; Wang, L., Metal–organic framework-derived copper nanoparticle@carbon nanocomposites as peroxidase mimics for colorimetric sensing of ascorbic acid. *Chemistry* **2014,** *20* (49), 16377-16383.

106. Wei, C.; Li, X.; Xu, F.; Tan, H.; Li, Z.; Sun, L.; Song, Y., Metal organic framework-derived anthill-like Cu@carbon nanocomposites for nonenzymatic glucose sensor. *Anal. Methods* **2014,** *6* (5), 1550-1557.

107. Santos, V. P.; Wezendonk, T. A.; Jaén, J. J. D.; Dugulan, A. I.; Nasalevich, M. A.; Islam, H.-U.; Chojecki, A.; Sartipi, S.; Sun, X.; Hakeem, A. A., Metal organic framework-mediated synthesis of highly active and stable Fischer-Tropsch catalysts. *Nat. Commun.* **2015,** *6*, 6451.

108. Xu, Y.-T.; Xiao, X.; Ye, Z.-M.; Zhao, S.; Shen, R.; He, C.-T.; Zhang, J.-P.; Li, Y.; Chen, X.-M., Cage-confinement pyrolysis route to ultrasmall tungsten carbide nanoparticles for efficient electrocatalytic hydrogen evolution. *J. Am. Chem. Soc.* **2017,** *139* (15), 5285-5288.

109. Yang, L.; Huang, J.; Ma, R.; You, R.; Zeng, H.; Rui, Z., Metal–Organic Framework-Derived IrO_2/CuO Catalyst for Selective Oxidation of Methane to Methanol. *ACS Energy Lett.* **2019,** *4* (12), 2945-2951.

110. Wu, R.; Qian, X.; Zhou, K.; Wei, J.; Lou, J.; Ajayan, P. M., Porous Spinel $Zn_xCo_{3-x}O_4$ Hollow Polyhedra Templated for High-Rate Lithium-Ion Batteries. *ACS Nano* **2014,** *8* (6), 6297-6303.

111. Wang, T.; Shi, L.; Tang, J.; Malgras, V.; Asahina, S.; Liu, G.; Zhang, H.; Meng, X.; Chang, K.; He, J.; Terasaki, O.; Yamauchi, Y.; Ye, J., A Co_3O_4-embedded porous ZnO rhombic dodecahedron prepared using zeolitic imidazolate frameworks as precursors for CO_2 photoreduction. *Nanoscale* **2016,** *8* (12), 6712-6720.

112. Liu, Y.; Wang, Z.; Zhong, Y.; Tade, M.; Zhou, W.; Shao, Z., Molecular Design of

Mesoporous $NiCo_2O_4$ and $NiCo_2S_4$ with Sub-Micrometer-Polyhedron Architectures for Efficient Pseudocapacitive Energy Storage. *Adv. Funct. Mater.* **2017,** *27* (28), 1701229.

113. Wezendonk, T. A.; Santos, V. P.; Nasalevich, M. A.; Warringa, Q. S. E.; Dugulan, A. I.; Chojecki, A.; Koeken, A. C. J.; Ruitenbeek, M.; Meima, G.; Islam, H.-U.; Sankar, G.; Makkee, M.; Kapteijn, F.; Gascon, J., Elucidating the Nature of Fe Species during Pyrolysis of the Fe-BTC MOF into Highly Active and Stable Fischer–Tropsch Catalysts. *ACS Catal.* **2016,** *6* (5), 3236-3247.

114. Oar-Arteta, L.; Wezendonk, T.; Sun, X.; Kapteijn, F.; Gascon, J., Metal organic frameworks as precursors for the manufacture of advanced catalytic materials. *Mater. Chem. Front.* **2017,** *1* (9), 1709-1745.

115. Sun, X.; Suarez, A. I. O.; Meijerink, M.; Van Deelen, T.; Ould-Chikh, S.; Zečević, J.; De Jong, K. P.; Kapteijn, F.; Gascon, J., Manufacture of highly loaded silica-supported cobalt Fischer–Tropsch catalysts from a metal organic framework. *Nat. Commun.* **2017,** *8* (1), 1680.

116. Wezendonk, T. A.; Warringa, Q. S.; Santos, V. P.; Chojecki, A.; Ruitenbeek, M.; Meima, G.; Makkee, M.; Kapteijn, F.; Gascon, J., Structural and elemental influence from various MOFs on the performance of Fe@ C catalysts for Fischer–Tropsch synthesis. *Faraday Discuss.* **2017,** *197*, 225-242.

117. Oar-Arteta, L.; Valero-Romero, M. J.; Wezendonk, T.; Kapteijn, F.; Gascon, J., Formulation and catalytic performance of MOF-derived Fe@C/Al composites for high temperature Fischer–Tropsch synthesis. *Catal. Sci. Technol.* **2018,** *8* (1), 210-220.

118. Ramirez, A.; Gevers, L.; Bavykina, A.; Ould-Chikh, S.; Gascon, J., Metal Organic Framework-Derived Iron Catalysts for the Direct Hydrogenation of CO_2 to Short Chain Olefins. *ACS Catal.* **2018,** *8* (10), 9174-9182.

119. Qiu, B.; Yang, C.; Guo, W.; Xu, Y.; Liang, Z.; Ma, D.; Zou, R., Highly dispersed Co-based Fischer–Tropsch synthesis catalysts from metal–organic frameworks. *J. Mater. Chem. A* **2017,** *5* (17), 8081-8086.

120. Zhang, C.; Guo, X.; Yuan, Q.; Zhang, R.; Chang, Q.; Li, K.; Xiao, B.; Liu, S.; Ma, C.; Liu, X., Ethyne-Reducing Metal–Organic Frameworks to Control Fabrications of Core/shell Nanoparticles as Catalysts. *ACS Catal.* **2018,** *8* (8), 7120-7130.

121. Pei, Y.; Li, Z.; Li, Y., Highly active and selective Co-based Fischer–Tropsch catalysts

derived from metal–organic frameworks. *AlChE J.* **2017,** *63* (7), 2935-2944.

122. Hermes, S.; Schröter, M. K.; Schmid, R.; Khodeir, L.; Muhler, M.; Tissler, A.; Fischer, R. W.; Fischer, R. A., Metal@ MOF: loading of highly porous coordination polymers host lattices by metal organic chemical vapor deposition. *Angew. Chem. Int. Ed.* **2005,** *44* (38), 6237-6241.

123. Müller, M.; Hermes, S.; Kähler, K.; van den Berg, M. W.; Muhler, M.; Fischer, R. A., Loading of MOF-5 with Cu and ZnO nanoparticles by gas-phase infiltration with organometallic precursors: properties of Cu/ZnO@ MOF-5 as catalyst for methanol synthesis. *Chem. Mater.* **2008,** *20* (14), 4576-4587.

124. Cavka, J. H.; Jakobsen, S.; Olsbye, U.; Guillou, N.; Lamberti, C.; Bordiga, S.; Lillerud, K. P., A new zirconium inorganic building brick forming metal organic frameworks with exceptional stability. *J. Am. Chem. Soc.* **2008,** *130* (42), 13850-13851.

125. Rungtaweevoranit, B.; Baek, J.; Araujo, J. R.; Archanjo, B. S.; Choi, K. M.; Yaghi, O. M.; Somorjai, G. A., Copper Nanocrystals Encapsulated in Zr-based Metal–Organic Frameworks for Highly Selective CO_2 Hydrogenation to Methanol. *Nano Lett.* **2016,** *16* (12), 7645-7649.

126. An, B.; Zhang, J.; Cheng, K.; Ji, P.; Wang, C.; Lin, W., Confinement of Ultrasmall Cu/ZnO_x Nanoparticles in Metal–Organic Frameworks for Selective Methanol Synthesis from Catalytic Hydrogenation of CO_2. *J. Am. Chem. Soc.* **2017,** *139* (10), 3834-3840.

127. Wang, Z.; Laddha, G.; Kanitkar, S.; Spivey, J. J., Metal organic framework-mediated synthesis of potassium-promoted cobalt-based catalysts for higher oxygenates synthesis. *Catal. Today* **2017,** *298*, 209-215.

128. Jiang, H.-L.; Liu, B.; Akita, T.; Haruta, M.; Sakurai, H.; Xu, Q., Au@ ZIF-8: CO oxidation over gold nanoparticles deposited to metal−organic framework. *J. Am. Chem. Soc.* **2009,** *131* (32), 11302-11303.

129. El-Shall, M. S.; Abdelsayed, V.; Abd El Rahman, S. K.; Hassan, H. M.; El-Kaderi, H. M.; Reich, T. E., Metallic and bimetallic nanocatalysts incorporated into highly porous coordination polymer MIL-101. *J. Mater. Chem.* **2009,** *19* (41), 7625-7631.

130. Abdel-Mageed, A. M.; Rungtaweevoranit, B.; Parlinska-Wojtan, M.; Pei, X.; Yaghi, O. M.; Behm, R. J., Highly Active and Stable Single-Atom Cu Catalysts Supported by a Metal–Organic Framework. *J. Am. Chem. Soc.* **2019,** *141* (13), 5201-5210.

131. Wang, W.; Li, Y.; Zhang, R.; He, D.; Liu, H.; Liao, S., Metal-organic framework as a host

for synthesis of nanoscale Co_3O_4 as an active catalyst for CO oxidation. *Catal. Commun.* **2011,** *12* (10), 875-879.

132. Zhang, F.; Chen, C.; Xiao, W.-m.; Xu, L.; Zhang, N., CuO/CeO_2 catalysts with well-dispersed active sites prepared from $Cu_3(BTC)_2$ metal–organic framework precursor for preferential CO oxidation. *Catal. Commun.* **2012,** *26*, 25-29.

133. Zamaro, J. M.; Pérez, N. C.; Miró, E. E.; Casado, C.; Seoane, B.; Téllez, C.; Coronas, J., HKUST-1 MOF: A matrix to synthesize CuO and $CuO–CeO_2$ nanoparticle catalysts for CO oxidation. *Chem. Eng. J.* **2012,** *195*, 180-187.

134. Ikuno, T.; Zheng, J.; Vjunov, A.; Sanchez-Sanchez, M.; Ortuño, M. A.; Pahls, D. R.; Fulton, J. L.; Camaioni, D. M.; Li, Z.; Ray, D., Methane Oxidation to Methanol Catalyzed by Cu-Oxo Clusters Stabilized in NU-1000 Metal–Organic Framework. *J. Am. Chem. Soc.* **2017,** *139* (30), 10294-10301.

135. Baek, J.; Rungtaweevoranit, B.; Pei, X.; Park, M.; Fakra, S. C.; Liu, Y.-S.; Matheu, R.; Alshmimri, S. A.; Alshehri, S.; Trickett, C. A.; Somorjai, G. A.; Yaghi, O. M., Bioinspired Metal–Organic Framework Catalysts for Selective Methane Oxidation to Methanol. *J. Am. Chem. Soc.* **2018,** *140* (51), 18208-18216.

136. Osadchii, D. Y.; Olivos-Suarez, A. I.; Szécsényi, Á.; Li, G.; Nasalevich, M. A.; Dugulan, I. A.; Crespo, P. S.; Hensen, E. J. M.; Veber, S. L.; Fedin, M. V.; Sankar, G.; Pidko, E. A.; Gascon, J., Isolated Fe Sites in Metal Organic Frameworks Catalyze the Direct Conversion of Methane to Methanol. *ACS Catal.* **2018,** *8* (6), 5542-5548.

Chapter 3 Research Methodology and Analytical Techniques

3.1 Introduction

This chapter presents the overall research methodologies employed to achieve the thesis objectives outlined in Chapter 1. A methodical approach was pursued to fabricate most promising MOF-derived catalysts for DME and higher alcohols synthesis, mainly consisting of catalyst design and preparation, catalyst characterization, and catalyst activity evaluation for DME and higher alcohols production. The detailed descriptions of experimental and analytical techniques are listed in the following sections.

3.2 Catalyst Design and Preparation

3.2.1 catalysis design

Considering the targets of this thesis, three types MOFs are selected for oxygenates production and different modification strategies have been conducted. In the first part, to prepare a MOF composite with bifunctionality for DME synthesis, a Zr-based MOF (UiO-66) was selected to incorporate solid acid molecules (12-silicontunstic acid, $H_4SiW_{12}O_{40}$) and support Cu species on the external surface owing to the exceptional thermostability and potential SMSI effect with Cu. In the second part, a series of CuZn bimetallic MOF with different compositions have been designed. Since CuZn-MOFs are not stable under DME synthesis conditions, the prepared MOFs were calcined to produce the Cu/ZnO catalyst. For the third session, as CoMo catalysts are widely reported to be active for higher alcohols synthesis, a carbon supported CoMo catalyst

was also fabricated via pyrolysis of a Co-MOF composite. The detailed catalyst preparation procedures are included in Section 3.2.2-3.2.4.

3.2.2 Cu deposited UiO-66 encapsulated 12-silicotungstic acid composite catalyst for DME synthesis

The pure UiO-66 was synthesized based on the reported protocol.[1] Briefly, 4.54 mmol of zirconium chloride and 4.54 mmol of terephthalic acid were mixed together in 810.76 mmol of N, N-dimethylformamide (DMF) for 30 min under stirring and then the mixture was poured into a Parr PTFE-lined digestion vessel of 125 mL. The vessel was placed inside an oven at 120 °C for 24 h. To prepare STA encapsulated UiO-66, 0.25 g STA and terephthalic acid were firstly added in DMF under stirring until fully dissolved. Then zirconium tetrachloride was added into the aforementioned solution and stirred for 30 min. The mixture was poured into a Parr PTFE-lined digestion and placed in an oven preheated to 120 °C for 24 h. All products were activated before being used with the following procedures. The white powder collected by centrifugation was washed thoroughly with DMF to remove the unreacted chemicals and then soaked in 50 mL methanol at 60 °C for 3 days to exchange DMF during which the solvent was replaced every 24 hours to exchange DMF in MOF cavities. The product was centrifuged and washed fully with methanol. Finally, the sample was vacuumed at 150 °C for 24 hours on a degas station to remove the encapsulated solvents within the cavities or channels.

To prepare Cu deposited UiO-66 and STA-UiO, An organometallic compound (copper acetylacetonate ($Cu(acac)_2$)) was selected as the copper precursor owing to its easy sublimation and decomposition at low temperatures. [2, 3] The Cu/UiO-66 and Cu/STA-UiO catalysts with 3 wt% Cu were prepared through the similar procedure. Typically, 0.1227g $Cu(acac)_2$ and 0.97g UiO-66 were mixed and ground well for 30 min in an agate mortar to form a light purple mixture, which was then heated in a muffle furnace at 180 °C for 4 hours to obtain uniformly dispersed $Cu(acac)_2$ on the surface of UiO-

66.

3.2.3 CuZn bimetallic MOFs derived catalyst for DME synthesis

The CuZn bimetallic MOF (CuZn-BTC) precursor was synthesized according to the procedure reported elsewhere.[4] Briefly, copper nitrate ($Cu(NO_3)_2{\cdot}3H_2O$) and zinc nitrate ($Zn(NO_3)_2{\cdot}6H_2O$) were dissolved into 90 mL N, N-Dimethylformamide. Then 3.0 g of 1,3,5-benzenetricarboxylic acid was added into the solution. After sonicated for 15 min, the resultant homogeneous solution was transferred into a 125 mL-Parr PTFE-lined autoclave and kept at 90 °C for 18 h. The product was filtered off, washed with DMF three times, and dried at 110 °C overnight.

The prepared CuZn-BTC was firstly pyrolyzed in a tubular furnace at 500 °C for 4 h in N_2 to obtain Cu/ZnO@C precursor. Then, the resultant Cu/ZnO@C was further calcined in a muffle furnace in air at 350 to 550 °C for 4 h. This catalysts were defined as CZ-X, where "X" following CZ represents the final calcination temperature. To prepare the final bifunctional catalyst for DME formation, the γ-Al_2O_3 was used as the methanol dehydration component and mixed with the prepared CZ-X catalysts.

3.2.4 Co-MOF encapsulated phosphomolybdic acid derived catalyst for HAS

The preparation of PMA@ZIF-67 and derived catalyst followed the procedures illustrated in Scheme 3-1. Briefly, cobalt nitrate ($Co(NO_3)_2.6H_2O$) and different amounts of phosphomolybdic acid (PMA) were dissolved in 120 mL methanol to get the solution A and 3.94 g of 2-methylimidazole was dissolved in 60 mL methanol to prepare the solution B. Then the solution B was poured into solution A and stirred for 15 mins. The resultant purple mixture was kept still for 24 h at room temperature.

The purple precipitate was collected after centrifuging, washing thoroughly with methanol, and drying at 80 °C overnight. The pure ZIF-67 was developed following the similar process without the addition of PMA. The resultant PMA@ZIF-67 composites were denoted as PZIF-1, PZIF-2 and PZIF-3, respectively. The synthesized MOFs (ZIF-67, PZIF-1, PZIF-2 and PZIF-3) were carbonized in a tube furnace under a nitrogen atmosphere. The temperature was ramped from room temperature to 600 °C with a heating rate of 1 °C/min and held for 4 h. The final black powders were referred to as Co@C, $Co_{4.7}$Mo@C, $Co_{2.2}$Mo@C and $Co_{7.3}$Mo@C.

3.3 Analysis Techniques for Catalyst Characterization

Catalyst characterization reveals valuable compositional and structural information of MOF-based catalysts. Through a combination of different characterization techniques, it is possible to detect the active centers for oxygenates and the chemistry behind the formation of active sites. All used characterization techniques are listed here.

3.3.1 Inductively Coupled Plasma Optical Emission Spectrometry (ICP-OES)

The bulk compositions of MOF-based catalyst were determined on an Optima 8300 (PerkinElmer) ICP-OES Spectrometer. Ten-milligram sample was dissolved in an acidic solution. The atomic compositions of each element were provided in parts per million (ppm).

3.3.2 Nitrogen adsorption/desorption analysis

The N_2 adsorption/desorption analysis is an important technique to detect the porosity of catalysts, such as the specific surface area and pore volume. N_2 adsorption/desorption isotherms were recorded using a Tristar II 3020 instrument (Micromeritics) under the boiling point of liquid nitrogen (-196 °C). The specific

surface area was estimated using Brunauer-Emmett-Teller (BET) method. Before analysis, sample (50 mg) was degassed at 200 °C under vacuum for 18 hours.

3.3.3 Thermogravimetric Analysis and Differential Scanning Calorimetry (TGA/DSC)

Thermal stability of MOF-based catalyst was determined on a TGA instrument (METTLER TOLEDO) equipped with alumina pan, from room temperature to targeted temperature at a heating rate of 15 °C and under different gas flows.

3.3.4 Fourier Transform Infrared (FT-IR) Spectra Analysis

Fourier Transform Infrared (FT-IR) Spectra were scanned from 600-2000 cm^{-1} with the resolution of 4 cm^{-1} on a PerkinElmer Spectrum 100 FTIR Spectrometer equipped with an ATR-Diamond/ZnSe IR detector.

3.3.5 Powder X-ray Diffraction (XRD) analysis

The powder X-ray diffraction is widely used to identify the phase compositions and to determine the crystallite size of prepared catalysts. In this study, Powder X-ray diffraction analyses were performed on an XRD diffractometer (Bruker D8 Advance) with Cu Kα radiation (λ=1.5406 Å). The spectra were obtained between the 2θ ranges of 5-90° at a scanning rate of 2°/min. The recorded patterns were identified by reference to the powder diffraction data (JCPDS-ICDD) with the standard spectra software, and the particle size was determined using the Scherrer equation ($D=k\lambda/\beta \cos\theta$).

3.3.6 Scanning Election Microscopy (SEM)

Scanning electron microscopy (SEM) is used to detect the morphology of fromed catalysts. The SEM images were obtained on a Zeiss Neon 40EsB FIBSEM to evaluate the morphologies of catalysts with an accelerating voltage of 3 kV. Before analysis, samples were coated with platinum to avoid charging.

3.3.7 Transmission Electron Microscopy (TEM)

Transmission electron microscopy (TEM) provides more professional knowledge about the morphology and compositional properties than SEM. The high-resolution TEM analysis can even present the lattice strain of active sites. In this study, TEM analysis was carried out using an FEI Talos FS200X G2 electron microscopy at an accelerating voltage of 200 kV.

3.3.8 X-ray Photoelectron Spectroscopy (XPS)

X-ray photoelectron spectroscopy (XPS) analysis provides valuable quantitative and chemical state information from the surface of the material being studied. The XPS spectra for different elements were scanned on a Kratos AXIS Ultra DLD machine with a monochromatic Al Kα X-Ray gun. Prior to fitting, the binding energy was calibrated using C 1s at 284.6 eV.

3.4 Catalytic Activity Evaluation for Oxygenates Production

3.4.1 Instruments for Catalyst Evaluation

The performance of prepared catalysts was tested on a high-pressure fixed-bed reactor system (Spider 3F-T instrument, AMTech, Germany). The Spider 3F-T is equipped

with 3 parallel reactor tubes (I.D. = 12.7 mm, L = 200 mm). The reaction temperature was monitored by thermocouple inserted into the reactor tube, and the pressure is controlled by a back-pressure controller. The ultra-pure gases (H_2 and N_2: 99.999%, CO: 99.5%) were connected to the reactor system. The products were analyzed online using a connected Agilent 7890 / 5977 GC/MS instrument. CO, H_2, CH_4, N_2, and CO_2 in the effluent gases were detected on the thermal conductivity detector (TCD) connected to a packed column (TDX-01, 2 m×80/100 mesh). Methanol and DME were detected on mass spectrometry detector (MSD) connected to an MS HP-5 column (30 m×0.32 mm×0.25 μm). To avoid any product condensation, the temperature of the gas lines connecting the reactor and GC/MS was maintained at 180 °C.

3.4.2 Oxygenates Synthesis from Syngas

The catalyst for DME synthesis was diluted with SiC and loaded into the Spider 3F-T facility. Prior to the reaction, the catalyst was firstly reduced *in situ* under ambient pressure using 20 vol.% of H_2 in N_2 at a flow rate of 100 mL min^{-1}. The temperature was raised to reduction temperature at a slow heating rate of 1 °C min^{-1} and then held overnight. Then, the reactor was pressurized to 3.0 MPa with pure nitrogen before switching to syngas feed. A mixture of H_2 and CO in a ratio of 2:1 was used as syngas feed for all catalysts with 50 vol.% of N_2 gas used as the internal calibration standard. The DME performance was detected at steady state under the reaction conditions for the required period of time.

The HAS catalysts were tested following similar procedures of STD reaction. The catalyst was firstly diluted with γ-Al_2O_3 and then loaded into the reactor. Prior to reaction, the catalyst was reduced at 450 °C.

3.4.3 Calculation Methods

CO conversion and selectivity of products were calculated based on the following equations:

$$CO\ conversion: \quad X_{CO}\ (mol\%) = \frac{Mole_{CO,in} - Mole_{CO,out}}{Mole_{CO,in}} \times 100\% \qquad (3\text{-}1)$$

$$Product\ selectivity: \quad S_i(mol\%) = \frac{Mole_i \times n_i}{Mole_{CO,converted}} \times 100\% \qquad (3\text{-}2)$$

where, $Mole_{CO,in}$ and $Mole_{CO,out}$ represent the molar content of CO in the feed gas and effluent gas; $Mole_i$ and n_i stand for the molar content of the product (CH_4, CO_2, DME, alcohols) and the number of carbon atoms in the product, respectively.

For HAS, the alcohol distribution was calculated by Equation (3-3):

$$Alcohol\ distribution: \quad S_A = \frac{Mole_A \times n_A}{\Sigma Mole_A \times n_A} \times 100\% \qquad (3\text{-}3)$$

$Mole_A$, n_A represent the moles of alcohol product *A* and the number of carbon atoms in alcohol *A*, respectively.

References

1. Abid, H. R.; Ang, H. M.; Wang, S., Effects of ammonium hydroxide on the structure and gas adsorption of nanosized Zr-MOFs (UiO-66). *Nanoscale* **2012,** *4* (10), 3089-3094.

2. Nasibulin, A. G.; Altman, I. S.; Kauppinen, E. I., Semiempirical dynamic phase diagrams of nanocrystalline products during copper (II) acetylacetonate vapour decomposition. *Chem. Phys. Lett.* **2003,** *367* (5-6), 771-777.

3. Goel, P.; Duragasi, G.; Singh, J., Copper (I) oxide micro-cubical structures formation by metal organic chemical vapor deposition from copper (II) acetylacetonate. *J. Mater. Sci.* **2013,** *48* (14), 4876-4882.

4. Zhang, J.; An, B.; Hong, Y.; Meng, Y.; Hu, X.; Wang, C.; Lin, J.; Lin, W.; Wang, Y.,

Pyrolysis of metal–organic frameworks to hierarchical porous Cu/Zn-nanoparticle@ carbon materials for efficient CO_2 hydrogenation. *Mater. Chem. Front.* **2017,** *1* (11), 2405-2409.

Chapter 4 Fabrication of A novel UiO-66 Encapsulated Silicotungstic Acid Catalyst for DME Synthesis from Syngas

Abstract

Dimethyl ether (DME) has received great attention as a promising clean fuel and industrially important intermediate. Tremendous efforts have been made to develop highly active and stable catalysts for DME production. Here, we present the first example of the application of metal-organic framework (MOF) catalyst in DME synthesis from syngas. A Zr-MOF (UiO-66) was selected as the catalyst host and support owing to its exceptionally high stability and porosity. UiO-66 was firstly functionalized by silicotungstic acid ($H_4SiW_{12}O_{40}$, STA) via a one-pot synthesis method and then loaded with Cu by a facile solid grinding method. The prepared catalysts were characterized using XRD, TGA, FT-IR, N_2 adsorption and TEM. The high porosity and thermal stability of acidified UiO-66 were maintained after 15% wt STA incorporation without any destruction of the Keggin structure of STA. The catalyst was tested for one step DME synthesis from syngas, showing higher DME selectivity and space-time yield than control catalysts. The superior activity of Cu/STA-UiO was attributed to the uniform dispersion of active centers with close intimacy and high density of Brønsted acid sites, as well as strong metal support interaction between Cu and Zr oxide SBU evidenced by XPS analysis.

The content of this chapter is published in Catalysis Today: 2020 (355)

4.1 Introduction

Seeking alternative energy sources is one of the hot topics to address the global environmental crisis and energy shortage issues. Syngas (CO + H_2), which can be produced from natural gas, coal and biomass, is acting as the crucial junction point that exclusively bridges the non-petroleum carbon resources and other basic chemicals.[1, 2] Dimethyl ether (DME) can be generated from syngas conversion via gas-to-liquid technology and has been considered as a clean fuel in the 21st century due to its environmental benign properties.[3] DME can partially replace diesel or liquefied petroleum gas (LPG). In addition, DME is also a key feedstock or intermediate for many chemicals synthesis, such as methyl acetate, formaldehyde, and light olefins.[4-7]

Currently, DME production can be realized via two different routes from syngas. One is the indirect method, where methanol synthesis and dehydration are conducted in separate plant. Another method is the direct synthesis (also referred as STD process) where methanol synthesis reaction and dehydration step occur simultaneously in one reactor. The latter STD method is more economically and thermodynamically favorable than the former indirect method, because the intermediate product methanol can be quickly catalyzed to form DME immediately once it's produced. Such synergetic effect can help to minimize the equilibrium constraints, thus leading to a higher syngas conversion and improving the overall economy of the process.[8, 9]

The conventional catalysts for the STD process are the hybrids of Cu/ZnO and solid acid functioning for methanol synthesis and methanol dehydration, respectively. ZnO has been believed as the essential promoter of Cu for methanol production due to the strong metal-support interaction (SMSI) between ZnO and Cu.[9] Other publications reveal that similar interaction exists between Cu and ZrO_2, with slightly lower activity than the support from ZnO.[10, 11] In addition to the γ-Al_2O_3, some zeolites (ZSM-5, Y,

and SAPO-18) can also be applied as the methanol dehydration component.[9, 12-14] However, the hybrid catalysts always suffer from Cu sintering, low DME production rate and coke deposition, showing quick deactivation in the STD process.

As a class of solid acids, heteropoly acid (HPA), especially Keggin-type HPAs, have attracted increasing attention in heterogeneous catalysis area. Their intrinsic properties such as high surface Brønsted acidity, good redox stabilities and eco-friendly properties have made them promising catalysts for acid-catalyzed reactions.[15] However, one obvious disadvantage of the bulk HPAs is their low surface area.[16] It has been reported that the catalytic performance of HPA can be significantly improved when loaded onto high surface area supports.[17] TiO_2 or SiO_2 supported HPA has shown outstanding performance in the production of dimethyl ether from methanol dehydration, even better than HZSM-5.[18, 19] The priority of HPA catalysts is assigned to their strong acidity and high Brønsted acid density.

In recent years, metal-organic-framework materials (MOFs) have become the subject of very active research due to their unparalleled properties, such as extreme high surface area/porosity, tunable pore apertures/window size, providing great potential in gas separation and heterogeneous catalysis as the perfect host or support for active centers.[20] Among these applications, the HPA-MOF composite has been widely studied since the first report of one-pot incorporation of HPAs in the large cavities of HKUST-1.[21] The large porosity and appropriate pore window size provide MOFs as the unique host for HPAs because the molecule size of HPAs is about 10.4 Å.[22] Such a strategy via composite formation has been regarded as the most promising approach to achieve high loading and homogeneous dispersion of HPA molecules, thus boosting their applications in acid catalyzed reactions (oxidative desulfurization, condensation, hydrolysis, esterification, *etc*).[23-27] Two examples have been reported about the application of HPA-MOF composite on DME synthesis from methanol dehydration. A low DME selectivity (less than 75%) was observed in one work with MIL-101 (Cr-MOF) encapsulated PTA ($H_3PW_{12}O_{40}$).[28] Large amount of hydrocarbons were formed,

might due to the strong acidity of PTA. It has been believed that strong Brønsted acid sites could give rise to hydrocarbons from DME deep dehydration thus lowering the selectivity.[29-31] Liang *et al.* chose silicotungstic acid ($H_4SiW_{12}O_{40}$, STA) with mild acidity as the immobilized acid and HKUST-1(Cu-MOF) as the host. The prepared STA-HKUST exhibited almost 100% DME selectivity and much higher methanol conversion than other catalysts like PTA-HKUST, γ-Al_2O_3 or γ-Al_2O_3 supported STA. The medium acidity, high loading of STA and the completely accessible active sites in STA-HKUST mainly contributed to the superior catalytic performance. However, to the best of our knowledge, no application of MOF-based catalyst has been reported in the STD process.

In this chapter, we look at the hypothesis that if the incorporation of MOF and solid acid can serve as an efficient bifunctional catalyst for the STD process. For this purpose, UiO-66 (Zr-MOF) was chosen as the host not only because of its exceptionally high thermal stability but also the possible synergetic effect between Cu and Zr oxide. Scheme 4-1 depicts the detailed preparation procedure. UiO-66 was firstly acidified by encapsulating STA into its framework, followed by Cu deposition on the prepared MOF composite via a facile solid grinding method. The structural and chemical properties were clarified via a series of characterization techniques and the catalytic activity was tested in the DME production from syngas.

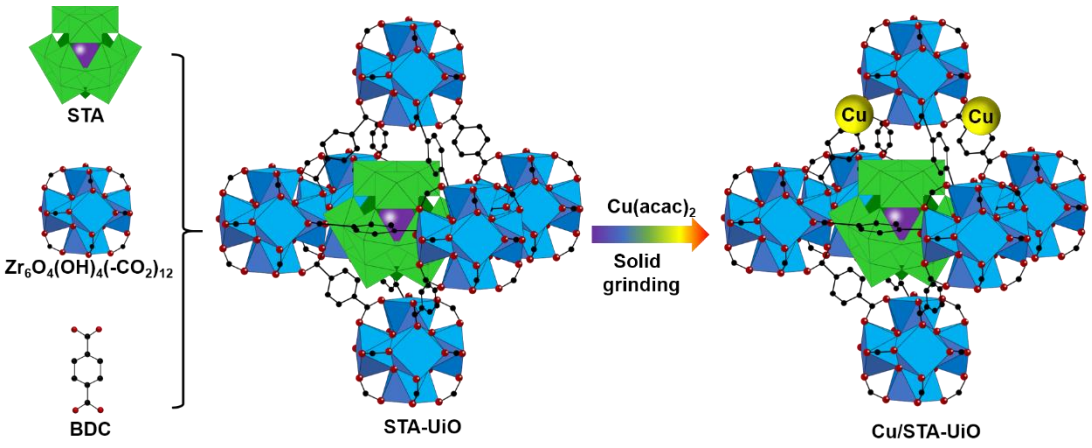

Scheme 4-1. Preparation of bifunctional Cu/STA-UiO

4.2 Results and discussion

4.2.1 Catalyst Characterization

The XRD patterns of pure STA and the synthesized UiO-66 samples are displayed in Figure 4.1A. The STA-UiO and bare UiO-66 show similar XRD patterns. This observation is consistent with the results from literature and suggests that both of their crystalline structures are well retained after STA encapsulation.[32] However, a minor peak shift with decreased intensity is detected at 7.36° and 8.48° (inset in Figure 4.1A) for STA-UiO, indicating STA encapsulation could lead to a lower crystallinity. This might be explained with the molecule size of STA. UiO-66 is a microporous MOF, with pore sizes from 10 to 14 Å, similar to the molecule size of STA.[33] During the encapsulation process, it might be difficult to get homogeneous growth of UiO-66 crystals, thus leading to a lower crystallinity. No characteristic peaks of STA are observed in the XRD pattern of STA-UiO, indicating that the STA molecule is evenly dispersed in UiO-66 without any aggregation.

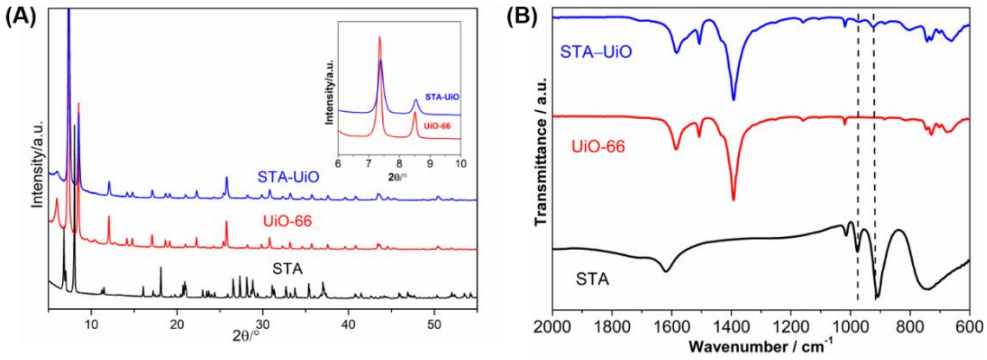

Figure 4.1. XRD patterns for STA, UiO-66 and STA-UiO (A). FT-IR spectra of STA, UiO-66 and STA-UiO (B).

The successful incorporation of STA in UiO-66 can also be confirmed by comparing their FT-IR spectra difference (Figure 4.1B). In addition to the appearance of similar peaks in the region of 1700-1300 cm^{-1},which indicates the intact framework of STA-

UiO, further inspection of the spectra exhibits that the peaks at 980 and 920 cm^{-1} of STA-UiO and pure STA are ascribed to the vibrations of W-O_d and Si-O_a in the Keggin-type anion of $SiW_{12}O_{40}^{4-}$, suggesting the integrity of STA molecule in STA-UiO.[34]

The effect of STA incorporation on UiO-66 morphology is clearly revealed from transmission electron microscopy (TEM) analysis (Figure 4.2A-F). Consistent with the previous analysis, pure UiO-66 (Figure 4.2A) possesses homogeneous shape with size around 150 nm in high crystallinity. However, after STA incorporation, the particles of STA-UiO have a more tendency to be aggregated (Figure 4.2B) as observed by other researchers.[35] Nevertheless, the high-angle annular dark field scanning transmission electron microscopy (HAADF-STEM) images and corresponding elemental mapping images (Figure 4.2C-F) clearly demonstrate the homogeneous distribution of Si and W atoms within MOF frameworks.

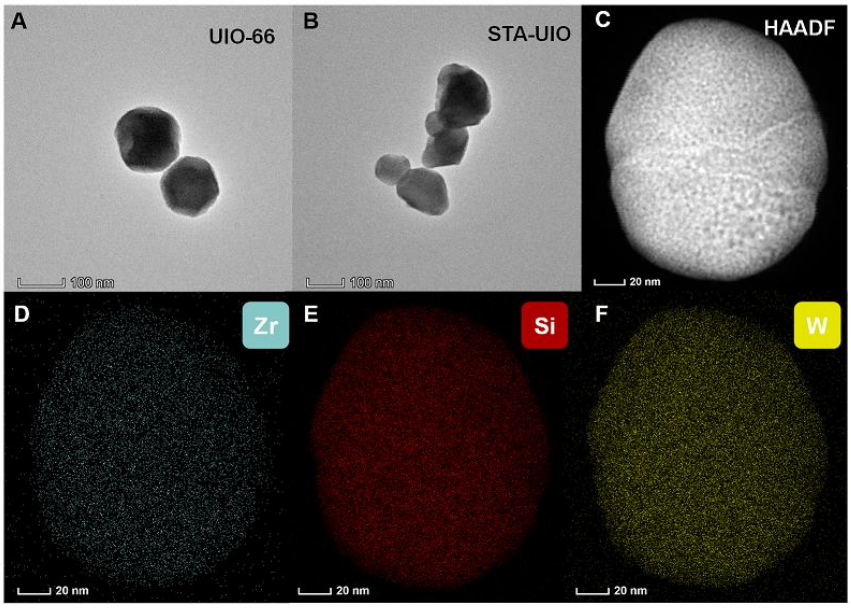

Figure 4.2. TEM images of UiO-66 (A) and STA-UiO (B). HAADF-STEM of STA-UiO (C) and corresponding EDS elemental mapping of Zr (D), Si (E) and W (F).

To seek its potential use in STD process, STA-UiO is further characterized to evaluate the porosity, thermal stability and acidity. As presented in Figure 4.3A and Table 4-1,

STA-UiO keeps high N_2 uptake ability and thus means the highly porous structure is maintained. The bulk STA shows a very low N_2 adsorption with BET surface area of 9.5 m^2/g and total pore volume of 0.01 cm^3/g, consistent with previous reports that bulk HPA always possesses low BET surface area.[36] After STA modification, the BET surface area of the composite was reduced from the original 1423 m^2/g (pure UiO-66) to 1094 m^2/g (STA-UiO) and total pore volume also shrank from 0.65 to 0.51 cm^3/g, due to the occupation of UiO-66 pore structure by large STA molecule. However, despite the loss of the porosity, nearly 80% of the highly porous space of UiO-66 is still maintained after the STA incorporation. More importantly, their high thermal stability is confirmed by the TGA curve as no significant weight change was observed when the temperature regime was controlled between 100 and 450 °C (Figure 4.3B). These observations confirm that the prepared STA-UiO is competent to be applied as the catalyst component for dimethyl ether (DME) synthesis normally performed below 400 °C.

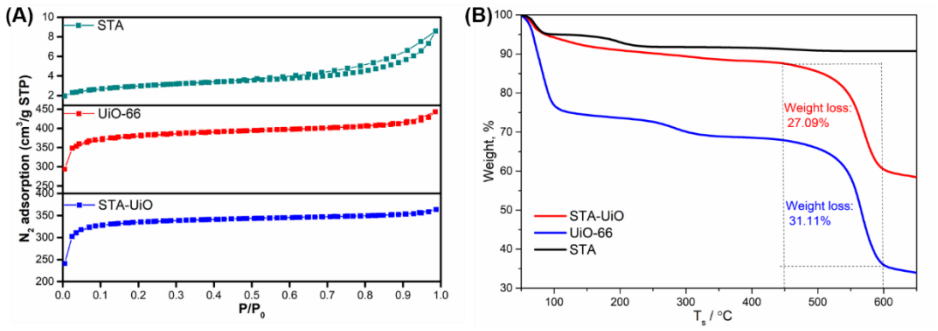

Figure 4.3. Nitrogen adsorption isotherms (A) and TGA patterns (B) of pure STA, UiO-66, and STA-UiO.

The number of acidic protons in STA-UiO was measured by the acid-base titration method to study the acidity and the results are listed in Table 4-1. For the sake of comparison, the number of protons in STA and UiO-66 were also studied. The results show that in pure STA, proton concentration was 1.39 mmol/g, but no proton was found in the pure UiO-66. After 15 wt% of STA encapsulation, proton concentration of 0.21 mmol/g was observed in STA-UiO, corresponding to the stoichiometric

composition of $SiW_{12}O_{40}^{4-}$. This indicates that the STA molecules present as the non-coordinating guests within the UiO-66 cages. [37]

Table 4-1 Physicochemical properties of STA, UiO-66, STA-UiO

Catalysts	S_{BET} (m^2/g)	Total pore volume (cm^3/g)	Average pore width (Å)	Number of protons (mmol/g)
STA	9.5	0.01	_	1.39
UiO-66	1423	0.65	9.7	0
STA-UiO	1094	0.51	11.3	0.21

To study the dispersion of Cu sites, the TEM scanning and mapping was carried out on the reduced Cu/STA-UiO (290 °C, 8 h). As can be seen from Figure 4.4, after reduction, copper sites mainly located on the surface of UiO-66. The homogenous dispersion of Cu and STA sites were also evidenced with overlapped EDS mapping of Cu and W. Thus, it is feasible to accommodate two types of active centers on a MOF framework by a facile one-pot synthesis and solid grinding method.

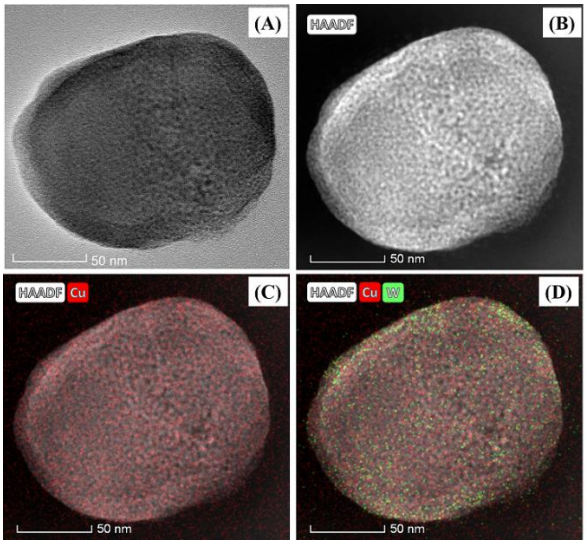

Figure 4.4. TEM image of reduced Cu/STA-UiO (A); HAADF (B), Cu EDS mapping (C) and overlapped mapping of Cu, W (D)

4.2.2 Catalytic Performance in the STD Process

The catalytic performance of prepared catalysts for DME production from syngas was evaluated at 290 °C and 3.0 MPa with an H_2/CO ratio of 2 as described in **Chapter 3** and the results are listed in Table 4-2.

Table 4-2 catalytic performance of prepared catalysts in the Syngas-to-DME process

Catalysts	Cu wt%	CO conversion, %	Product selectivity, %			
			DME	Methanol	CO_2	Other
STA-UiO	/	/	/	/	/	/
Cu/UiO-66	3.0	1.13	2.4	85.8	6.5	5.3
Cu/STA-UiO	3.0	1.99	69.3	3.20	24.94	2.56
Cu-ZnO/γ-Al_2O_3	24.0	10.15	43.02	3.21	38.54	15.23
Cu/γ-Al_2O_3	3.0	4.48	29.9	1.19	42.18	26.73

Reaction conditions: P=3.0 MPa, T=290 °C, H_2/CO/N_2 = 2/1/3, GHSV = 3000 mL/g_{cat}.h, TOS = 20 h; Cu loading is 3 *wt*% for Cu/STA-UiO, Cu/UiO-66 and Cu/γ-Al_2O_3. Other products are mainly CH_4 and C_{2+} hydrocarbons.

As can be seen in Table 4-2, there was no any activity observed on the sample of STA-UiO during the reaction owing to the lack of active centers for the unavoidable CO hydrogenation step. For Cu supported on UiO-66, methanol is the main product as the synergetic effect between Zr and Cu can facilitate the methanol formation. However, a very limited DME was produced on it due to the absence of acid function. When accommodating both Cu and STA in UiO-66, CO conversion raised from 1.13% to 1.99%, and DME selectivity was improved significantly from 2.4% to 69.3% on Cu/STA-UiO. The result vividly proves that the combination of methanol synthesis reaction and in situ dehydration reaction is thermodynamically more favourable than either of the individual reaction.[38]

Two conventional catalysts (Cu-ZnO/γ-Al_2O_3 and Cu/γ-Al_2O_3) were also prepared and tested under similar conditions for comparison purpose. Cu-ZnO/γ-Al_2O_3, the most

frequently used catalyst for DME production, gave CO conversion of 10.15% and DME selectivity of 43.02%, respectively. Even without Zn, the Cu/γ-Al_2O_3 still displayed 29.9% of DME selectivity, but which for CO_2 and other undesirable by-products were increased. In terms of selectivity, Cu/STA-UiO performed best for DME production among all five tested catalysts. This can be explained by its unique structure as presented in Figure 4.5.

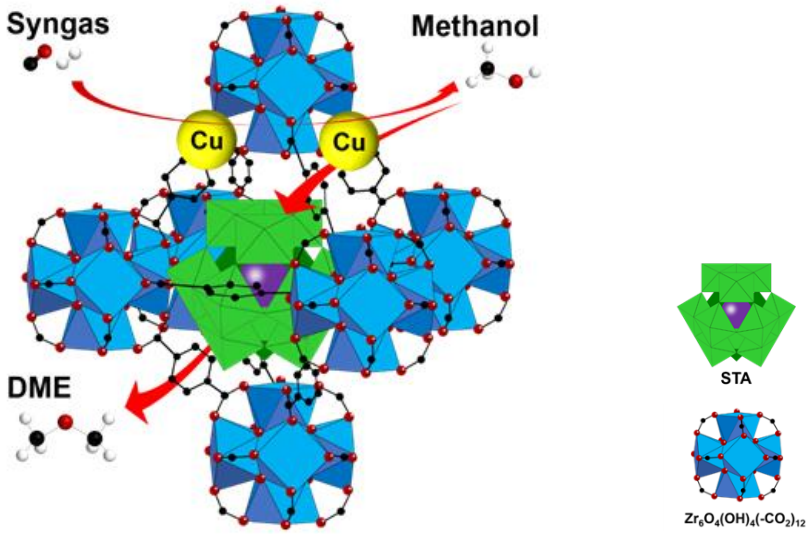

Figure 4.5. Crystal structure of Cu/STA-UiO and the possible reaction pathways for DME production. Atom labelling scheme: Zr, blue polyhedral; O, red; C, black; Si, purple; W, green polyhedron; Cu, yellow; hydrogen, white.

Firstly, the UiO-66 host can ensure the suitable distance between Cu and STA. STA molecule is encapsulated in the UiO-66 cavities, so it would not be blocked by Cu deposition on the surface of UiO-66. As elucidated previously, a detrimental effect could be induced from the partial blockage of methanol dehydration function by the methanol synthesis component and would lower DME formation and catalyst stability.[39] For a similar reason, low DME selectivity on Cu impregnated γ-Al_2O_3 was observed. Secondly, Cu and STA maintain close intimacy at one UiO-66 molecule thus the formed methanol on Cu can be dehydrated on STA immediately when it passes

through the UiO-66 framework.

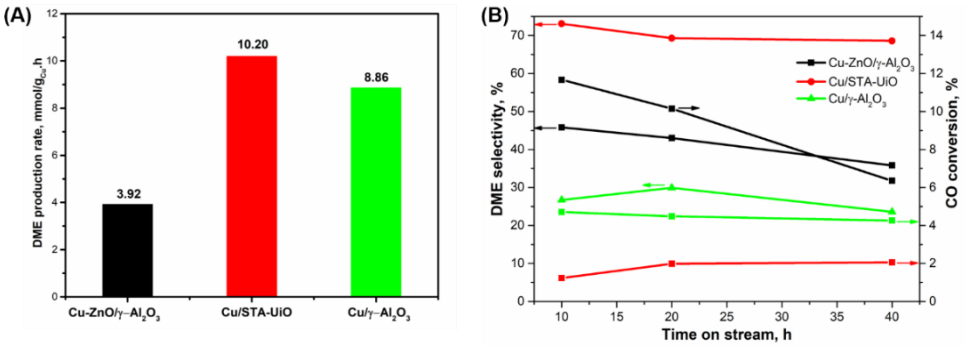

Figure 4.6. DME space-time yield (A) and stability (B) of three different catalysts

Figure 4.6A shows the space-time yield to DME of three active catalysts based on Cu content. Cu/STA-UiO exhibited a STY_{DME} of 10.2 mmol/g_{Cu}.h, greatly exceeding the STY_{DME} of 3.92 mmol/g_{Cu}.h for the Cu-ZnO/γ-Al_2O_3 and 8.86 mmol/g_{Cu}.h for the Cu impregnated γ-Al_2O_3. Two factors contribute to its superior catalytic performance. One is the large surface area and porous structure provided by the UiO-66 to disperse the active centers more homogeneously and avoid Cu sintering and the diffusion limitation of feed gas and products during the reaction. Another one is the mild Brønsted acidity of STA. It is well believed that DME formation from methanol dehydration is much favorable on Brønsted acid than Lewis acid sites.[40-42] The large density of proton in STA can improve the methanol dehydration rate thus boost the DME formation rate. While only Lewis acid sites with weak acidity exist in γ-Al_2O_3, thus DME selectivity and production rate are both low for γ-Al_2O_3 containing catalyst. Due to the above-mentioned merits, the prepared Cu/STA-UiO showed very high stability in 40 h of time on stream, with DME selectivity over 65%, as observed in long-term stability test (Figure 4.6B). However, the DME selectivity on Cu-ZnO/γ-Al_2O_3 and Cu/γ-Al_2O_3 dropped from 46% and 29.9% to 38% and 26%, respectively.

Additionally, a comparison of the catalytic performance of several representative catalysts in the literatures was also investigated and the result is listed in Table 4-3. It

is clearly showing that the prepared Cu/STA-UiO is most selective for DME formation from syngas, even under lowest syngas partial pressure (15 bar) in the feed gas. It is generally accepted that high syngas partial pressure in the feed gas favors better activity and DME selectivity. However, most traditional catalysts exhibited lower DME selectivity (below 65%) under higher pressure (40 bar or above) using almost pure syngas with short time on stream (no more than 25 h). This indicates that MOF based catalysts are potential alternatives for conventional catalysts under harsh reaction conditions.

Table 4-3 Comparisons of the catalytic performance from previous reports

Catalysts	Gas composition	Temperature (°C)	Pressure (bar)	CO conv. (%)	Selectivity (%)			TOS (h)	Ref
					DME	Methanol	CO_2		
Cu/STA-UiO	$N_2/H_2/CO$ = 3/2/1	290	30	2.0	68.7	3.3	25.5	40	This work
Cu/mesoAl	$N_2/H_2/CO$ = 5.5/63/31.5	250	50	9.6	58.9	11.4	25.0	25	[43]
Core-shell CZA@HZSM 5	$H_2/CO/CO_2/Ar$ = 59.2/32.6/5.2/3	250	50	5.59	96.6	3.4	N/A	N/A	[38] *
CZA/Nb-γ-Al_2O_3	H_2/CO = 2	265	50	8.0	64.9	6.8	27.7	~6	[44]
CZA/γ-Al_2O_3	H_2/CO = 2	240	50	53.3	58.3	8.6	31.0	~10	[45]
Pd- CZA/γ-Al_2O_3	$N_2/H_2/CO$ = 4/64/32	220	40	63	60	N/A	N/A	N/A	[46]
CZA/STA-γ-Al_2O_3	H_2/CO = 1	275	50	42	62	N/A	N/A	1	[47]

*: DME selectivity is calculated CO_2-free

Despite the high DME selectivity and space-time yield, the CO conversion of Cu/STA-UiO was lower than that of control catalysts. This could be explained by the introduction method of Cu during catalyst preparation. For Cu-ZnO/γ-Al_2O_3 and Cu/γ-Al_2O_3, copper nitrate solution was used. This will result in more homogeneous-dispersed Cu atoms on the support, more accessible to the feed gas molecules. While the solid grinding method might lead to partial Cu aggregation on the surface of STA-

UiO. To improve the catalytic performance of UiO-based catalysts, further work will be needed to address the effects of Cu introduction method, Cu/STA ratio and to optimize the reaction conditions for DME synthesis.

4.2.3 Characterization of Spent Catalysts

The XRD patterns of the prepared STA-UiO before and after reaction are exhibited in Figure 4.7. The peaks with strong intensity at 2θ values of 34.10°, 35.66°, 38.14° and 60.01° are assigned to SiC as catalyst dilute (JCPDS 01-073-1663). The characteristic peaks of UiO-66 at 2θ of 7.36° and 8.48° are also present in the XRD pattern of spent catalyst, mirroring the framework is well maintained after reaction. This confirms that UiO-66 based catalyst still has a good hydrothermal stability under high temperature and high pressure in the reducing atmosphere. However, the chemical state of Cu cannot be determined from the obtained XRD pattern. The characteristic peaks for Cu^0 at 2θ = 43.48° and 50.38° (JCPDS 00-001-1241) overlap with that of UiO-66. Thus, further XPS analysis is necessary to get more information of Cu state.

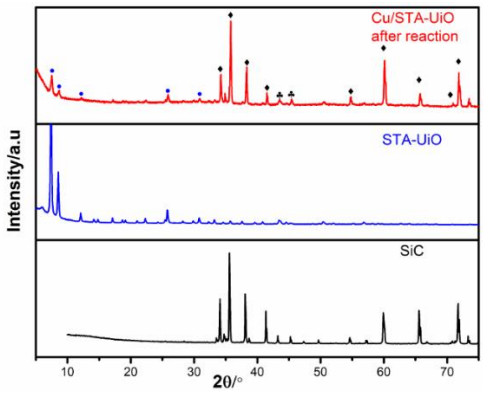

Figure 4.7. XRD pattern of fresh and spent catalysts: ♦–SiC, ●–UiO-66, ♣ – undetermined

Figure 4.8 shows the high-resolution XPS spectra of Cu and Zr in fresh and spent catalysts. Before reaction, Cu only exists in the form of Cu^{2+} (Cu 2p3/2 and Cu 2p1/2 at 934.2 and 954.3 eV) without any Cu^+ or Cu^0. In the spent catalysts, the Cu 2p3/2 band split into two peaks at 934.2 and 932.5 eV, and Cu 2p1/2 split into two peaks at

954.3 and 952.3 eV, respectively, suggesting the existence of Cu^0. Cu^{2+} also exists in the spent catalyst which might be derived from the oxidation of Cu^0 during handling and exposure in the air.

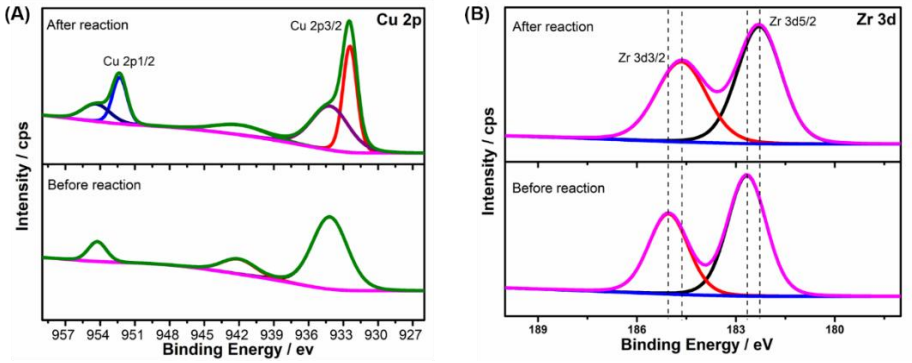

Figure 4.8. High-resolution XPS of Cu (A) and Zr (B) in fresh and spent Cu/STA-UiO

As for Zr, the Zr 3d3/2 and Zr 3d5/2 spectrum exhibit binding energy of 185.1 and 182.6 eV corresponding to Zr (IV) oxidation state in the Zr_6 cluster $[Zr_6O_4(OH)_4(CO_2)_{12}]$ of UiO-66. However, in the spent catalyst, both peaks shift to lower binding energy (182.6 to 182.2 eV, 185.1 to 184.7 eV), indicating that part of Zr (IV) was reduced to Zr(III). The change of Zr existence state suggests the strong interaction between Zr and Cu known as the SMSI effect. A spillover model over Cu and ZrO_2 has been proposed in previous studies for CO and CO_2 hydrogenation to produce methanol [10]**.** In this mechanism, spillover of adsorbed CO from metallic Cu sites to ZrO_2 can facilitate the formation of formate species, in the meanwhile, the atom H generated from dissociated adsorption of hydrogen on Cu migrates to the adjacent ZrO_2 surface and further reacts with formate stepwise to form methylenebisoxy, methoxide and finally methanol. In this work, the peak shift for Zr 3d clearly demonstrates the SMSI effect derived from spillover between Cu and $Zr_6O_4(OH)_4(CO_2)_{12}$, which is also detected in the recent study on CO_2 hydrogenation using Zr-MOF.[48, 49]

4.3 Conclusions

The catalytic conversion of syngas to DME was investigated on a novel Cu loaded STA-UiO catalyst. The STA (15%) encapsulated UiO-66 catalyst was synthesized by dissolving STA into the staring raw material solutions for UiO-66 formation. After heat-treatment at 120 °C for 24 h, the STA encapsulation and UiO-66 growth were completed simultaneously. Cu was introduced via the solid grinding of $Cu(acac)_2$ and STA-UiO. TGA, FT-IR and BET analysis reveal similar thermal and textural properties of STA-UiO to that of pure UiO-66. No STA aggregation or framework destruction was observed with XRD/TEM analysis. A DME selectivity of 69.6% is achieved on Cu/STA-UiO, much higher than that on Cu/UiO-66, Cu-ZnO/γ-Al_2O_3 and Cu/γ-Al_2O_3. This is explained by the close intimacy between Cu atoms and STA molecules as well as the increased Brønsted acid sites. Meanwhile, the prepared Cu/STA-UiO results in the highest DME production rate, almost threefold of conventional Cu-ZnO based catalyst. The strong interaction between Cu and Zr oxide is clearly proved by XPS analysis of fresh and spent catalysts. This work presents the possibility of application of MOF based material in complicated reactions which need two or more active functions. However, the catalyst design should be further studied to get more homogeneous dispersion of active centers and thus better catalytic performance.

References

1. Sun, J.; Yang, G.; Yoneyama, Y.; Tsubaki, N., Catalysis chemistry of dimethyl ether synthesis. *ACS Catal.* **2014,** *4* (10), 3346-3356.

2. Zhang, P.; Tan, L.; Yang, G.; Tsubaki, N., One-pass selective conversion of syngas to para-xylene. *Chem. Sci.* **2017,** *8* (12), 7941-7946.

3. Fleisch, T.; Basu, A.; Gradassi, M.; Masin, J., Dimethyl ether: a fuel for the 21st century. In *Stud. Surf. Sci. Catal.*, Elsevier: 1997; Vol. 107, pp 117-125.

4. García-Trenco, A.; Martínez, A., Direct synthesis of DME from syngas on hybrid

CuZnAl/ZSM-5 catalysts: New insights into the role of zeolite acidity. *Appl. Catal. A-Gen.* **2012,** *411*, 170-179.

5. Xu, M.; Lunsford, J. H.; Goodman, D. W.; Bhattacharyya, A., Synthesis of dimethyl ether (DME) from methanol over solid-acid catalysts. *Appl. Catal. A-Gen.* **1997,** *149* (2), 289-301.

6. Garcia-Trenco, A.; White, E. R.; Shaffer, M. S. P.; Williams, C. K., A one-step Cu/ZnO quasi-homogeneous catalyst for DME production from syn-gas. *Catal. Sci. Technol.* **2016,** *6* (12), 4389-4397.

7. Moradi, G.; Nosrati, S.; Yaripor, F., Effect of the hybrid catalysts preparation method upon direct synthesis of dimethyl ether from synthesis gas. *Catal. Commun.* **2007,** *8* (3), 598-606.

8. Asthana, S.; Samanta, C.; Voolapalli, R. K.; Saha, B., Direct conversion of syngas to DME: synthesis of new Cu-based hybrid catalysts using Fehling's solution, elimination of the calcination step. *J. Mater. Chem. A* **2017,** *5* (6), 2649-2663.

9. Asthana, S.; Samanta, C.; Bhaumik, A.; Banerjee, B.; Voolapalli, R. K.; Saha, B., Direct synthesis of dimethyl ether from syngas over Cu-based catalysts: Enhanced selectivity in the presence of MgO. *J. Catal.* **2016,** *334*, 89-101.

10. Fisher, I. A.; Bell, A. T., In Situ Infrared Study of Methanol Synthesis from H_2/CO over Cu/SiO_2 and Cu/ZrO_2/SiO_2. *J. Catal.* **1998,** *178* (1), 153-173.

11. Liu, X.-M.; Lu, G.; Yan, Z.-F.; Beltramini, J., Recent advances in catalysts for methanol synthesis via hydrogenation of CO and CO_2. *Ind. Eng. Chem. Res.* **2003,** *42* (25), 6518-6530.

12. García-Trenco, A.; Martínez, A., A rational strategy for preparing Cu–ZnO/H-ZSM-5 hybrid catalysts with enhanced stability during the one-step conversion of syngas to dimethyl ether (DME). *Appl. Catal. A-Gen.* **2015,** *493*, 40-49.

13. Fei, J.; Hou, Z.; Zhu, B.; Lou, H.; Zheng, X., Synthesis of dimethyl ether (DME) on modified HY zeolite and modified HY zeolite-supported Cu–Mn–Zn catalysts. *Appl. Catal. A-Gen.* **2006,** *304*, 49-54.

14. Ateka, A.; Pérez-Uriarte, P.; Sánchez-Contador, M.; Ereña, J.; Aguayo, A. T.; Bilbao, J., Direct synthesis of dimethyl ether from syngas on CuO-ZnO-MnO/SAPO-18 bifunctional catalyst. *Int. J. Hydrog. Energy* **2016,** *41* (40), 18015-18026.

15. Ciftci, A.; Varisli, D.; Cem Tokay, K.; Asli Sezgi, N.; Dogu, T., Dimethyl ether, diethyl ether & ethylene from alcohols over tungstophosphoric acid based mesoporous catalysts.

Chem. Eng. J. **2012,** *207-208*, 85-93.

16. Varisli, D.; Dogu, T.; Dogu, G., Novel mesoporous nanocomposite WO_x-silicate acidic catalysts: ethylene and diethylether from ethanol. *Ind. Eng. Chem. Res.* **2008,** *48* (21), 9394-9401.

17. Ciftci, A.; Varisli, D.; Dogu, T., Dimethyl Ether Synthesis over Novel Silicotungstic Acid Incorporated Nanostructured Catalysts. *Int. J. Chem. React. Eng.* **2010,** *8* (1).

18. Ladera, R. M.; Fierro, J. L. G.; Ojeda, M.; Rojas, S., TiO_2-supported heteropoly acids for low-temperature synthesis of dimethyl ether from methanol. *J. Catal.* **2014,** *312*, 195-203.

19. Alharbi, W.; Kozhevnikova, E. F.; Kozhevnikov, I. V., Dehydration of methanol to dimethyl ether over heteropoly acid catalysts: The relationship between reaction rate and catalyst acid strength. *ACS Catal.* **2015,** *5* (12), 7186-7193.

20. Wang, X. S.; Li, L.; Liang, J.; Huang, Y. B.; Cao, R., Boosting Oxidative Desulfurization of Model and Real Gasoline over Phosphotungstic Acid Encapsulated in Metal–Organic Frameworks: The Window Size Matters. *ChemCatChem* **2017,** *9* (6), 971-979.

21. Yang, L.; Naruke, H.; Yamase, T., A novel organic/inorganic hybrid nanoporous material incorporating Keggin-type polyoxometalates. *Inorg. Chem. Commun.* **2003,** *6* (8), 1020-1024.

22. Zhou, E. L.; Qin, C.; Wang, X. L.; Shao, K. Z.; Su, Z. M., Steam-Assisted Synthesis of an Extra-Stable Polyoxometalate-Encapsulating Metal Azolate Framework: Applications in Reagent Purification and Proton Conduction. *Chem. - Eur. J.* **2015,** *21* (37), 13058-13064.

23. Ribeiro, S.; Granadeiro, C. M.; Silva, P.; Paz, F. A. A.; de Biani, F. F.; Cunha-Silva, L.; Balula, S. S., An efficient oxidative desulfurization process using terbium-polyoxometalate@ MIL-101 (Cr). *Catal. Sci. Technol.* **2013,** *3* (9), 2404-2414.

24. Ribeiro, S.; Barbosa, A. D. S.; Gomes, A. C.; Pillinger, M.; Gonçalves, I. S.; Cunha-Silva, L.; Balula, S. S., Catalytic oxidative desulfurization systems based on Keggin phosphotungstate and metal-organic framework MIL-101. *Fuel Process. Technol.* **2013,** *116*, 350-357.

25. Deng, Q.; Nie, G.; Pan, L.; Zou, J.-J.; Zhang, X.; Wang, L., Highly selective self-condensation of cyclic ketones using MOF-encapsulating phosphotungstic acid for renewable high-density fuel. *Green Chem.* **2015,** *17* (8), 4473-4481.

26. Bromberg, L.; Diao, Y.; Wu, H.; Speakman, S. A.; Hatton, T. A., Chromium (III)

terephthalate metal organic framework (MIL-101): HF-free synthesis, structure, polyoxometalate composites, and catalytic properties. *Chem. Mater.* **2012,** *24* (9), 1664-1675.

27. Zang, Y.; Shi, J.; Zhao, X.; Kong, L.; Zhang, F.; Zhong, Y., Highly stable chromium (III) terephthalate metal organic framework (MIL-101) encapsulated 12-tungstophosphoric heteropolyacid as a water-tolerant solid catalyst for hydrolysis and esterification. *React. Kinet. Mech. Catal.* **2013,** *109* (1), 77-89.

28. Juan-Alcañiz, J.; Ramos-Fernandez, E. V.; Lafont, U.; Gascon, J.; Kapteijn, F., Building MOF bottles around phosphotungstic acid ships: One-pot synthesis of bi-functional polyoxometalate-MIL-101 catalysts. *J. Catal.* **2010,** *269* (1), 229-241.

29. Mao, D.; Xia, J.; Chen, Q.; Lu, G., Highly effective conversion of syngas to dimethyl ether over the hybrid catalysts containing high-silica HMCM-22 zeolites. *Catal. Commun.* **2009,** *10* (5), 620-624.

30. Jin, D.; Zhu, B.; Hou, Z.; Fei, J.; Lou, H.; Zheng, X., Dimethyl ether synthesis via methanol and syngas over rare earth metals modified zeolite Y and dual Cu–Mn–Zn catalysts. *Fuel* **2007,** *86* (17), 2707-2713.

31. Mao, D.; Yang, W.; Xia, J.; Zhang, B.; Song, Q.; Chen, Q., Highly effective hybrid catalyst for the direct synthesis of dimethyl ether from syngas with magnesium oxide-modified HZSM-5 as a dehydration component. *J. Catal.* **2005,** *230* (1), 140-149.

32. Zhang, W.; Lu, G.; Cui, C.; Liu, Y.; Li, S.; Yan, W.; Xing, C.; Chi, Y. R.; Yang, Y.; Huo, F., A Family of Metal-Organic Frameworks Exhibiting Size-Selective Catalysis with Encapsulated Noble-Metal Nanoparticles. *Adv. Mater.* **2014,** *26* (24), 4056-4060.

33. Cavka, J. H.; Jakobsen, S.; Olsbye, U.; Guillou, N.; Lamberti, C.; Bordiga, S.; Lillerud, K. P., A new zirconium inorganic building brick forming metal organic frameworks with exceptional stability. *J. Am. Chem. Soc.* **2008,** *130* (42), 13850-13851.

34. Rocchiccioli-Deltcheff, C.; Fournier, M.; Franck, R.; Thouvenot, R., Vibrational investigations of polyoxometalates. 2. Evidence for anion-anion interactions in molybdenum(VI) and tungsten(VI) compounds related to the Keggin structure. *Inorg. Chem.* **1983,** *22* (2), 207-216.

35. Sabyrov, K.; Jiang, J.; Yaghi, O. M.; Somorjai, G. A., Hydroisomerization of n-Hexane Using Acidified Metal–Organic Framework and Platinum Nanoparticles. *J. Am. Chem. Soc.*

2017, *139* (36), 12382-12385.

36. Sun, C.-Y.; Liu, S.-X.; Liang, D.-D.; Shao, K.-Z.; Ren, Y.-H.; Su, Z.-M., Highly stable crystalline catalysts based on a microporous metal− organic framework and polyoxometalates. *J. Am. Chem. Soc.* **2009,** *131* (5), 1883-1888.

37. Zhang, F.; Jin, Y.; Shi, J.; Zhong, Y.; Zhu, W.; El-Shall, M. S., Polyoxometalates confined in the mesoporous cages of metal–organic framework MIL-100(Fe): Efficient heterogeneous catalysts for esterification and acetalization reactions. *Chem. Eng. J.* **2015,** *269*, 236-244.

38. Yang, G.; Tsubaki, N.; Shamoto, J.; Yoneyama, Y.; Zhang, Y., Confinement effect and synergistic function of H-ZSM-5/Cu-ZnO-Al_2O_3 capsule catalyst for one-step controlled synthesis. *J. Am. Chem. Soc.* **2010,** *132* (23), 8129-8136.

39. García-Trenco, A.; Vidal-Moya, A.; Martínez, A., Study of the interaction between components in hybrid CuZnAl/HZSM-5 catalysts and its impact in the syngas-to-DME reaction. *Catal. Today* **2012,** *179* (1), 43-51.

40. Yaripour, F.; Baghaei, F.; Schmidt, I.; Perregaard, J., Catalytic dehydration of methanol to dimethyl ether (DME) over solid-acid catalysts. *Catal. Commun.* **2005,** *6* (2), 147-152.

41. Yaripour, F.; Baghaei, F.; Schmidt, I.; Perregaard, J., Synthesis of dimethyl ether from methanol over aluminium phosphate and silica–titania catalysts. *Catal. Commun.* **2005,** *6* (8), 542-549.

42. Blaszkowski, S. R.; van Santen, R. A., The Mechanism of Dimethyl Ether Formation from Methanol Catalyzed by Zeolitic Protons. *J. Am. Chem. Soc.* **1996,** *118* (21), 5152-5153.

43. Ham, H.; Kim, J.; Cho, S. J.; Choi, J. H.; Moon, D. J.; Bae, J. W., Enhanced Stability of Spatially Confined Copper Nanoparticles in an Ordered Mesoporous Alumina for Dimethyl Ether Synthesis from Syngas. *ACS Catal.* **2016,** *6* (9), 5629-5640.

44. Lima, S. H.; Forrester, A. M. S.; Amparo Palacio, L.; Faro, A. C., Niobia-alumina as methanol dehydration component in mixed catalyst systems for dimethyl ether production from syngas. *Appl. Catal. A-Gen.* **2014,** *488*, 19-27.

45. Moradi, G.; Nazari, M.; Yaripour, F., The interaction effects of dehydration function on catalytic performance and properties of hybrid catalysts upon LPDME process. *Fuel Process. Technol.* **2008,** *89* (12), 1287-1296.

46. Huang, M. H.; Lee, H. M.; Liang, K. C.; Tzeng, C. C.; Chen, W. H., An experimental study

on single-step dimethyl ether (DME) synthesis from hydrogen and carbon monoxide under various catalysts. *Int. J. Hydrog. Energy* **2015,** *40* (39), 13583-13593.

47. Bayat, A.; Dogu, T., Optimization of CO_2/CO Ratio and Temperature for Dimethyl Ether Synthesis from Syngas over a New Bifunctional Catalyst Pair Containing Heteropolyacid Impregnated Mesoporous Alumina. *Ind. Eng. Chem. Res.* **2016,** *55* (44), 11431-11439.

48. Rungtaweevoranit, B.; Baek, J.; Araujo, J. R.; Archanjo, B. S.; Choi, K. M.; Yaghi, O. M.; Somorjai, G. A., Copper Nanocrystals Encapsulated in Zr-based Metal–Organic Frameworks for Highly Selective CO_2 Hydrogenation to Methanol. *Nano Lett.* **2016,** *16* (12), 7645-7649.

49. An, B.; Zhang, J.; Cheng, K.; Ji, P.; Wang, C.; Lin, W., Confinement of Ultrasmall Cu/ZnO_x Nanoparticles in Metal–Organic Frameworks for Selective Methanol Synthesis from Catalytic Hydrogenation of CO_2. *J. Am. Chem. Soc.* **2017,** *139* (10), 3834-3840.

Chapter 5 Cu/ZnO catalysts derived from bimetallic metal-organic framework for dimethyl ether synthesis from syngas with enhanced selectivity and stability

Abstract

Direct syngas-to-dimethyl ether (STD) process allows higher CO conversion and simpler reactor design that translates to lower production cost relative to the conventional two-step process that involves methanol synthesis and its dehydration to dimethyl ether (DME). Although the potential of Cu/ZnO-based catalysts highly active for methanol synthesis in STD process has been recognized, the sintering of Cu during extended reaction operation generally leads to their performance deterioration. In this work, we synthesized a bimetallic Cu/ZnO catalyst that inherits the octahedron structure of its precursor, i.e., Zn-doped Cu-BTC metal-organic framework (MOF) via one-pot solvothermal route followed by two-step calcination in N_2 and air. Powder X-ray diffraction and energy dispersive spectroscopy results reveal that the resultant Cu/ZnO MOF-derived catalysts contain mainly CuO and ZnO phases, which are distributed homogeneously over the catalyst surface. Increasing temperature from 350 to 550 ^{o}C in the final calcination step in air leads to the reduction in the porosity and surface area but an increase of CuO crystallite size. The catalytic performance of the best catalyst, i.e., CZ-350/A (calcined in air at 350 ^{o}C) was evaluated by combining it with γ-Al_2O_3 as the methanol dehydration component where up to 7.74% CO conversion and 70.05% DME selectivity were achieved. Such performance is superior to the conventional Cu/ZnO catalyst counterpart (CZ-CP/A) of CZ-350/A, which was made via co-precipitation route. CZ-350/A also showed lower CO conversion deterioration rate and higher DME selectivity during the long term continuous STD reaction due to the confinement of Cu nanoparticles within octahedron matrix which

hinders their migration and aggregation. Moreover, partial reduction of ZnO in the activated CZ-350 prompts the formation of Cu^{+}-O-Zn, facilitating the DME production with the highest selectivity compared to literature results.

The content of this chapter is published in Small 2020, 16 (14).

5.1 Introduction

Syngas, the mixture of CO and H_2, is a key chemical intermediate for the utilization of non-petroleum carbon resources.[1] Syngas can be produced from natural gas, shale gas, coal, biomass, and organic wastes.[1-3] Through a versatile "Fischer-Tropsch synthesis (FTS)" process, syngas can be transformed into valuable chemicals such as hydrocarbons (gasoline, diesel fuel, light olefins, and aromatics) and oxygenates (alcohols and ether).[4-8] One of the most attractive oxygenates products from FTS process is dimethyl ether (DME) given its eco-friendly properties. DME is both a promising alternative of diesel fuel with higher cetane number (between 55 and 60) and low soot emission as well as an important feedstock for the production of methyl acetate, fuel cells, and aromatics.[9-11]

DME production has traditionally been realized via a two-step process, where methanol is firstly synthesized from syngas and then dehydrated to DME. However, the first step, methanol synthesis, is limited by the thermodynamic constraints and as a result, the overall CO conversion is relatively low. As an alternative to such process, a one-step process, where direct "syngas-to-DME (STD)" conversion occurs in a single reactor via consecutive methanol synthesis and methanol dehydration reactions, has been developed. Compared to the two-step process, the STD process is more thermodynamically and economically attractive to achieve higher CO conversion.[12] Catalyst for STD reaction is typically a composite (hybrid) catalyst made by combining methanol synthesis catalyst component (Cu/Zn, Cu/Zn/Al, and/or Zn/Cr) with methanol dehydration catalyst component (zeolite, γ-Al_2O_3, SiO_2-Al_2O_3, and/or heteropoly acid).[13-15]

Since copper/zinc oxide (Cu/ZnO)-based catalysts have been widely used as a

methanol synthesis catalyst component in STD process, the interaction between Cu and ZnO and the role of their interfacial areas have been widely documented.[16-19] The presence of ZnO in particular, is reported to be essential to achieve high dispersion of Cu during the catalyst preparation given its role as a geometrical spacer between Cu nanoparticles.[20, 21] Moreover, a strong metal-support interaction (SMSI) between ZnO and Cu is demonstrated to be responsible for the *in situ* formation of methanol-active copper.[14] Partial coverage of Cu nanoparticles with ZnO was also determined as the main contributing factor behind the formation of stable surface intermediates such as HCO during the methanol synthesis reaction.[22]

A main obstacle towards the large-scale application of Cu/ZnO-based catalysts nonetheless comes from their rapid deactivation due to the sintering of Cu at high temperature (above 500 K).[23] This issue becomes even more severe in STD process given the water presence during the methanol dehydration step.[11, 24] To solve this issue, for example, several promoters such as Al_2O_3, ZrO_2, Li_2O, and MgO can be added to obtain and retain homogeneous dispersion of Cu and Zn on the catalysts.[13, 14, 25, 26] These promoter-containing catalysts are normally prepared using sodium carbonate (Na_2CO_3) as a precipitant. However, the presence of residual Na^+ may enhance the aggregation of Cu, which leads to lower catalytic activity.[27] Alternatively, several recent works have also achieved homogeneous dispersion of Cu and Zn on the catalysts by loading Cu/ZnO onto SBA-15 or carbon nanotubes or by forming colloidal nanoparticles of Cu/ZnO.[28-31] These two methods nevertheless require expensive raw materials and lengthy preparation procedure. Thus, it becomes necessary to develop new synthesis procedure to achieve highly active and stable Cu/ZnO-based catalysts.

A relatively new class of crystalline materials made of “metal” ions or clusters coordinated to “organic” ligands with one-, two-, or three-dimensional arrangements, the so-called metal-organic frameworks (MOFs) have recently

emerged, which offers a unique platform to design a novel catalyst with tunable morphology, porous properties, and catalytic activity.[32, 33] A few recent studies have attempted to apply MOF-derived metal oxides to the catalytic gas conversion. For example, Zheng *et al*. prepared a Cu/Zn bimetallic MOF ($Cu_{1.1}Zn_{1.9}(BTC)_2 \cdot 9.4(H_2O)$, BTC:1,3,5-benzenetricarboxylic acid) and obtained a core-shell Cu@ZnO framework by performing subsequent controlled calcination of the prepared MOF.[34] Using such framework, relatively high interfacial area between Cu and ZnO can be achieved while minimizing the tendency for Cu sintering since the outer ZnO shell serves as a physical spacer between Cu particles layers. The resultant MOF-derived $Cu_{1.1}Zn_{1.9}O_3$ showed higher activity and stability relative to its $Cu_{1.1}Zn_{1.9}O_3$ analog, which was prepared by co-precipitation method. Zhang *et al.* also reported that a mixture of copper and zinc oxide supported on carbon framework (Cu/ZnO@C) prepared *via* pyrolysis of Zn-doped Cu-MOF in argon exhibited stable catalytic activity in reverse water-gas shift reaction performed at 500 °C.[35]

To date, few studies have evaluated the application of MOF-derived Cu/ZnO in STD reaction. Herein, Zn-doped Cu-BTC MOF, also known as HKUST-1 ($Cu_3(BTC)_2 \cdot 9.4(H_2O)$) was synthesized *via* one-pot solvothermal process. The resultant product was then subjected to two-step thermal treatment process (i.e., carbonization in N_2 followed by calcination in air at different temperatures) to obtain the final Cu/ZnO-containing products as illustrated in Scheme 5-1. The structure and physicochemical properties of the synthesized MOF and Cu/ZnO catalysts were carefully characterized. Their catalytic activities for syngas to DME conversion in STD process were subsequently evaluated.

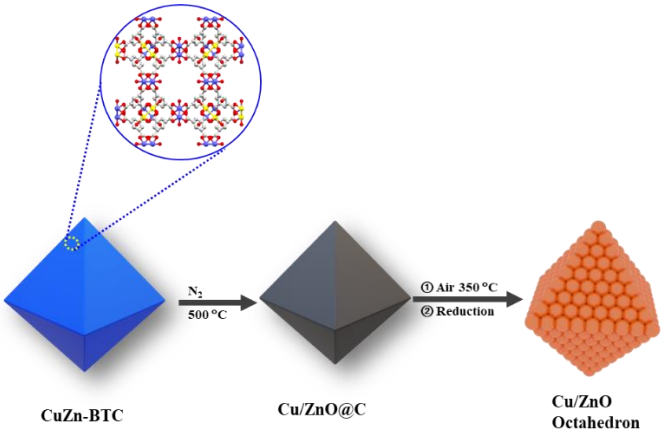

Scheme 5-1. Preparation of octahedral Cu/ZnO catalyst via pyrolysis of CuZn-BTC MOF.

5.2. Results and discussion

5.2.1 Catalyst Characterization

Two different CuZn-BTC precursors (CuZn-BTC-1 and CuZn-BTC-2) were synthesized. Both precursors were made *via* identical solvothermal process as described in the Chapter 3, during which the molar ratio of Cu to Zn was kept at 1:2 for CuZn-BTC-1 and 1:3 for CuZn-BTC-2. Excess Zn was applied here to achieve Zn doping in the MOF framework. Nonetheless, inductively coupled plasma optical emission spectroscopy (ICP-OES) results show that the final Cu to Zn molar ratios in CuZn-BTC-1 and CuZn-BTC-2 were 3.3:1 (Zn^{2+} constitutes 23% of the total metal ions (Cu^{2+} and Zn^{2+})) and 2:1 (Zn^{2+} constitutes 33% of the total metal ions), respectively; suggesting that the CuZn-BTC MOF framework can only accommodate much lower amount of Zn than the intended amount during the solvothermal process. This can be rationalized in terms of the size mismatch between Zn^{2+} and Cu^{2+}, i.e., Zn^{2+} has a slightly larger ionic radius (0.68 Å) relative to Cu^{2+} (0.65 Å) [36], which hinders Zn^{2+} incorporation into Cu^{2+}-containing MOF framework as is observed also in the work of Zhang *et al*.[35]

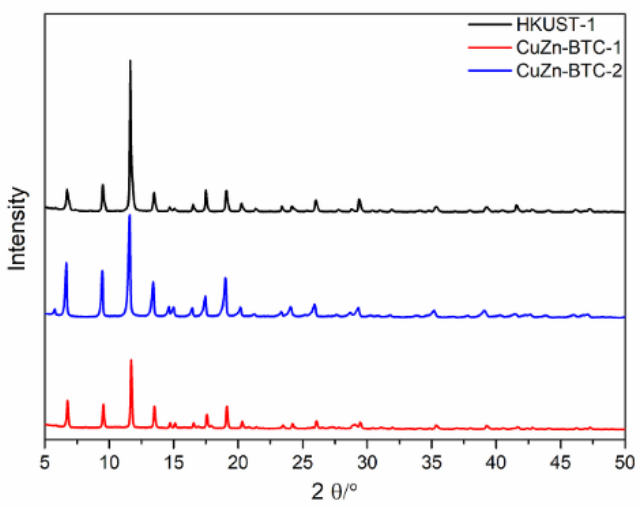

Figure 5.1. Powder XRD patterns of HKUST-1, CuZn-BTC-1, and CuZn-BTC-2.

The successful formation of Cu and Zn bimetallic MOFs *via* the reaction of 1,3,5-benzenetricarboxylic acid with Cu and Zn ions in a dimethylformamide (DMF) solution was confirmed using powder XRD, SEM, and TEM. Figure 5.1 shows the powder XRD patterns of CuZn-BTC-1 and CuZn-BTC-2. The pattern of HKUST-1 is also included as comparison (JCPDS 00-064-0936).[37] CuZn-BTC-1 and CuZn-BTC-2 clearly exhibit identical characteristic peaks at the same 2θ positions as HKUST-1, which indicates the presence of MOF structure and also the fact that Zn doping into HKUST-1 did not lead to the formation of phase impurities or structure modification with respect to HKUST-1. Figure 5.2 display the low magnification (Figure 5.2a, d) and high magnification (Figure 5.2b, e) SEM images of MOF particle of CuZn-BTC-1 and CuZn-BTC-2, respectively, and Figure 5.2c and Figure 5.2f show their respective TEM images. Both samples have octahedron shape with base length size that varies between 2 and 20 μm. SEM-EDS elemental mapping was also performed on the single MOF particle of CuZn-BTC-2, the results of which are shown in Figure 5.2g-i. Cu and Zn were clearly distributed homogeneously on the surface of CuZn-BTC-2, which suggests the successful formation of CuZn-BTC MOF in single crystalline phase.

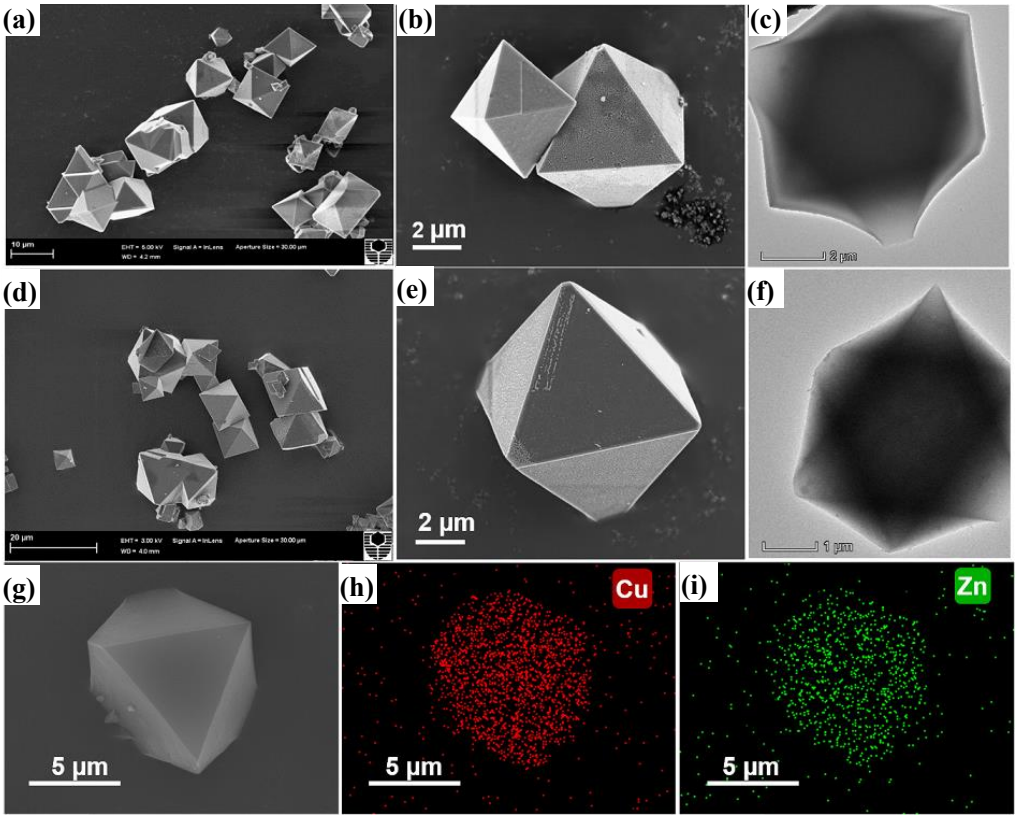

Figure 5.2. (a, d) Low magnification and (b, e) high magnification SEM images and (c, f) TEM images of CuZn-BTC-1, and CuZn-BTC-2; (g, h, i) SEM-EDS mapping results and respective distributions of Cu and Zn in the single CuZn-BTC-2 crystal.

Pre-calcination step in inert gas atmosphere is required to achieve porous structure with polyhedral morphology characteristics of MOF, during which the carbonization of organic linker portion, i.e., BTC, occurred. Direct calcination of MOF in oxidizing air atmosphere, on the other hand, may cause serious structure damage from the combustion of organic ligands.[33, 38] Zhang *et al*. has demonstrated that their CuZn-BTC MOF can be transformed into Cu/ZnO@C via carbonization at 500 °C.[35] Therefore, here we denote CuZn-BTC-2 sample subjected to the first calcination in N_2 but not yet subjected to the second calcination in air as "Cu/ZnO@C precursor". Thermal gravimetric analysis (TGA) results in air shows that Cu/ZnO@C precursor started to decompose upon heating above 300 °C (Figure 5.3). This suggests that the subsequent calcination in air at 350-550 °C for 4 hours should lead to the almost complete

decomposition of carbon, leaving mostly CuO and ZnO constituents in the framework.

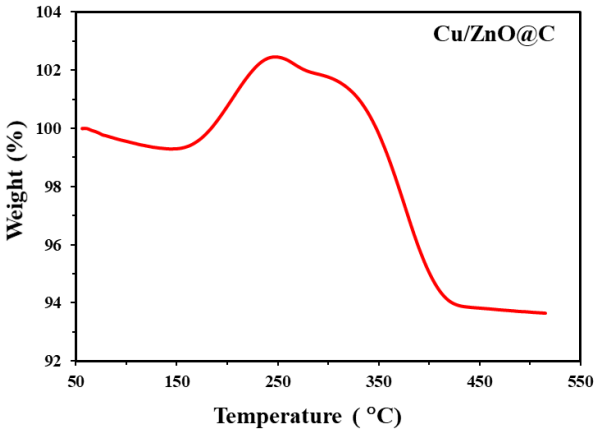

Figure 5.3. Weight change profile of Cu/ZnO@C precursor during thermal gravimetric analysis in air upon heating from 50 ˚C to 500 °C.

Figure 5.4 shows the powder XRD patterns of CZ-350, CZ-450, and CZ-550. The pattern of CZ-1, i.e., CuZn-BTC-1 that was subjected to calcination at 500 ^{o}C in N_2 and another calcination at 350 ^{o}C in air is also included as comparison. The characteristic peaks of HKUST-1 MOF observed earlier in Figure 5.1 for CuZn-BTC-1 and CuZn-BTC-2 disappear after the two-step calcination process. All of the diffraction peaks in CZ-350, CZ-450, CZ-550, and CZ-1 can be attributed to the characteristic peaks of CuO (JCPDS 01-080-1268) and ZnO (JCPDS 00-036-1451). Our calculations using half-width of CuO (111) peak and the Scherrer equation ($D=k\lambda/\beta \cos\theta$) reveal increasing crystallite size of the metal oxide with increasing calcination temperature where the crystallite size of CuO in CZ-350, CZ-450, and CZ-550, for example, are 28.9 nm, 33.6 nm, and 58.2 nm, respectively (shown in Table 5-1). Such trend is consistent with that observed by others.[32] Relative to these three samples, CuO in CZ-1 nonetheless has significantly larger crystallite size of 95.2 nm. The smaller CuO size in CZ-350 or CZ-450 is due to the larger Zn content playing the role of nanospacers to

restrict CuO nanoparticle growth. Apparently, the reduced Zn content in the MOF skeleton (CuZn-BTC-1) could not sufficiently prevent such particle overgrowth during the pyrolysis process thus large particle with size up to 95.2 nm was observed in CZ-1. We also synthesized two conventional Cu/ZnO catalyst samples via co-precipitation of Cu^{2+} and Zn^{2+} with sodium carbonate (Na_2CO_3) followed by calcination at 350 °C in air as baseline comparison, which contain Cu:Zn in identical molar ratios to CuZn-BTC-1 (3.3:1) and CuZn-BTC-2 (2:1). The former and the latter are labelled as CZ-CP-1 and CZ-CP, respectively. It is noteworthy that CZ-CP-1 and CZ-CP actually have significantly smaller CuO crystallite sizes of 52.1 nm and 9.6 nm, respectively, relative to their MOF-derived analogues, i.e., CZ-1 and CZ-350. Powder XRD patterns of CZ-CP-1 and CZ-CP are given as Figure 5.4 as well. Such discrepancy in the crystallite sizes is consistent with the higher calcination temperature and the longer calcination duration applied to MOF-derived Cu/ZnO catalysts samples.

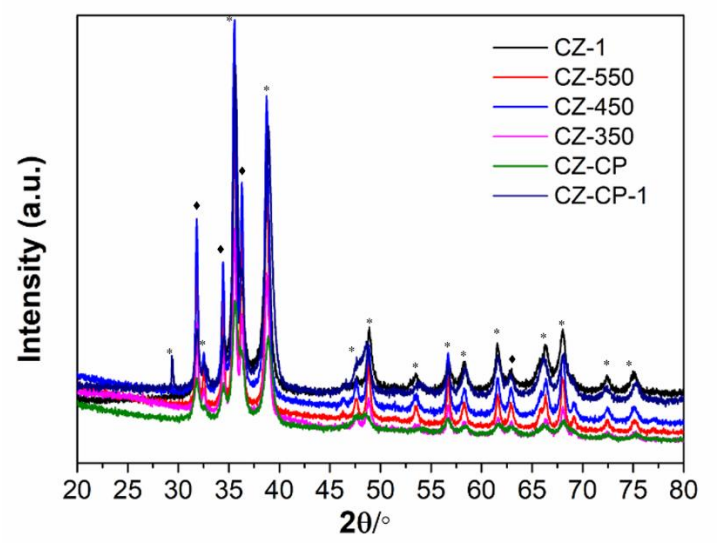

Figure 5.4. Powder XRD patterns of CZ-350, CZ-450, CZ-550, and CZ-1 derived from MOF and CZ-CP and CZ-CP-1 prepared by co-precipitation method. Note that "∗" and "♦" symbols represent characteristic peaks of CuO and ZnO, respectively.

Figure 5.5a-d display the SEM images of four MOFs-derived Cu/ZnO catalysts, i.e., CZ-350, CZ-450, CZ-550 and CZ-1, respectively. The octahedron morphology and MOF structure originally observed in CuZn-BTC-2 were retained at the end of the two-step calcination process. It is worth noting however that the surface of CZ-350 looks much rougher than that of CuZn-BTC-2 and contains some numerous open pores. Such structure preservation can be achieved since the carbon matrix, which was obtained at the end of the carbonization step, functions as a skeleton host for CuO and ZnO particles during the 2nd calcination step in air. High-angle annular dark-field-scanning transmission electron microscopy image of CZ-350 and the corresponding EDS profile map (Figure 5.5g-i) reveal homogeneous distribution of Cu and Zn on the octahedron structure. The two conventional Cu/ZnO catalyst samples, i.e., CZ-CP-1 and CZ-CP, on the other hand, have irregular, loose floccules morphology made of CuO and ZnO nanoparticles as observed in Figure 5.5e and f, respectively.

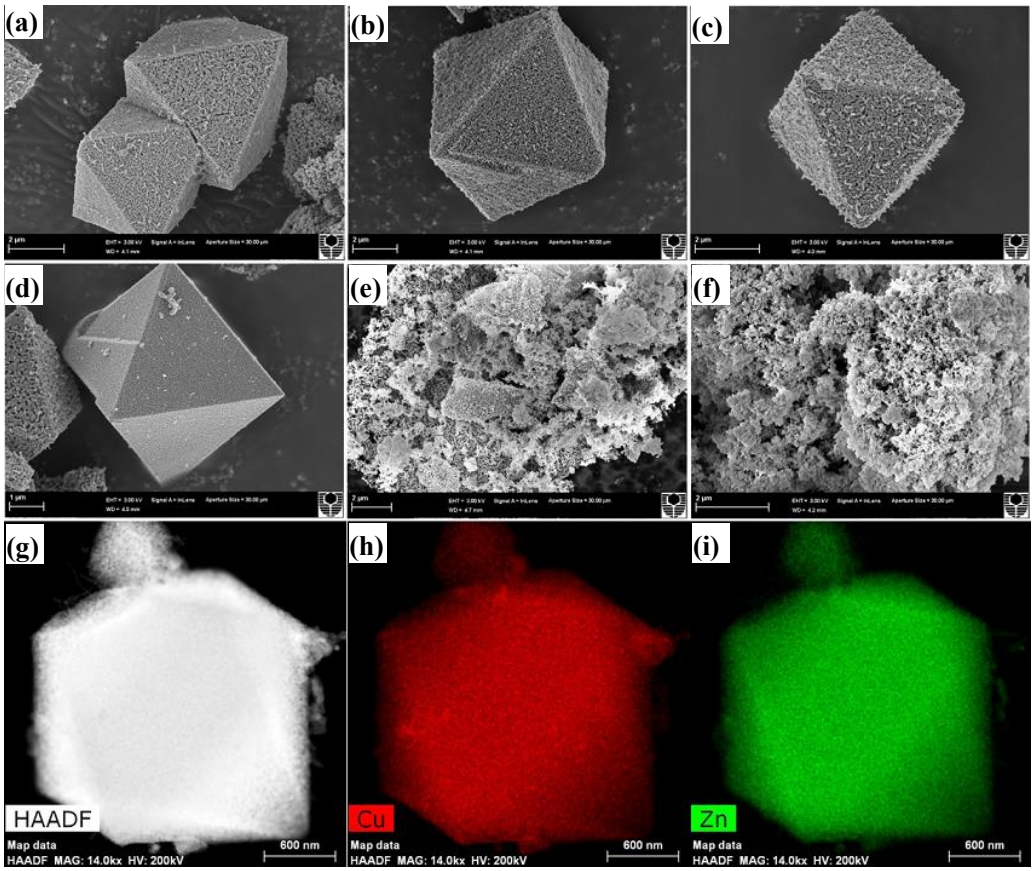

Figure 5.5. SEM images of (a) CZ-350, (b) CZ-450, (c) CZ-550, (d) CZ-1, (e) CZ-CP-1 and (f) CZ-CP; and (g) HAADF-STEM image and the respective distributions of (h) Cu and (i) Zn for CZ-350.

Nitrogen (N_2) sorption experiments were additionally performed to evaluate the porosities and the specific surface areas of CZ-350, CZ-450, CZ-550, and CZ-CP; the results of which are given in Figure 5.6 and Table 5-1. All four samples exhibit type II N_2 adsorption/desorption isotherm (according to IUPAC classification) with hysteresis loop, which indicates the presence of mesopores. Increasing the calcination temperature from 350 to 550 ºC leads to a decrease in N_2 uptake, which translates to the reduction in the Brunauer-Emmett-Teller (BET) surface area from 17.8 $m^2\ g^{-1}$ for CZ-350 to 8 $m^2\ g^{-1}$ for CZ-550 (Table 5-1). CZ-CP sample, i.e., the conventional Cu/ZnO sample counterpart of CZ-350 nonetheless exhibits larger surface area of 30 $m^2\ g^{-1}$, relative to CZ-350, CZ-450, and CZ-550 given its loose floccule structure (Table 5-1 and Figure 5.5

e and f).

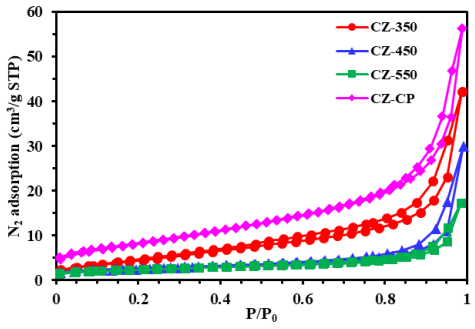

Figure 5.6. Nitrogen sorption isotherms of CZ-350, CZ-450, CZ-550, and CZ-CP.

Table 5-1. Specific surface areas and CuO crystallite sizes (from powder XRD analysis) of CZ-350, CZ-450, CZ-550, and CZ-CP.

Catalysts	BET surface area (m^2/g)	CuO crystallite size (nm)
CZ-350	17.8	28.9
CZ-450	9.3	33.6
CZ-550	8.0	58.2
CZ-1	-	95.2
CZ-CP	30	9.6
CZ-CP-1	-	52.1

5.2.2 Catalytic Performance for DME synthesis

To test their catalytic activities in STD reaction, each of the resultant MOF-derived Cu/ZnO catalysts, i.e., CZ-350, CZ-450, or CZ-550 was physically mixed with an equivalent (weight) amount of γ-Al_2O_3; resulting in the final sample that is denoted as CZ-350/A, CZ-450/A, or CZ-550/A, respectively. γ-Al_2O_3 was added as a methanol dehydration catalyst component. The STD reaction was performed at 250 ^oC and 3.0 MPa in a fixed-bed reactor. Lower calcination temperature is essential to achieve higher catalytic activity and selectivity as evidenced by the significant reduction in CO conversion and the minor reduction in DME selectivity in the order of CZ-350/A > CZ-450/A >

CZ-550/A (Figure 5.7a). CZ-350/A for example exhibited the highest CO conversion of 7.74% and the highest DME selectivity of 70.05% after 10 hours on stream. CZ-550/A, on the other hand, displayed the lowest CO conversion of 3.48% and the lowest DME selectivity of 67.64% at the same reaction time. The decrease in DME selectivity and CO conversion with the catalysts prepared from a higher calcination temperature was accompanied by the increased formation of CO_2 and other by-products. This observation reflects the decrease in the amount of accessible active centers due to the aggregation of Cu^0 nanoparticles, which becomes more severe at higher calcination temperatures as confirmed by powder XRD results above.

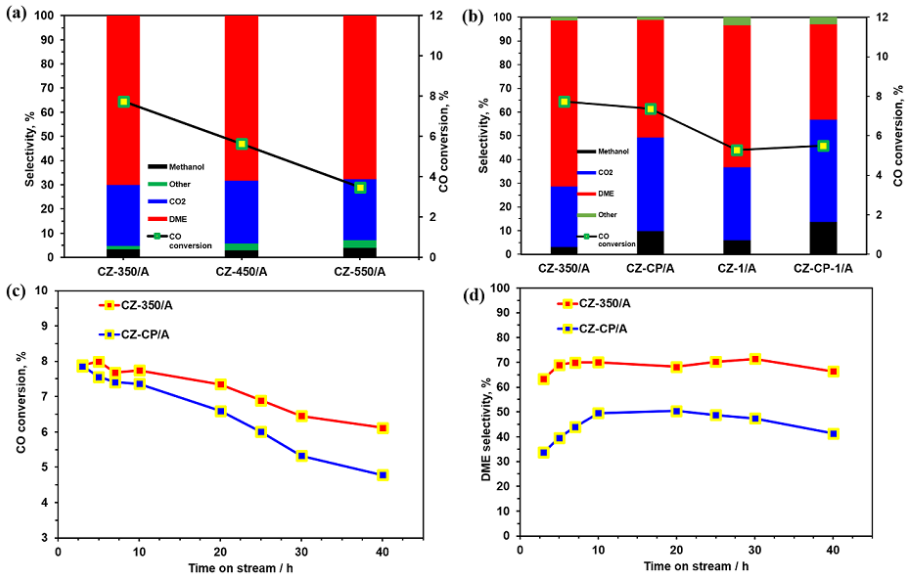

Figure 5.7. DME synthesis performance over various Cu/ZnO catalysts synthesized here in terms of CO conversion and methanol, DME, and CO_2 selectivity. (a) Comparison between CuZn-BTC-2 (Cu:Zn=2:1) MOF-derived Cu/ZnO catalysts calcined at three different temperatures, i.e., CZ-350, CZ-450, or CZ-550; and (b) Comparison between MOF-derived and conventional Cu/ZnO catalysts. The profile of (c) CO conversion and (d) DME selectivity for DME synthesis over CZ-350/A and CZ-CP/A catalysts during the 40-hour continuous reaction. Note: reaction was performed at 3 MPa, 250 ^oC, H_2:CO:N_2 volume ratio of 2:1:3, and gas hourly space velocity (GHSV) of 2500 mL $gcat^{-1}$ h^{-1}.

Smaller Cu nanoparticles were previously reported to provide large turnover frequencies for methanol synthesis.[39] Such effect nonetheless does not appear to be applicable to STD reaction catalyzed by conventional and MOF-derived Cu/ZnO in this work. Figure 5.7b compares CO conversion and methanol, DME, and CO_2 selectivities of CZ-350/A, CZ-CP, CZ-1/A, and CZ-CP-1/A. CZ-350/A displayed the highest CO conversion and the highest DME selectivity despite its largest CuO nanoparticles size among these four samples. The conventional Cu/ZnO sample counterpart of CZ-350/A, i.e., CZ-CP/A, which has the smallest CuO nanoparticle size among the four samples, exhibited almost identical CO conversion (7.36%) and significantly lower DME selectivity (49.51%) with respect to CZ-350/A. CZ-1/A, i.e., CuZn-BTC-1 MOF-derived Cu/ZnO catalyst, on the other hand, showed slightly lower CO conversion (5.29%) and significantly higher DME selectivity (59.8%) relative to those of CZ-CP-1/A (5.51% and 40.3%, respectively), which is the conventional Cu/ZnO sample counterpart of CZ-1A. These results suggest that DME formation depends primarily upon the catalyst structure. Cu/ZnO interface was previously reported to play a key role in the methanol formation from CO or CO_2.[40, 41] During the whole span of synthesis process, which involves consecutive thermal treatment processes, the octahedron structure with a homogenous confinement and distribution of CuO and ZnO was preserved. Such an ordered structure enables high interfacial area to be achieved between Cu and ZnO particles. Platelet-like ZnO however manifested from conventional co-precipitation synthesis route, which leads to random dispersion of CuO into ZnO support.[29] Under high operation temperature, these unconfined CuO particles may easily migrate and aggregate. Higher DME selectivities for samples containing higher amount of Zn dopant, i.e., CZ-350/A and CZ-CP/A (both of which have Cu:Zn molar ratio of 2:1) relative to CZ-1/A and CZ-CP-1/A (both of which have Cu:Zn molar ratio of 3.3:1) additionally indicate the essential role of Cu/ZnO interface.

Stability is another key important factor for practical application of a catalyst. In the literature, the deactivation of Cu/ZnO-based catalysts has mainly been related to the sintering of Cu.[26, 28, 42-44] Small Cu particles are easy to aggregate into large particles *via* Ostwald ripening or particle migration, which further leads to the reduced methanol formation rate.[45, 46] In this context, the 40-hour continuous performances of STD reaction over CZ-350/A and CZ-CP/A were monitored; the results of which are displayed in Figure 5.7c and d in terms of CO conversion and DME selectivity, respectively. In CZ-350/A case, CO conversion decreased by about 22%, i.e., from 7.99% at the beginning to 6.23% at the end of 40 hour while DME selectivity fluctuated at about 65% (Figure 5.7c). This is much better than the performance of CZ-CP/A catalyst, the conventional Cu/ZnO catalyst counterpart of CZ-350/A, which displayed about 40% reduction in CO conversion during the 40-hour continuous operation, i.e., from 7.96% at the beginning to 4.73% at the end of 40 hour (Figure 5.7d). DME selectivity in CZ-CP/A case was also consistently lower, i.e., below 50% during the 40-hour continuous operation.

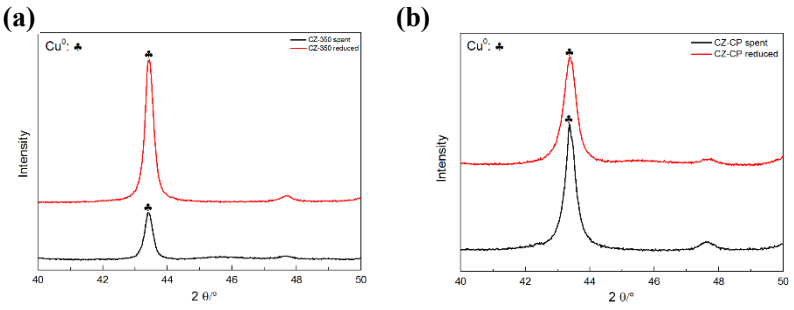

Figure 5.8. XRD patterns of (a) CZ-350 and (b) CZ-CP after reduction and after reaction.

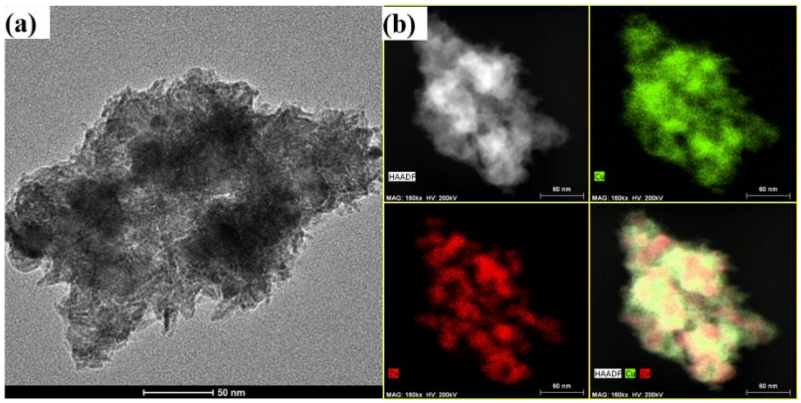

Figure 5.9. TEM image (a), HAADF-STEM and EDS mapping (b) of Cu, Zn for reduced CZ-CP.

Such stable catalytic performance for CZ-350/A likely comes from the confinement of Cu particles within the octahedron structure. Powder XRD results reveal that the particle size of Cu in CZ-350/A case was similar before and after the 40-hour continuous test (Figure 5.8a and Table 5-2), which confirms our hypothesis. In CZ-CP/A case however, the crystallite size of Cu increased significantly from 9.3 nm to 24.8 nm over 40 hour- operation duration (Figure 5.8b and Table 5-2). The severe Cu^0 agglomeration and irregular distribution of Cu and Zn on reduced CZ-CP were clearly observed via TEM analysis and EDS mapping (Figure 5.9). On the other hand, homogenous dispersion of Cu and Zn was retained on reduced CZ-350, without obvious particle aggregation (Figure 5.10a-b). HRTEM image (Figure 5.10c) reveals the presence of Cu^0 and ZnO nanoparticles in close contact. As shown in Figure 5.10c, the lattice spacing of 0.209, 0.191 and 0.247 nm were indexed to the interplanar spcing of Cu (1 1 1), ZnO (1 0 2) and ZnO (1 0 1), respectively. At the same time, XPS analysis confirmed that the mole ratio of Cu/Zn for reduced CZ-350 and CZ-CP were 2.01 and 2.89, respectively (Table 5-2). These results are consistent with the above XRD and TEM analysis that the unconfined Cu nanoparticles in CZ-CP are easy to grow into Cu clusters on the surface, which would cause rapid deactivation during the reaction. It is also worth mentioning

that the binding energy of Zn 2p1/2 and Zn 2p3/2 in reduced CZ-350 were 1044.1 eV and 1021.1 eV, which were 0.3-0.4 eV lower than that in reduced conventional CZ-CP (Figure 5.10d). The results disclose that a small quantity of Zn^{2+} in reduced CZ-350 became oxygen-deficient and $Zn^{(2-\delta)+}$ ($0<\delta<2$) was formed as the new species. It is proposed that the electronic interaction between Cu and $Zn^{(2-\delta)+}$ would generate the active site Cu^{+}-O-Zn, which provides the synergetic effect between Cu and ZnO favorable for the DME production.[13, 47]

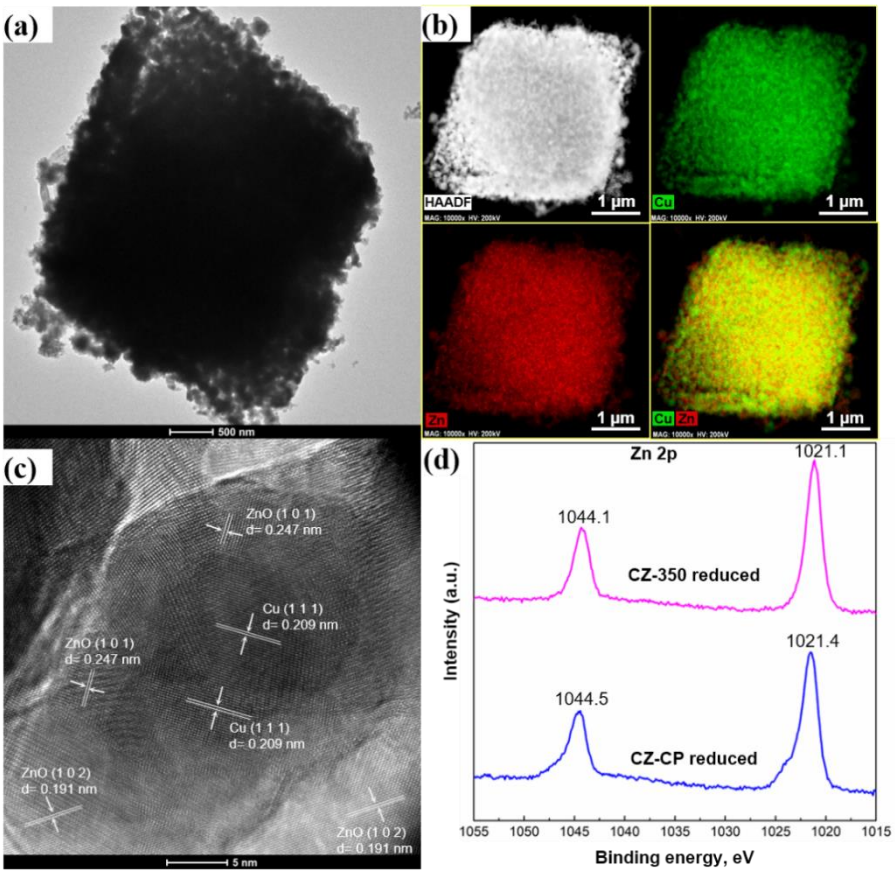

Figure 5.10 (a) TEM image, (b) HAADF-STEM and EDS mapping of Cu, Zn, (c) high resolution TEM for reduced CZ-350. (d) XPS spectra of Zn in reduced CZ-350 and reduced CZ-CP.

Table 5-2. The structure of fresh, reduced and used CZ-350 and CZ-CP

Catalysts	Cu^0 crystallite size (nm) [a]		Cu/Zn molar ratio after reduction [b]
	Reduced	Used	
CZ-350	26.4	28.3	2.01
CZ-CP	9.3	24.8	2.89

[a] Calculated from powder XRD peak of Cu (111) using Scherrer equation.

[b] Calculated from survey scan results of XPS.

The catalytic performances of several bifunctional catalysts for DME production in terms of CO conversion and DME selectivity are comparatively listed in Table 5-3. Although similar process conditions in STD process do not exist in previous reports for a straightforward comparison, the prepared CZ-350 derived from metal-organic framework precursor in this work reached high level of DME selectivity compared to other catalysts, considering relatively similar reaction conditions.

Table 5-3. Comparisons of the catalytic performance from previous reports

Catalysts	Feed gas	Temperature (°C)	Pressure (bar)	CO conversion	Selectivity (%)		Ref
					DME	CO_2	
CZ-350/A	$N_2/H_2/CO$ = 3/2/1	250	30	7.74	70.05	25.36	This work
Cu/mesoAl	$N_2/H_2/CO$ = 5.5/63/31.5	250	50	9.6	58.9	25.0	[48]
CuZnAl/γ-Al_2O_3	H_2/CO =1/1	250	40	34.1	49.7	4.01	[49]
Cu-Mn/Y	H_2/CO =1.5/1	245	20	25.4	62.6	30.0	[50]
CuZnAl/γ-Al_2O_3	H_2/CO =1/1	250	51	11.1	64.3	30.7	[30]

5.3 Conclusions

The association between the catalyst morphology, structure, component contact and the catalytic performance in DME synthesis using Cu/ZnO catalysts derived from Zn-doped Cu-BTC bimetallic MOFs was fundamentally studied. The catalyst synthesis was completed via one-pot solvothermal route followed by two-step calcination of CuZn-BTC-2. The resultant Cu/ZnO catalysts can retain the octahedron morphology stemmed from their original MOFs. The specific surface area and CuO crystallite size were carefully evaluated. The homogeneous distribution of Cu and Zn in the unique octahedron morphology significantly reduced the aggregation and migration of Cu^0 nanoparticles, leading to superior activity and stability for DME production. This novel structured Cn/ZnO catalyst from bimetallic MOF precursors displayed good DME selectivity 70% higher than its counterpart from conventional co-precipitation synthesis. During the 40-hour continuous DME synthesis reaction operated at 250 ^oC and 30 bar, the MOF-derived catalyst displayed much higher catalytic stability than its counterpart conventionally prepared. Compared to the literature, the MOF-derived catalyst also exhibited the highest DME selectivity, because of the formation of more active species of Cu^+-O-Zn favourable for DME production. This work was based on Cu/ZnO catalyst for DME synthesis, but it may also open a new avenue using MOF as the precursor to design these catalysts where the intimate contact or interface between multi-components is vital to achieve high catalytic performance.

References

1. Cheng, K.; Zhou, W.; Kang, J.; He, S.; Shi, S.; Zhang, Q.; Pan, Y.; Wen, W.; Wang, Y., Bifunctional catalysts for one-step conversion of syngas into aromatics with excellent selectivity and stability. *Chem* **2017,** *3* (2), 334-347.

2. Kasipandi, S.; Bae, J. W., Recent Advances in Direct Synthesis of Value-Added Aromatic Chemicals from Syngas by Cascade Reactions over Bifunctional Catalysts. *Adv. Mater.* **2019**, 1803390.

3. Ni, Y.; Liu, Y.; Chen, Z.; Yang, M.; Liu, H.; He, Y.; Fu, Y.; Zhu, W.; Liu, Z., Realizing and Recognizing Syngas-to-olefins Reaction via a Dual-bed Catalyst. *ACS Catal.* **2018**.

4. Zhao, Z.; Lu, W.; Yang, R.; Zhu, H.; Dong, W.; Sun, F.; Jiang, Z.; Lyu, Y.; Liu, T.; Du, H., Insight into the formation of Co@Co_2C catalysts for direct synthesis of higher alcohols and olefins from syngas. *ACS Catal.* **2017,** *8* (1), 228-241.

5. Zhang, P.; Tan, L.; Yang, G.; Tsubaki, N., One-pass selective conversion of syngas to para-xylene. *Chem. Sci.* **2017,** *8* (12), 7941-7946.

6. Ao, M.; Pham, G. H.; Sage, V.; Pareek, V., Structure and activity of strontium substituted $LaCoO_3$ perovskite catalysts for syngas conversion. *J. Mol. Catal. A: Chem.* **2016,** *416*, 96-104.

7. Yang, G.; Tsubaki, N.; Shamoto, J.; Yoneyama, Y.; Zhang, Y., Confinement effect and synergistic function of H-ZSM-5/Cu-ZnO-Al_2O_3 capsule catalyst for one-step controlled synthesis. *J. Am. Chem. Soc.* **2010,** *132* (23), 8129-8136.

8. Cheng, K.; Gu, B.; Liu, X.; Kang, J.; Zhang, Q.; Wang, Y., Direct and highly selective conversion of synthesis gas into lower olefins: design of a bifunctional catalyst combining methanol synthesis and carbon–carbon coupling. *Angew. Chem. Int. Ed.* **2016,** *55* (15), 4725-4728.

9. Takeishi, K.; Wagatsurna, Y.; Ariga, H.; Kon, K.; Shimizu, K., Promotional Effect of Water on Direct Dimethyl Ether Synthesis from Carbon Monoxide and Hydrogen Catalyzed by Cu-Zn/Al_2O_3. *ACS Sustain. Chem. Eng.* **2017,** *5* (5), 3675-3680.

10. Wang, Y.; Chen, Y. X.; Yu, F.; Pan, D. H.; Fan, B. B.; Ma, J. H.; Li, R. F., One-step synthesis of dimethyl ether from syngas on ordered mesoporous copper incorporated alumina. *J. Energy Chem.* **2016,** *25* (5), 775-781.

11. Sun, J.; Yang, G.; Yoneyama, Y.; Tsubaki, N., Catalysis chemistry of dimethyl ether synthesis. *ACS Catal.* **2014,** *4* (10), 3346-3356.

12. Lu, W.-Z.; Teng, L.-H.; Xiao, W.-D., Simulation and experiment study of dimethyl ether synthesis from syngas in a fluidized-bed reactor. *Chem. Eng. Sci.* **2004,** *59* (22), 5455-5464.

13. Sun, K.; Lu, W.; Qiu, F.; Liu, S.; Xu, X., Direct synthesis of DME over bifunctional catalyst: surface properties and catalytic performance. *Appl. Catal. A-Gen.* **2003,** *252* (2), 243-249.

14. Asthana, S.; Samanta, C.; Bhaumik, A.; Banerjee, B.; Voolapalli, R. K.; Saha, B., Direct synthesis of dimethyl ether from syngas over Cu-based catalysts: Enhanced selectivity in the presence of MgO. *J. Catal.* **2016,** *334*, 89-101.

15. Bayat, A.; Dogu, T., Optimization of CO_2/CO Ratio and Temperature for Dimethyl Ether Synthesis from Syngas over a New Bifunctional Catalyst Pair Containing Heteropolyacid Impregnated Mesoporous Alumina. *Ind. Eng. Chem. Res.* **2016,** *55* (44), 11431-11439.

16. Poels, E. K.; Brands, D. S., Modification of Cu/ZnO/SiO_2 catalysts by high temperature reduction. *Appl. Catal. A-Gen.* **2000,** *191* (1), 83-96.

17. van den Berg, M. W. E.; Polarz, S.; Tkachenko, O. P.; Klementiev, K. V.; Bandyopadhyay, M.; Khodeir, L.; Gies, H.; Muhler, M.; Grünert, W., Cu/ZnO aggregates in siliceous mesoporous matrices: Development of a new model methanol synthesis catalyst. *J. Catal.* **2006,** *241* (2), 446-455.

18. Greeley, J.; Gokhale, A. A.; Kreuser, J.; Dumesic, J. A.; Topsøe, H.; Topsøe, N. Y.; Mavrikakis, M., CO vibrational frequencies on methanol synthesis catalysts: a DFT study. *J. Catal.* **2003,** *213* (1), 63-72.

19. Grunwaldt, J. D.; Molenbroek, A. M.; Topsøe, N. Y.; Topsøe, H.; Clausen, B. S., In Situ Investigations of Structural Changes in Cu/ZnO Catalysts. *J. Catal.* **2000,** *194* (2), 452-460.

20. Álvarez, A.; Bansode, A.; Urakawa, A.; Bavykina, A. V.; Wezendonk, T. A.; Makkee, M.; Gascon, J.; Kapteijn, F., Challenges in the greener production of formates/formic acid, methanol, and DME by heterogeneously catalyzed CO_2 hydrogenation processes. *Chem. Rev.* **2017,** *117* (14), 9804-9838.

21. Kasatkin, I.; Kurr, P.; Kniep, B.; Trunschke, A.; Schlögl, R., Role of lattice strain and defects in copper particles on the activity of Cu/ZnO/Al_2O_3 catalysts for methanol synthesis. *Angew. Chem. Int. Ed.* **2007,** *46* (38), 7324-7327.

22. Behrens, M.; Studt, F.; Kasatkin, I.; Kühl, S.; Hävecker, M.; Abild-Pedersen, F.; Zander, S.; Girgsdies, F.; Kurr, P.; Kniep, B.-L., The active site of methanol synthesis over Cu/ZnO/Al_2O_3 industrial catalysts. *Science* **2012,** *336* (6083), 893-897.

23. Tohji, K.; Udagawa, Y.; Mizushima, T.; Ueno, A., The structure of the copper/zinc oxide

catalyst by an in-situ EXAFS study. *J. Phys. Chem.* **1985,** *89* (26), 5671-5676.

24. Wang, D.; Han, Y.; Tan, Y.; Tsubaki, N., Effect of H_2O on Cu-based catalyst in one-step slurry phase dimethyl ether synthesis. *Fuel Process. Technol.* **2009,** *90* (3), 446-451.

25. Flores, J. H.; Solórzano, G.; da Silva, M. I. P., Effect of aluminum on the morphological and textural properties of CuO–ZnO/H-Ferrierite. *Appl. Surf. Sci.* **2008,** *254* (20), 6461-6466.

26. Zuo, H.; Mao, D.; Guo, X.; Yu, J., Highly efficient synthesis of dimethyl ether directly from biomass-derived gas over Li-modified Cu-ZnO-Al_2O_3/HZSM-5 hybrid catalyst. *Renew. Energy* **2018,** *116*, 38-47.

27. Prieto, G.; de Jong, K. P.; de Jongh, P. E., Towards 'greener' catalyst manufacture: Reduction of wastewater from the preparation of Cu/ZnO/Al_2O_3 methanol synthesis catalysts. *Catal. Today* **2013,** *215*, 142-151.

28. García-Trenco, A.; Martínez, A., A rational strategy for preparing Cu–ZnO/H-ZSM-5 hybrid catalysts with enhanced stability during the one-step conversion of syngas to dimethyl ether (DME). *Appl. Catal. A-Gen.* **2015,** *493*, 40-49.

29. Zhang, Q.; Zuo, Y.-Z.; Han, M.-H.; Wang, J.-F.; Jin, Y.; Wei, F., Long carbon nanotubes intercrossed Cu/Zn/Al/Zr catalyst for CO/CO_2 hydrogenation to methanol/dimethyl ether. *Catal. Today* **2010,** *150* (1-2), 55-60.

30. Gentzen, M.; Habicht, W.; Doronkin, D.; Grunwaldt, J.-D.; Sauer, J.; Behrens, S., Bifunctional hybrid catalysts derived from Cu/Zn-based nanoparticles for single-step dimethyl ether synthesis. *Catal. Sci. Technol.* **2016,** *6* (4), 1054-1063.

31. Garcia-Trenco, A.; White, E. R.; Shaffer, M. S. P.; Williams, C. K., A one-step Cu/ZnO quasi-homogeneous catalyst for DME production from syn-gas. *Catal. Sci. Technol.* **2016,** *6* (12), 4389-4397.

32. Wang, T.; Shi, L.; Tang, J.; Malgras, V.; Asahina, S.; Liu, G.; Zhang, H.; Meng, X.; Chang, K.; He, J.; Terasaki, O.; Yamauchi, Y.; Ye, J., A Co_3O_4-embedded porous ZnO rhombic dodecahedron prepared using zeolitic imidazolate frameworks as precursors for CO_2 photoreduction. *Nanoscale* **2016,** *8* (12), 6712-6720.

33. Xu, X.; Cao, R.; Jeong, S.; Cho, J., Spindle-like Mesoporous α-Fe_2O_3 Anode Material Prepared from MOF Template for High-Rate Lithium Batteries. *Nano Lett.* **2012,** *12* (9), 4988-4991.

34. Zheng, L.; Li, X.; Du, W.; Shi, D.; Ning, W.; Lu, X.; Hou, Z., Metal-organic framework derived Cu/ZnO catalysts for continuous hydrogenolysis of glycerol. *Appl. Catal. B-Environ.* **2017,** *203*, 146-153.

35. Zhang, J.; An, B.; Hong, Y.; Meng, Y.; Hu, X.; Wang, C.; Lin, J.; Lin, W.; Wang, Y., Pyrolysis of metal–organic frameworks to hierarchical porous Cu/Zn-nanoparticle@ carbon materials for efficient CO_2 hydrogenation. *Mater. Chem. Front.* **2017,** *1* (11), 2405-2409.

36. Shannon, R. D., Revised effective ionic radii and systematic studies of interatomic distances in halides and chalcogenides. *Acta Crystallogr. A* **1976,** *32* (5), 751-767.

37. Domán, A.; Madarász, J.; László, K., In situ evolved gas analysis assisted thermogravimetric (TG-FTIR and TG/DTA–MS) studies on non-activated copper benzene-1,3,5-tricarboxylate. *Thermochim. Acta* **2017,** *647*, 62-69.

38. Liu, Y.; Wang, Z.; Zhong, Y.; Tade, M.; Zhou, W.; Shao, Z., Molecular Design of Mesoporous $NiCo_2O_4$ and $NiCo_2S_4$ with Sub-Micrometer-Polyhedron Architectures for Efficient Pseudocapacitive Energy Storage. *Adv. Funct. Mater.* **2017,** *27* (28), 1701229.

39. Natesakhawat, S.; Lekse, J. W.; Baltrus, J. P.; Ohodnicki, P. R.; Howard, B. H.; Deng, X.; Matranga, C., Active Sites and Structure–Activity Relationships of Copper-Based Catalysts for Carbon Dioxide Hydrogenation to Methanol. *ACS Catal.* **2012,** *2* (8), 1667-1676.

40. Kuld, S.; Thorhauge, M.; Falsig, H.; Elkjær, C. F.; Helveg, S.; Chorkendorff, I.; Sehested, J., Quantifying the promotion of Cu catalysts by ZnO for methanol synthesis. *Science* **2016,** *352* (6288), 969-974.

41. Kuld, S.; Conradsen, C.; Moses, P. G.; Chorkendorff, I.; Sehested, J., Quantification of Zinc Atoms in a Surface Alloy on Copper in an Industrial-Type Methanol Synthesis Catalyst. *Angew. Chem. Int. Ed.* **2014,** *53* (23), 5941-5945.

42. Baek, S.-C.; Kang, S.-H.; Bae, J. W.; Lee, Y.-J.; Lee, D.-H.; Lee, K.-Y., Effect of Copper Precursors to the Activity for Dimethyl Ether Synthesis from Syngas over Cu–ZnO/γ-Al_2O_3 Bifunctional Catalysts. *Energy Fuels* **2011,** *25* (6), 2438-2443.

43. Xie, Q.; Chen, P.; Peng, P.; Liu, S.; Peng, P.; Zhang, B.; Cheng, Y.; Wan, Y.; Liu, Y.; Ruan, R., Single-step synthesis of DME from syngas on CuZnAl–zeolite bifunctional catalysts: the influence of zeolite type. *RSC Adv.* **2015,** *5* (33), 26301-26307.

44. Ateka, A.; Sánchez-Contador, M.; Ereña, J.; Aguayo, A. T.; Bilbao, J., Catalyst

configuration for the direct synthesis of dimethyl ether from CO and CO_2 hydrogenation on CuO–ZnO–MnO/SAPO-18 catalysts. *React. Kinet. Mech. Catal.* **2018**, 1-18.

45. Bhunia, M. K.; Hughes, J. T.; Fettinger, J. C.; Navrotsky, A., Thermochemistry of paddle wheel MOFs: Cu-HKUST-1 and Zn-HKUST-1. *Langmuir* **2013,** *29* (25), 8140-8145.

46. Kung, H. H., Deactivation of methanol synthesis catalysts - a review. *Catal. Today* **1992,** *11* (4), 443-453.

47. Kanai, Y.; Watanabe, T.; Fujitani, T.; Uchijima, T.; Nakamura, J., The synergy between Cu and ZnO in methanol synthesis catalysts. *Catal. Lett.* **1996,** *38* (3-4), 157-163.

48. Ham, H.; Kim, J.; Cho, S. J.; Choi, J. H.; Moon, D. J.; Bae, J. W., Enhanced Stability of Spatially Confined Copper Nanoparticles in an Ordered Mesoporous Alumina for Dimethyl Ether Synthesis from Syngas. *ACS Catal.* **2016,** *6* (9), 5629-5640.

49. Bae, J.-W.; Potdar, H.; Kang, S.-H.; Jun, K.-W., Coproduction of methanol and dimethyl ether from biomass-derived syngas on a Cu−ZnO−Al_2O_3/γ-Al_2O_3 hybrid catalyst. *Energy Fuels* **2007,** *22* (1), 223-230.

50. Tang, X.-J.; Fei, J.-H.; Hou, Z.-Y.; Zheng, X.-M.; Lou, H., Characterization of Cu−Mn/Zeolite-Y Catalyst for One-Step Synthesis of Dimethyl Ether from CO−H_2. *Energy Fuels* **2008,** *22* (5), 2877-2884.

Chapter 6 Co/Co_6Mo_6C@C nanoreactors derived from ZIF-67 composite for Higher Alcohols Synthesis

Abstract

Direct production of higher alcohols from syngas provides a promising route for the conversion of methane-rich feedstocks into value-added commodity chemicals. However, the rationale catalyst design for this process remains a challenge due to severe long-standing sintering problem, low dispersion of active sites and uncontrollable synergism between CO dissociation and CO insertion. Here, we demonstrate the successful development of highly active catalyst for higher alcohols production based on the confined carbonization in metal-organic framework (MOF) matrix. Starting from a compound consisting of cobalt-based MOF host (ZIF-67) and molybdenum-based polyoxometalates guest ($H_3PMo_{12}O_{40}$), Co/Co_6Mo_6C confined in the carbon matrix are achieved with well-defined morphology and high porosity after carbonation in N_2. The $Co_{4.7}Mo$@C with optimal fraction of Co^0 and Co_6Mo=C exhibits remarkable performance for higher alcohols synthesis, with a CO conversion of 48% and $C_{2+}OH$ space time yield of 99 $mg/g_{cat}.h$ under 275 °C and 3.0 MPa. Compared to the literature, the developed $Co_{4.7}Mo$@C catalyst from MOF displayed favourable higher alcohols production rates. The balance of Co^0/ Co_6Mo_6C is found to be crucial for the observed reactivity, where Co^0 is for CO dissociation and C-C chain growth and Co_6Mo_6C is highly efficient for CO nondissociation and CO insertion. Moreover, the synthesized catalyst also displays exceptional stability in a 100 h long-term stability test owing to the uniform dispersion of active centres, demonstrating great potential for large-scale application.

6.1 Introduction

Higher alcohols, containing two or more carbon atoms, have shown great potential as the alternative energy source owing to their vast applications including fuel additives, hydrogen carriers or precursors for major platform chemicals.[1-4] Catalytic upgrading of syngas to higher alcohols via a tandem strategy is currently attracting prominent research interest due to the facile and economical merits. To date, great efforts have been devoted to optimizing the catalytic system for industrial implementation. Many active metals including Cu, Fe, Co, Mo have shown good activity for this reaction. Among these elements, Co-based catalysts are most favored over others owing to their low cost, high chain growth capability and excellent stability.[5, 6]

It is widely believed that HAS from syngas follows CO insertion mechanism, coupling C-O bond cleavage to form alkyl chains C_nH_{2n}* via CH_x* addition and CO* insertion to produce alcohols.[7, 8] Both reaction steps should occur simultaneously to boost the formation of higher alcohols. However, the active sites for CO dissociation and insertion are usually different. For Co-based catalysts, Co^0 nanoparticles are always responsible to produce paraffins, whereas $Co^{\delta+}$ species with higher valence have been reported to be active for alcohols formation.[9, 10] Normally, modification of Co catalyst with Cu or Mo can facilitate the formation of Co_2C, thus promotes CO insertion rate towards the production of higher alcohols.[11-14] It is reported that the Co_2C species are critical for selective HA formation in the Cu modified Co catalysts. Moreover, bimetallic carbide Co_3Mo_3C has been found active for CO insertion during HAS in the prepared Co-Mo catalysts.[15, 16] Except for the nature of active sites, their microenvironment in the catalysts also plays important role in HAS, such as dispersion and proximity between the active centers. Highly dispersed active sites are the primary reason for efficient CO conversion, whereas low distribution of active sites in bulk Co catalysts usually leads to poor CO conversion and quick deactivation due to particle aggregation. Using supports with high surface area, such as active carbon, γ-Al_2O_3,

could solve this problem. Additionally, the close affinity of two functional groups for CO dissociation and CO insertion is essential to promote a synergistic effect between two species for high HA output.[17] However, the impregnation method for conventional catalyst preparation always evokes randomly distribution of active sites and reduces the synergism, which remains a crucial challenge for the design of efficient catalyst for HAS. As a result, it is highly imperative to develop a rational strategy to accurately control the dispersion of active sites and their proximity for HAS reaction.

Metal-organic frameworks (MOFs), the assembly of metal nodes and organic linkers, have attracted tremendous research interests for sustainable catalysis as a new class of porous materials.[18-20] The well-defined structure of MOFs allows the isolation of metal sites by the organic ligands. Besides, functional groups, such as polyoxometalates ($H_nXM_{12}O_{40}$, where X is P, Si, *etc*. and M is Mo, W, *etc*.) can be installed in the MOF cavities due to their high porosity and the matched size of polyoxometalates molecule and MOF cage.[21, 22] Our previous efforts demonstrated that the successful incorporation of $H_4SiW_{12}O_{40}$ in the UiO-66 can lead to a sturdy catalyst in a favourable hierarchical texture for dimethyl ether formation.[23] It is inspiring us to further explore the possibility to incorporate a Mo-based polyoxometalate in a Co-based MOF to achieve the homogenous arrangement of Co and Mo with intimate contact. With precisely controlled calcination in inert atmosphere, a novel catalyst can be produced with multiple active sites for HAS, such as Co^0, CoMo bimetallic carbide, or $Mo^{\delta+}$. Furthermore, the organic linkers in MOF can transform to a robust carbon skeleton after pyrolysis, thus providing an excellent architecture where these active centres can be in an optimum arrangement not only to keep their intimacy but also to prevent their aggregation under HAS. However, such strategy has been rarely reported for F-T synthesis, in particular for higher alcohols production.

Herein, we report a novel catalyst derived from phosphomolybdic acid (PMA, $H_3PMo_{12}O_{40}$)-MOF composite for higher alcohols production from syngas. For this purpose, the PMA molecule was firstly trapped in zeolitic imidazolate framework-67

(ZIF-67) cages via a facile one-pot synthesis strategy, as can be seen in the Scheme 6-1. Through precise calcination in inert atmosphere, the resultant carbon supported Co/Co_6Mo_6C catalyst shows very high activity with exceptional stability for HAS. The strategy to use MOF as the precursor to prepare dual or multi-components may be expanded to other catalysts to improve more catalytic reaction systems.

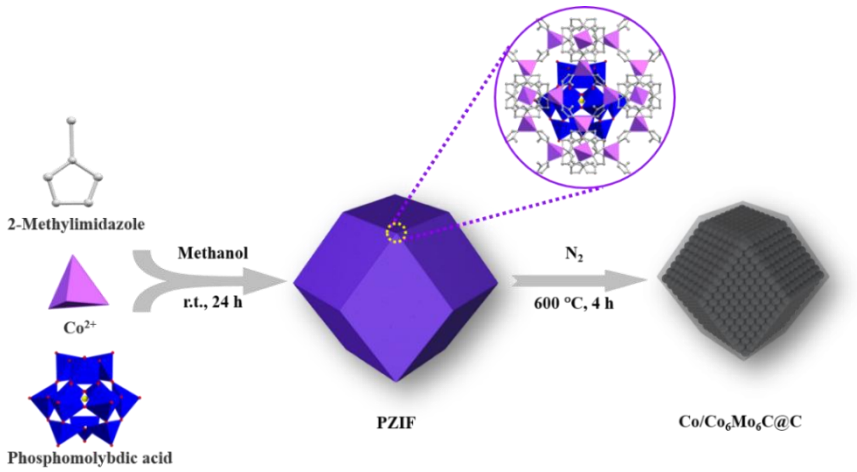

Scheme 6-1. A Schematic illustration of the synthesis of the carbon supported Co/Co_6Mo_6C catalyst via pyrolysis of phosphomolybdic acid encapsulated ZIF. All hydrogen atoms are omitted for clarity.

6.2 Results and discussions

6.2.1 Catalyst Characterization

We developed PMA modulated ZIF-67 precursors by adding different amounts of PMA into the precursor mixture. This strategy allows for homogeneously dispersed PMA to enter into the ZIF-67 channels without jeopardizing the structural and compositional features of both ZIF-67 and PMA clusters.[24] Here, the representative samples ZIF-67, PZIF-1 and PZIF-2 were precisely characterized due to their vast difference in composition. Elemental analysis evidenced that PZIF-1 and PZIF-2

contain 12.69 % and 23.66 % (by weight) of PMA, as shown in Table 6-1.

Table 6-1. Properties of prepared MOF precursors and calcined products.

Sample	Calcinating temperature (°C)	PMA wt%	Co wt%	Mo wt%	Co/Mo molar ratio	BET surface area (m^2/g)
ZIF-67		-	26.3	-	-	1960
PZIF-1		12.7	23.3	8.0	4.7	1655
PZIF-2		23.6	20.4	14.9	2.2	1035
PZIF-3		8.6	24.4	5.4	7.3	-
Co@C	600	-	36.8	-	-	334
$Co_{4.7}Mo$@C	600	-	31.7	10.90	4.7	132
$Co_{2.2}Mo$@C	600	-	33.1	24.3	2.2	38
$Co_{7.3}Mo$@C	600	-	33.9	7.5	7.3	-

The successful formation of PZIF samples was verified via different characterization techniques. The XRD patterns of all prepared MOFs (Figure 6.1a), for instance, are identical with the simulated ZIF-67 patterns (CCDC#671073), indicating the intact framework of ZIF-67 after PMA modulation. The lack of crystalline PMA domains clearly confirms that the PMA clusters are fully enclosed in the well-developed ZIF-67 pores. N_2 adsorption/desorption analysis (Figure 6.1b) provides another convincing evidence of PMA trapping in ZIF-67. The pristine ZIF-67 provides the largest BET surface area of 1960 m^2/g. The PZIF-1 and PZIF-2 with increased PMA loading remain highly porous, with clearly reduced S_{BET} values of 1655 and 1035 m^2/g, respectively. Furthermore, TGA under air atmosphere (Figure 6.1c) reveals that the weight loss of ZIF-67 between 50 and 600 °C was 65%, much higher than that of PZIF-1 (58%) and PZIF-2 (51%). This clearly demonstrates the effect of PMA trapping on the compositional feature of ZIF-67. To ensure the intact architecture of prepared MOFs, SEM and TEM analysis were also employed, as shown in Figure 6.2. All synthesized MOFs are rhombic dodecahedral in shape, typical morphology of ZIF-67. Moreover, the ordered polyhedral crystals with 6 exposed [110] facets demonstrate high symmetry with smooth surfaces.[25]

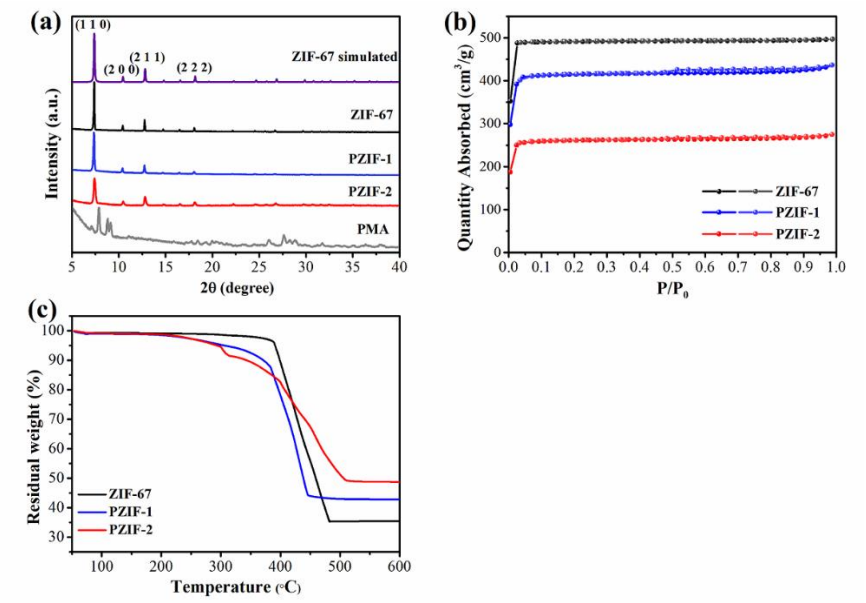

Figure 6.1. (a) XRD spectra, (b) N_2 adsorption / desorption isotherms and (c) TGA patterns of prepared ZIF-67, PZIF-1 and PZIF-2.

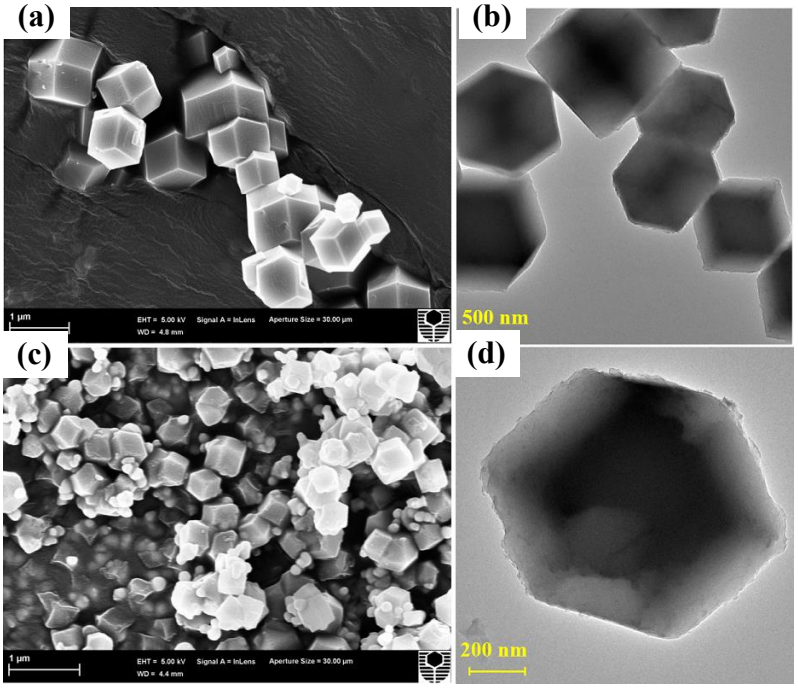

Figure 6.2. (a-b) SEM images and (c-d) TEM images of ZIF-67 and PZIF-1.

The above discussions corroborate that the PMA molecules are successfully anchored into the ZIF-67 cages via the facile one-pot synthesis method. After pyrolysis in the

N_2 atmosphere, the MOF precursors were decomposed and new species emerged, as observed in XRD patterns in Figure 6.3. All the characteristic peaks for ZIF-67 and PZIFs disappear after calcination at 600 °C. For the pure Co containing sample Co@C, only Co^0 phase is presented with three peaks located at 44.3°, 51.6° and 75.9° corresponding to the (1 1 1), (2 0 0) and (2 2 0) planes of metallic cobalt (JCPDS 001-015-0806). For another two Mo containing samples $Co_{4.7}Mo@C$ and $Co_{2.2}Mo@C$, it's interesting to find that a novel bimetallic carbide Co_6Mo_6C was formed along with extra Co^0 phase. The peaks located at 2θ = 32.7°, 35.8º, 40.5°, 43.0°, 47.1°, 60.4°, 65.6° and 73.6° are indexed to the (4 0 0), (3 3 1), (4 2 2), (5 1 1), (4 4 0), (5 5 1), (7 3 1) and (8 2 2) planes of Co_6Mo_6C (JCPDS 01-080-0338). Especially, as the Co/Mo ratio decreased from 4.7 for $Co_{4.7}Mo@C$ to 2.2 for $Co_{2.2}Mo@C$, strengthened Co_6Mo_6C peaks and weakened Co^0 peaks are observed, indicative of enhanced Co_6Mo_6C formation and less Co^0 content in the catalyst. No peaks corresponding to monometallic carbide can be observed, for instance, Co_2C and Mo_xC. This is a striking observation because the formation of bimetallic carbides is generally favored through the interaction of cobalt molybdate ($CoMoO_4$) with a carbon source at a higher temperature (800-1000 ºC).[26] The corresponding mechanism behind this phenomenon is described as follows. The encapsulation of PMA in ZIF-67 leads to the homogeneous C, Co and Mo elemental distribution with optimum arrangement maintaining not only the required intimacy but also proper close distance to prevent aggregation via the MOF framework. During the pyrolysis step in N_2 atmosphere, 2-methylimidazole molecules in MOF framework were transformed to carbon skeleton with reducing gas release, whereas the PMA will be converted initially to MoO_3. After the decomposition step, the formed carbon will react with adjacent Mo and Co, leading to the formation of Co_6Mo_6C. The same phenomenon was also observed in the previous report.[27] Based on ICP analysis, the molar content of Co is 4.7 and 2.2 times that of Mo in PZIF-1 and PZIF-2. Thus, the excessive Co was reduced to metallic Co^0 nanoparticles simultaneously.

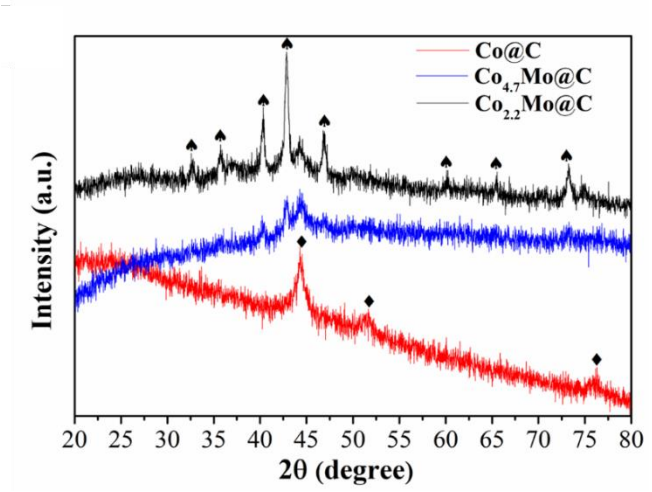

Figure 6.3. XRD patterns of Co@C, $Co_{4.7}Mo@C$ and $Co_{2.2}Mo@C$; ♦-Co^0, ♠-Co_6Mo_6C.

To further verify the existence of Co_6Mo_6C, X-ray photoelectron spectroscopy (XPS) was applied to $Co_{4.7}Mo@C$ sample derived from PZIF-1 precursor MOF. The survey spectrum verifies the coexistence of C, N, P, Co and Mo with the corresponding peaks located at binding energy of 284, 398, 134, 779 and 231 eV (**Figure 6.4a**). The high-resolution Co 2p peak (**Figure 6.4b**) can be deconvoluted into eight sub-peaks with four components corresponding to Co^0, Co^{2+}, Co^{3+} and satellite peaks. The peaks located at 793.4 and 778.2 eV are assigned to metallic Co (Co^0). Co^{2+} is observed with binding energy peaks at 796.4 eV for 2p 1/2 and 780.4 eV for 2p 3/2, indicative of the presence of Co_6Mo_6C. Co^{3+} is also shown at 798.9 and 783.0 eV, which was formed due to passivation upon air exposure.[26] In the case of Mo 3d spectrum (Figure 6.4c), after curve deconvolution, the peaks located at 232.9 and 228.5 eV are ascribed to Mo^{2+} 3d3/2 and Mo^{2+} 3d5/2 of C-Mo bond from cobalt molybdenum carbide.[16, 27] Other four peaks at 229.8 eV /235.4 eV (3d3/2 / 3d5/2) and 232.2 eV / 236.8 eV (3d3/2 / 3d5/2) are assigned to Mo^{4+} and Mo^{6+}, which are also due to the surface oxidation. The XPS results of Co 2d and Mo 3d solidly confirm the formation of cobalt molybdenum carbide through the facile pyrolysis of heteropolyacid-MOF composite. The C 1s peak can be fitted into five peaks, indexing to C-C (284.6 eV), C-P (285.3 eV), C-N (286.0 eV), C-O (287.3 eV) and Metal-C (283.9 eV), as shown in Figure 6.4d.[28, 29] The spectrum of N 1s (Figure 6.4e) can be deconvoluted into 3 peaks at 398.5,

299.5 and 400.9 eV, corresponding to pyridinic N, pyrrolic N and graphitic N, respectively, suggesting the successful incorporation of N into the carbon framework.[30] In the high-resolution P 2p peaks (Figure 6.4f), except the P-O bond (134.2 eV) and P-C bond (133.2 eV), P-Metal bond (P-Co or P-Mo) is also formed, peaking at 129.8 eV.[27] Although beyond the detecion of XRD, the existence of metal phosphide is clearly revealed from the XPS results. This can be attributed to the unique strucuture of PMA molecule, where one P atom is closely surrounded by twelve Mo atoms. Thus, MoP can be easily formed during the thermal treatment process. As reported elsewhere, the MoP or CoP is also found to be able to improve the catalytic activity and selectivity of C_{2+} alcohols.[31, 32] Thus, the prepared $Co_{4.7}Mo@C$ catalyst might exhibit exceptional activity for HAS.

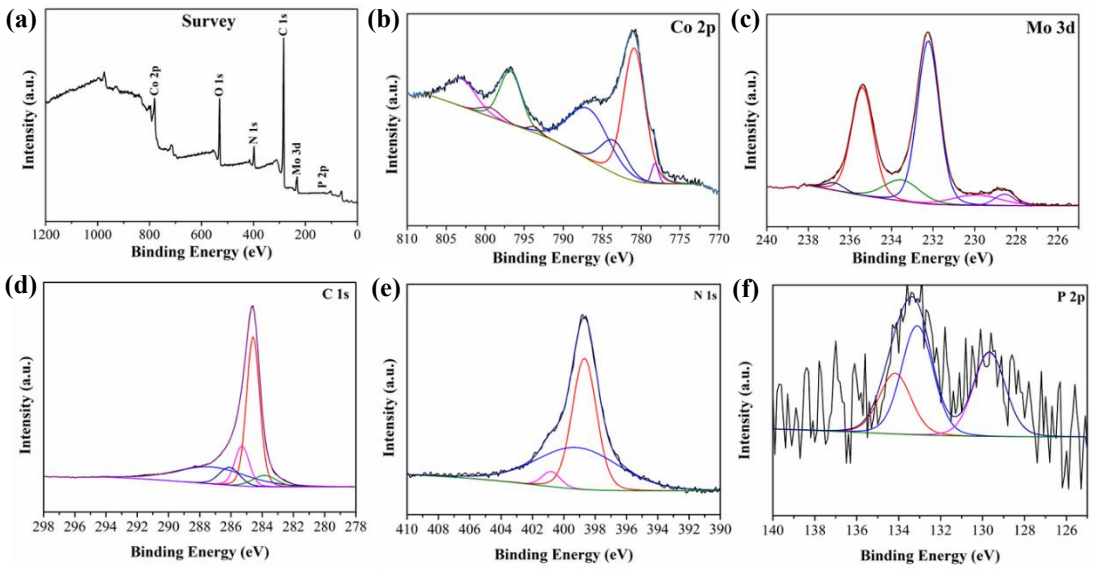

Figure 6.4. (a) XPS survey of $Co_{4.7}Mo@C$; (b-f) High resolution scans of Co 2p, Mo 3d, C1s, N1s and P 2p.

With the formation of bimetallic carbide, $Co_{4.7}Mo@C$ exhibits slight difference with Co@C in morphology. Co@C has retained the rhombic dodecahedral morphology and nanocage size of ZIF-67, with a rough surface as shown in SEM and TEM images (Figure 6.5a-b). The high-resolution TEM (HRTEM) of Co@C (Figure 6.5c) shows an interplanar distance of 0.177 nm, corresponding to the (2 0 0) plane of Co^0.[33] However,

the SEM image for $Co_{4.7}Mo@C$ reveals that the nanocage of PZIF-1 exhibit severe shrinkage after carbonization at 600 °C, leaving distorted surface with much smaller nanocages (Figure 6.5d). This is because that the oxygen atoms from PMA inside the MOF cages consume larger amount of carbon in the ZIF-67 during pyrolysis, rendering indentation in the structure. The HRTEM image (Figure 6.5f) provides further evidence for the formation of bimetallic carbide and metallic Co. Along with Co^0 (2 0 0) plane, the (5 1 1) and (3 3 1) plane for Co_6Mo_6C are also observed with the lattice spacing of 0.210 and 0.250 nm, respectively.[26] It is also observed that Co^0 is closely adjacent to Co_6Mo_6C, which promotes an intimate and extensive interface. Moreover, the EDS mapping further manifests the homogeneous dispersion of Co, Mo, C, N and P in the formed polyhedrons (Figure 6.5g).

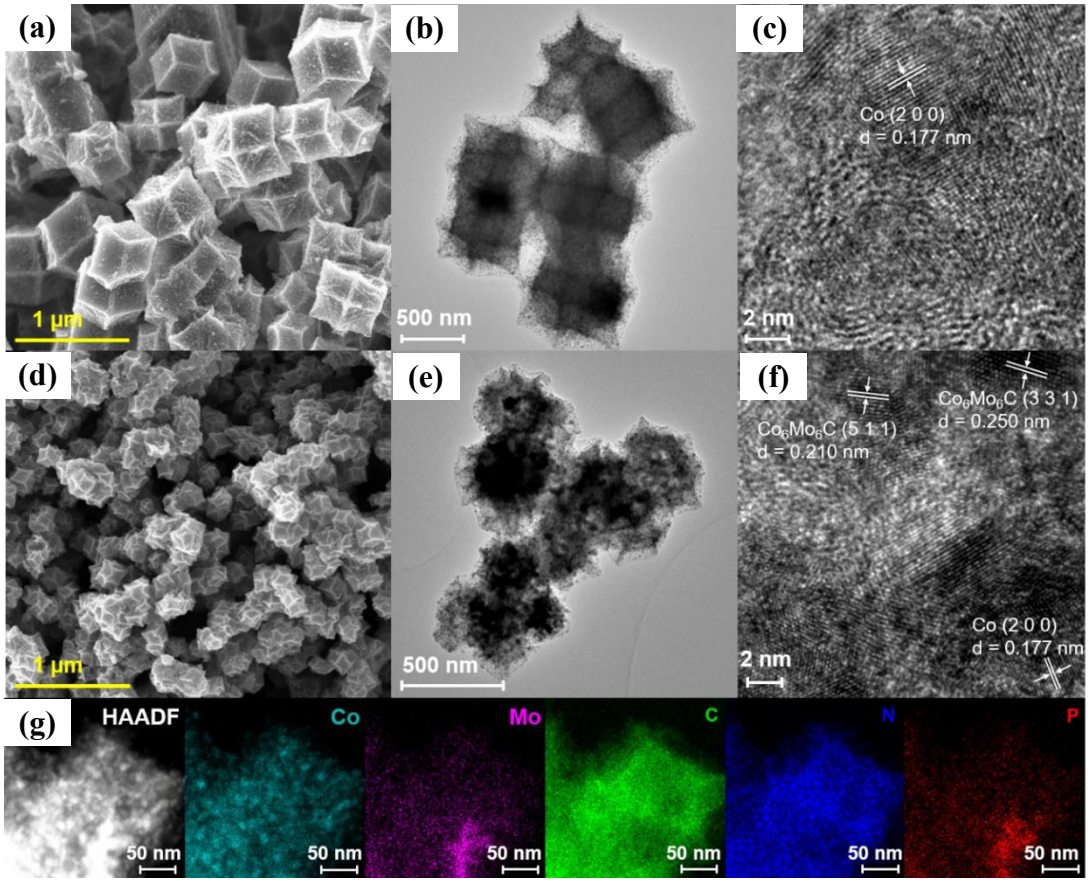

Figure 6.5. SEM images, TEM images, HRTEM images of Co@C (a-c) and $Co_{4.7}Mo@C$ (d-f); (g) HAADF-EDS mapping of $Co_{4.7}Mo@C$.

The porosities and specific surface areas of ZIF-derived catalysts were also altered sharply with the Mo modulation, as investigated by N_2 adsorption/desorption measurement. The results are shown in Figure 6.6 and Table 6-1. A vast decrease of N_2 uptake volume is clearly observed with the increasing amount of Mo in the final catalyst. Co@C, which was developed from thermal treatment of pure ZIF-67, has the largest N_2 uptake with a surface area reached up to 334 m^2/g. In the case of Mo containing samples $Co_{4.7}Mo@C$ and $Co_{2.2}Mo@C$, they own smaller uptake and the corresponding surface areas have substantially decreased to 132 and 38 m^2/g, respectively. This is consistent with the morphology changes for both samples, that the oxygen would take away more carbon atoms in the MOF and make the resultant catalysts less porous. Similarly, the pore volume values of $Co_{4.7}Mo@C$ and $Co_{2.2}Mo@C$ are 0.08 and 0.05 cm^3/g, respectively, much lower than Co@C (0.13 cm^3/g).

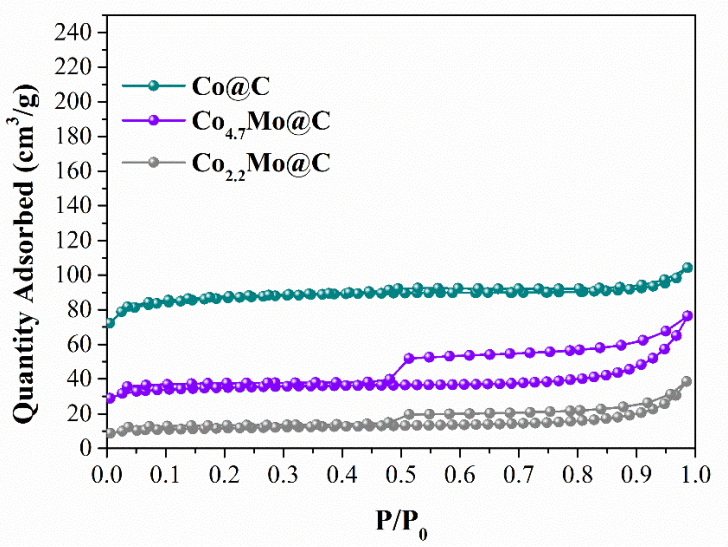

Figure 6.6. N_2 adsorption/desorption isotherms of Co@C, $Co_{4.7}Mo@C$ and $Co_{2.2}Mo@C$

6.2.2 Catalytic Performance for Higher Alcohols Synthesis

To investigate the impact of Mo modification on higher alcohols formation, herein, we have tested these ZIF-derived catalysts for HAS at 275 °C and 3.0 MPa with a GHSV

of 15000 mL_{syngas}/g_{cat}.h. The catalytic performance was evaluated in terms of CO conversion, product selectivity, alcohol distribution and space time yield, as shown in Figure 6.7 and Table 6-2.

Table 6-2. Summary of the HAS performance of PZIF derived catalyst

Catalyst	CO conversion (%)	Product Selectivity (%)				ROH Space-Time-Yield (mg/g_{cat}.h)		
		CH_4	CO_2	ROH	Others	Total	MeOH	$C_{2+}OH$
Co@C	22.2	40.6	2.3	8.6	48.5	54.6	28.6	26
$Co_{7.3}Mo$@C	42.6	35.7	16.3	9.8	38.2	98	22.3	75.7
$Co_{4.7}Mo$@C	48	28.3	21.1	11.9	38.7	123	24	99
$Co_{2.2}Mo$@C	37	31.9	23.3	6.5	38.3	57.6	16	41.6

Reaction conditions: T = 275 °C, P = 3.0 MPa, $H_2/CO/N_2$ = 2/1/3, GHSV = 15000 mL_{syngas}/g_{cat}.h, 0.2 g of catalyst.

The pure Co sample Co@C under the reaction conditions exhibited the lowest CO conversion of 22.2% with a CO conversion rate of 92 $\mu mol/g_{metal}$.h. CH_4 and others (mainly hydrocarbons) were the dominant products. The corresponding selectivity towards alcohols was only 8.6%. Moreover, methanol accounts for 52.5 wt % of total alcohols, with a space-time-yield (STY) of 28.6 mg/g_{cat}.h. As for Mo containing samples, for example, the $Co_{4.7}Mo$@C catalyst demonstrated a remarkable CO conversion of 48%, which is 2.2 times that of Co@C. Despite the slightly lower BET surface area, the CO conversion rate of $Co_{4.7}Mo$@C reached a higher level of 174 $\mu mol/g_{metal}$.h. In the meantime, the alcohols selectivity significantly increased to 11.9% and CH_4 selectivity was significantly reduced. A high $C_{2+}OH$ portion in total alcohols (80.3 wt %) is obtained, signifying that methanol formation was greatly suppressed. Moreover, the $C_{2+}OH$ STY was greatly raised to 99 mg/g_{cat}.h, which is 3.8 times that of Co@C (26 mg/g_{cat}.h). However, the $Co_{2.2}Mo$@C exhibits slightly inferior performance. The corresponding $C_{2+}OH$ fraction and STY were 73% and 41.6 mg/g_{cat}.h, respectively, at a CO conversion of 37%. As identified by XRD results, $Co_{2.2}Mo$@C contains the largest fraction of Co_6Mo_6C and the lowset content of Co^0. The catalyst of $Co_{7.3}Mo$@C containing the least amount of Co_6Mo_6C exhibited slightly

higher activity than $Co_{2.2}Mo@C$ in HAS, with a CO conversion of 42.6% and a $C_{2+}OH$ STY of 75.7 $mg/g_{cat}.h$. Therefore, we envision that a synergetic effect exists between Co and Co_6Mo_6C and the equilibrium of two species would shift the reaction toward higher alcohols formation.

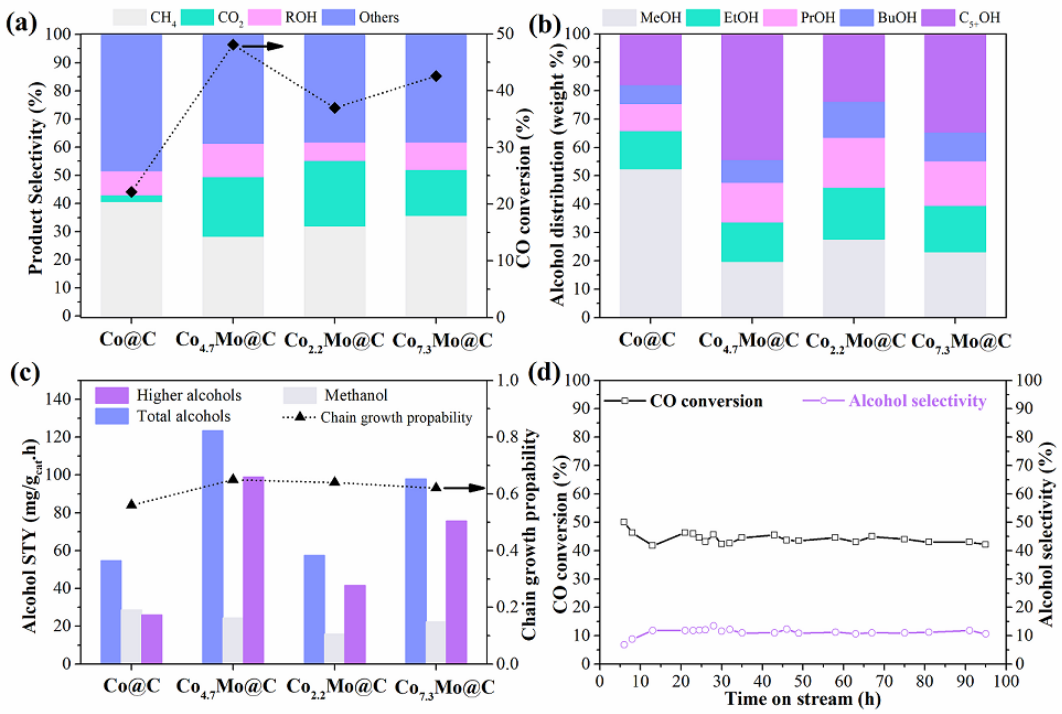

Figure 6.7. Catalytic performance of prepared MOF derived catalysts: (a) CO conversion and product selectivity, (b) Alcohol distribution, (c) Alcohols space-time yield (STY) and chain-growth ability (α), (d) Time-on-stream evolution of CO conversion and alcohol selectivity for the Co4.7Mo@C. Reaction conditions: T = 275 °C, P = 3.0 MPa, $H_2/CO/N_2$ = 2/1/3, GHSV = 15000 $mL_{syngas}/g_{cat}.h$, 0.2 g of catalyst.

Additionally, linear Anderson-Schulz-Flory (ASF) distributions for the alcohol products of all three catalysts are observed, suggesting that the higher alcohols formation on these catalysts follows same mechanism (Figure 6.8), and the carbon chain growth possibly occurs mainly on the metallic Co^0 component providing the active centres for CO dissociation and hydrogenation to form CHx* monomer and following chain propagation via C_nH_{2n}* formation.[34] Nevertheless, the bimetallic

carbide Co_6Mo_6C undoubtedly promotes the carbon chain propagation ability towards higher alcohols. The calculated chain growth probability (α) to alcohols over $Co_{4.7}Mo$@C and $Co_{2.2}Mo$@C catalysts are 0.67 and 0.64, respectively. Both values exceed that for Co@C (0.56). Therefore, the essence of Co_6Mo_6C in $Co_{4.7}Mo$@C and $Co_{2.2}Mo$@C catalysts could be rationalized by providing the active centres for CO nondissociative adsorption, coupling the C_nH_{2n}* formed on the Co^0 part at the Co^0/Co_6Mo_6C interface to produce oxygenate intermediates, which undergo further hydrogenation to produce the final alcohols.

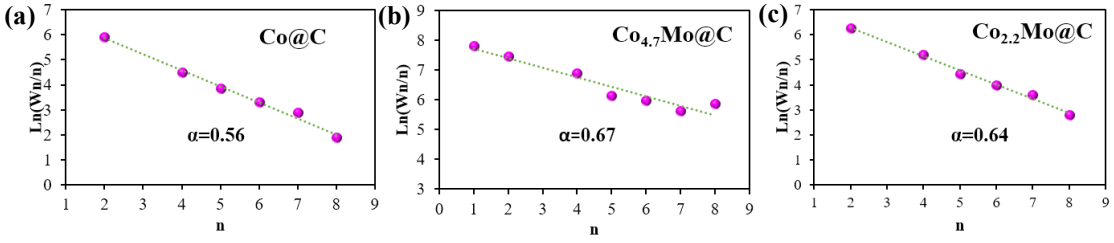

Figure 6.8. The ASF distribution patterns of Co@C (a), $Co_{4.7}Mo$@C (c), and $Co_{2.2}Mo$@C (c).

To gain further insight about the role of the bimetallic carbide Co_6Mo_6C in HAS, the counterpart sample Co_6Mo_6C@C was fabricated by etching away the metallic Co^0 particles in $Co_{4.7}Mo$@C using 1 M HCl solution. The corresponding Co/Mo ratio dropped to 1.18 after etching treatment based on the ICP analysis, close to the theoretical value of Co_6Mo_6C. Under the same reaction conditions, the Co_6Mo_6C@C only exhibits a CO conversion of 3% and a $C_{2+}OH$ STY of 5.5 $mg/g_{cat}.h$, much lower than that of $Co_{4.7}Mo$@C. This remarkable difference in catalytic performance demonstrates that sole Co_6Mo_6C phase exhibits poor activity for HAS reaction, which is in good agreement with previous report that metal carbides are usually less active than the corresponding metals.[35]

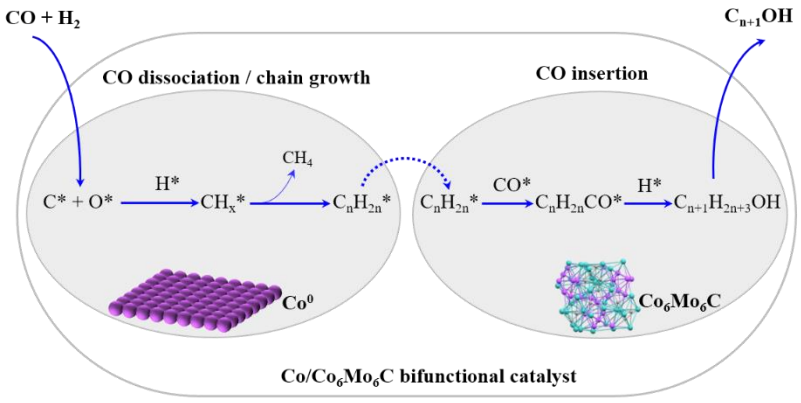

Figure 6.9. Reaction scheme for syngas conversion to higher alcohols. The CO hydrogenation reaction over the prepared carbon supported Co/Co_6Mo_6C bifunctional catalyst takes place in 2 steps namely (1) an initially CO and H_2 dissociation to form the C_nH_{2n}* intermediate on metal Co and (2) the CO* insertion in the C_nH_{2n}* groups over the Co/Co_6Mo_6C interface and subsequent hydrogenation to produce the higher alcohols.

It is widely known that the HAS process requires different active sites to complete C-C chain growth step and CO insertion step simultaneously. Based on the catalytic properties and corresponding performance, it is conclusive that the individual components of Co^0 and Co_6Mo_6C in the carbon supported Co^0/Co_6Mo_6C nanoreactors are responsible for different steps in the relay reactions of higher alcohols production from syngas, as illustrated in Figure 6.9**.** Metal Co firstly dissociatively adsorbs CO to produce CH_x*, followed by chain propagation to promote the C_nH_{2n}* intermediate. The short distance between Co^0 and Co_6Mo_6C provides more feasibility for the fast transfer of C_nH_{2n}* from Co^0 phase to Co_6Mo_6C phase. Meanwhile, the Co_6Mo_6C assists in the nondissociative adsorption of CO to produce the active CO*, which inserts in the adjacent C_nH_{2n}* species to give the acyl intermediate $C_nH_{2n}CO$* and then hydrogenate to the final $C_{n+1}H_{2n+3}OH$ alcohols. A recent study revealed that CO* insertion is the rate-determining step for C_{2+} oxygenates production.[36] Thus, the integration of Co and Co-Mo carbide will shift the reaction towards higher alcohols formation, rendering larger output. Indeed, monometallic carbides (Co_2C, Mo_2C, *etc*.) are well acknowledged to exhibit typical noble-metal-like features in the

hydrogenation process and water gas shift (WGS) reaction.[37, 38] Density functional theory (DFT) calculations proved that CO molecules can be adsorbed associatively on Co_2C (111) and then insert in the CH_2 intermediates.[34] Likewise, the formed bimetallic carbide Co_6Mo_6C in our experiment is very likely to perform the similar function as Co_2C. Moreover, the above discussion proves that the relative concentration of Co and Co_6Mo_6C on the catalyst surface is pivotal for the catalytic performance in HAS reaction. The catalyst $Co_{4.7}Mo@C$ with Co/Mo ratio of 4.7 exhibits the largest higher alcohol formation because it offers the best compromise between chain growth and CO insertion. However, the larger Co fraction in catalyst $Co_{7.3}Mo@C$ produces more CH_4 due to enhanced CO dissociation (Table 6-2), whereas the highest concentration of carbide component in $Co_{2.2}Mo@C$ has resulted in the slightly lower CO conversion with the largest CO_2 selectivity owing to the enhanced water gas shift reaction. The WGS reaction would change the H_2/CO ratio and contribute to the decrease in CO insertion and carbon chain growth.[3]

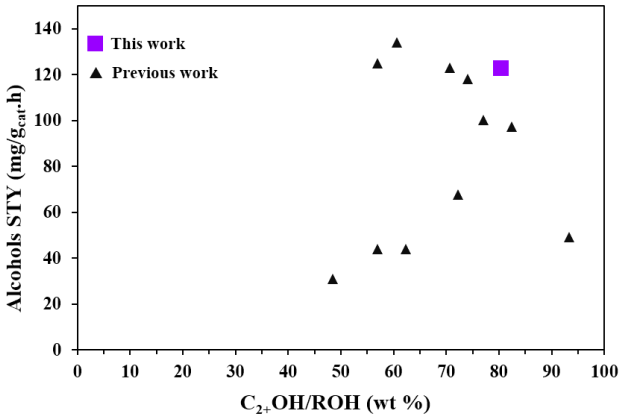

Figure 6.10. Total alcohols STY and $C_{2+}OH$ weight fraction obtained in this work for $Co_{4.7}Mo@C$ at 275 ºC (■) and catalysts from previous reports (▲).[3, 16, 36, 39-47]

Despite the high activity and selectivity to higher alcohols, long-term stability plays vital role concerning the industrial implementation of PZIF derived catalysts. The time-on-stream evolution of CO conversion and alcohols selectivity for $Co_{4.7}Mo@C$

catalysts is summarized in Figure 6.7d. Significantly, superior stability is achieved in a 100 h on-stream evaluation. After 20 h of reaction, the catalytic system reached the steady state, CO conversion ranging between 42% and 48% with alcohols selectivity above 10%. The outstanding stability is ascribed to the homogenously dispersed Co and Co_6Mo_6C components on the formed carbon skeletons after pyrolysis in N_2 atmosphere. Moreover, the catalytic performance achieved in our experiment is comparable with the relevant results from previous literature as shown in Figure 6.10 and Table 6-3, demonstrating the high prospects of MOFs derived catalysts for large-scale application.

Table 6-3. Summary of the HAS performance of different catalysts in the literatures

Catalyst	Reaction Conditions				CO	ROH STY	Alcohol distribution (wt%)		Ref
	T (°C)	P (MPa)	H_2/CO	GHSV (mL/g_{cat}.h)	conversion (%)	(mg/g_{cat}.h)	MeOH	C_{2+}OH	
$Co_{4.7}Mo$@C	275	3.0	2	15000	48	123	19.7	80.3	This work
$K_{0.2}$-$Co_{0.5}$-Mo/C	310	6.0	2	1200	27.5	100.4	23.0	77.0	[39]
K/Co/β-Mo_2C	300	8.0	1	2000	36.7	134	39.4	60.6	[16]
K_6-$Co_{4.5}$-Mo_{22}/AC	320	8.3	1	3600	32.1	118	26.0	74.0	[41]
Co-Mo-K/MWCNTs	320	8.3	1	3600	34.6	123	29.3	70.7	[42]
Cu-Co/Silica gel	300	5.0	1	5100	31.6	125	43.0	57.0	[40]
CoCu/MoO_x	270	4.0	1	120000	<2	30			[43]
CoMn | CuZnAlZr	230	6.0	2	2000	17.8	49	6.7	93.3	[36]
Fe-Cu/Al_2O_3	380	4.0	2.68	10000		44	37.7	62.3	[44]
$La_{0.9}Sr_{0.1}Co_{0.9}Ni_{0.1}O_3$	320	3.0	2	10995	49.2	67.7	27.8	72.2	[3]
$5Cu_{15}Co/Al_2O_3$	250	2.0	2	4500	30.9	43.8	43.1	56.9	[47]
$LaCo_{0.7}Cu_{0.3}O_3/ZrO_2$	310	3.0	2	3900	35.3	97.3	17.6	82.4	[45]
$LaRhO_3$	300	0.6	1			31.0	51.6	48.4	[46]
S-$Co_1Mo_1K_{0.3}$-10%CNT	340	5.0	1	3600	18	223.9	47.5	52.5	[48]

To date, there are only a few reports about the MOF-derived catalysts for HAS. Wang *et al*. reported the K-promoted Co_3O_4 catalysts derived from ZIF-67 exhibited a high selectivity to C_{2+} oxygenates in virtue of the homogenous distribution of Co nanoparticles and formation of Co_2C species under reaction conditions.[49]

Unfortunately, the CO conversion at 270 °C is below 1% and the stability is unknown. Compared with this monometallic catalyst, the Co-Mo bimetallic catalysts have shown great advantages in catalytic activity and chain growth probability in the formed $Co/Co_6Mo_6C@C$ nanoreactors. The close affinity of Co^0 and Co_6Mo_6C ensures fast transfer of reaction intermediates and thus high production of higher alcohols.

6.3 Conclusions

In summary, we report a novel MOF-assisted strategy for developing well confined Co-Mo bifunctional catalyst with unique polyhedral nanocages as a highly active catalyst for HAS. This strategy relies on the confined and in situ carbonization of the ZIF-67 composites (PZIF-1 and PZIF-2) consisting of ZIF-67 host and PMA ($H_3PMo_{12}O_{40}$) guest resided in the nanopores, which enables close contact between C, Co and Mo source and facilitates the simultaneous formation of cobalt molybdenum carbide (Co_6Mo_6C) and metal Co (Co^0) nanoparticles embedded in the N doped carbon matrix after pyrolysis in N_2 atmosphere.

Under HAS conditions of 275 °C and 3.0 MPa, the as-prepared $Co_{4.7}Mo@C$ stemmed from PZIF-1exhibited remarkable activity for higher alcohols formation from syngas with a CO conversion of 48% and $C_{2+}OH$ STY of 99 $mg/g_{cat}.h$. much better than its counterpart Co@C or Co_6Mo_6C catalyst. Benefiting from the protection of resultant N-doped carbon scaffold, this catalyst displays exceptional stability, and no catalyst deactivation was observed during the 100 h long-term stability test. Moreover, the relative content of Co and Co_6Mo_6C in the nanoreactors play crucial role for higher alcohols production. Higher fraction of Co_6Mo_6C in $Co_{2.2}Mo@C$ derived from PZIF-2 with higher Mo content enhances water-gas shift reaction and prohibits the formation of higher alcohols. Correlating the nature of Co@C, $Co_{4.7}Mo@C$ and $Co_{2.2}Mo@C$ and their corresponding catalytic performance in HAS, a strong synergism between Co and Co_6Mo_6C species in the catalyst is well defined, where Co^0 is mainly for CO

dissociation and carbon chain growth, and Co_6Mo_6C is responsible for CO nondissocative adsorption and subsequent CO insertion to produce HA.

Moreover, our results open new opportunities for rational design of bifunctional catalyst for HAS with optimized activity. By tuning the types of MOF, such as Fe- or Ni-MOF, highly porous Fe_xMo_xC or Ni_xMo_xC can also be developed which might be exclusively active for HAS.

References

1. Luk, H. T.; Mondelli, C.; Ferré, D. C.; Stewart, J. A.; Pérez-Ramírez, J., Status and prospects in higher alcohols synthesis from syngas. *Chem. Soc. Rev.* **2017,** *46* (5), 1358-1426.

2. Lu, Y.; Zhang, R.; Cao, B.; Ge, B.; Tao, F. F.; Shan, J.; Nguyen, L.; Bao, Z.; Wu, T.; Pote, J. W., Elucidating the Copper–Hägg Iron Carbide Synergistic Interactions for Selective CO Hydrogenation to Higher Alcohols. *ACS Catal.* **2017,** *7* (8), 5500-5512.

3. Ao, M.; Pham, G. H.; Sage, V.; Pareek, V., Selectivity enhancement for higher alcohol product in Fischer-Tropsch synthesis over nickel-substituted $La_{0.9}Sr_{0.1}CoO_3$ perovskite catalysts. *Fuel* **2017,** *206*, 390-400.

4. Ao, M.; Pham, G. H.; Sage, V.; Pareek, V.; Liu, S., Perovskite-derived trimetallic Co-Ni-Cu catalyst for higher alcohol synthesis from syngas. *Catal. Today* **2019,** *193*, 141-148.

5. Ao, M.; Pham, G. H.; Sunarso, J.; Tade, M. O.; Liu, S., Active Centers of Catalysts for Higher Alcohol Synthesis from Syngas: A Review. *ACS Catal.* **2018,** *8* (8), 7025-7050.

6. Subramanian, N. D.; Balaji, G.; Kumar, C. S. S. R.; Spivey, J. J., Development of cobalt–copper nanoparticles as catalysts for higher alcohol synthesis from syngas. *Catal. Today* **2009,** *147* (2), 100-106.

7. Xiaoding, X.; Doesburg, E. B. M.; Scholten, J. J. F., Synthesis of higher alcohols from syngas - recently patented catalysts and tentative ideas on the mechanism. *Catal. Today* **1987,** *2* (1), 125-170.

8. Xiang, Y.; Chitry, V. r.; Liddicoat, P.; Felfer, P.; Cairney, J.; Ringer, S.; Kruse, N., Long-

chain terminal alcohols through catalytic CO hydrogenation. *J. Am. Chem. Soc.* **2013,** *135* (19), 7114-7117.

9. Zhao, Z.; Lu, W.; Yang, R.; Zhu, H.; Dong, W.; Sun, F.; Jiang, Z.; Lyu, Y.; Liu, T.; Du, H., Insight into the formation of $Co@Co_2C$ catalysts for direct synthesis of higher alcohols and olefins from syngas. *ACS Catal.* **2017,** *8* (1), 228-241.

10. Liu, J.-X.; Su, H.-Y.; Sun, D.-P.; Zhang, B.-Y.; Li, W.-X., Crystallographic Dependence of CO Activation on Cobalt Catalysts: HCP versus FCC. *J. Am. Chem. Soc.* **2013,** *135* (44), 16284-16287.

11. Mouaddib, N.; Perrichon, V.; Martin, G., Characterization of copper-cobalt catalysts for alcohol synthesis from syngas. *Appl. Catal. A-Gen.* **1994,** *118* (1), 63-72.

12. Su, J.; Zhang, Z.; Fu, D.; Liu, D.; Xu, X.-C.; Shi, B.; Wang, X.; Si, R.; Jiang, Z.; Xu, J., Higher alcohols synthesis from syngas over $CoCu/SiO_2$ catalysts: Dynamic structure and the role of Cu. *J. Catal.* **2016,** *336*, 94-106.

13. Hensley, J. E.; Pylypenko, S.; Ruddy, D. A., Deactivation and stability of $K\text{-}CoMoS_x$ mixed alcohol synthesis catalysts. *J. Catal.* **2014,** *309*, 199-208.

14. Li, X.; Feng, L.; Liu, Z.; Zhong, B.; Dadyburjor, D. B.; Kugler, E. L., Higher alcohols from synthesis gas using carbon-supported doped molybdenum-based catalysts. *Ind. Eng. Chem. Res.* **1998,** *37* (10), 3853-3863.

15. Kiai, R. M.; Nematian, T.; Tavasoli, A.; Karimi, A., Effect of elemental molar ratio on the synthesis of higher alcohols over Co-promoted alkali-modified Mo_2C catalysts supported on CNTs. *J. Energy Chem.* **2015,** *24* (3), 278-284.

16. Xiang, M.; Li, D.; Li, W.; Zhong, B.; Sun, Y., Synthesis of higher alcohols from syngas over $K/Co/\beta\text{-}Mo_2C$ catalysts. *Catal. Commun.* **2007,** *8* (3), 503-507.

17. Li, Y.; Gao, W.; Peng, M.; Zhang, J.; Sun, J.; Xu, Y.; Hong, S.; Liu, X.; Liu, X.; Wei, M.; Zhang, B.; Ma, D., Interfacial Fe_5C_2-Cu catalysts toward low-pressure syngas conversion to long-chain alcohols. *Nat. Commun.* **2020,** *11* (1), 61.

18. Wang, C.; An, B.; Lin, W., Metal–Organic Frameworks in Solid–Gas Phase Catalysis. *ACS Catal.* **2018,** *9* (1), 130-146.

19. An, B.; Cheng, K.; Wang, C.; Wang, Y.; Lin, W., Pyrolysis of Metal–Organic Frameworks to $Fe_3O_4@Fe_5C_2$ Core–Shell Nanoparticles for Fischer–Tropsch Synthesis. *ACS Catal.* **2016,**

6 (6), 3610-3618.

20. Wezendonk, T. A.; Santos, V. P.; Nasalevich, M. A.; Warringa, Q. S. E.; Dugulan, A. I.; Chojecki, A.; Koeken, A. C. J.; Ruitenbeek, M.; Meima, G.; Islam, H.-U.; Sankar, G.; Makkee, M.; Kapteijn, F.; Gascon, J., Elucidating the Nature of Fe Species during Pyrolysis of the Fe-BTC MOF into Highly Active and Stable Fischer–Tropsch Catalysts. *ACS Catal.* **2016,** *6* (5), 3236-3247.

21. Sun, C.-Y.; Liu, S.-X.; Liang, D.-D.; Shao, K.-Z.; Ren, Y.-H.; Su, Z.-M., Highly stable crystalline catalysts based on a microporous metal−organic framework and polyoxometalates. *J. Am. Chem. Soc.* **2009,** *131* (5), 1883-1888.

22. Li, R.; Ren, X.; Zhao, J.; Feng, X.; Jiang, X.; Fan, X.; Lin, Z.; Li, X.; Hu, C.; Wang, B., Polyoxometallates trapped in a zeolitic imidazolate framework leading to high uptake and selectivity of bioactive molecules. *J. Mater. Chem. A* **2014,** *2* (7), 2168-2173.

23. Li, F.; Ao, M.; Pham, G. H.; Jin, Y.; Nguyen, M. H.; Alawi, N. M.; Tade, M. O.; Liu, S., A novel UiO-66 encapsulated 12-silicotungstic acid catalyst for dimethyl ether synthesis from syngas. *Catal. Today* **2019**.

24. Sabyrov, K.; Jiang, J.; Yaghi, O. M.; Somorjai, G. A., Hydroisomerization of n-Hexane Using Acidified Metal–Organic Framework and Platinum Nanoparticles. *J. Am. Chem. Soc.* **2017,** *139* (36), 12382-12385.

25. Liu, Y.; Wang, Z.; Zhong, Y.; Tade, M.; Zhou, W.; Shao, Z., Molecular Design of Mesoporous $NiCo_2O_4$ and $NiCo_2S_4$ with Sub-Micrometer-Polyhedron Architectures for Efficient Pseudocapacitive Energy Storage. *Adv. Funct. Mater.* **2017,** *27* (28), 1701229.

26. He, C.; Tao, J., Three-dimensional hollow porous Co_6Mo_6C nanoframe as an highly active and durable electrocatalyst for water splitting. *J. Catal.* **2017,** *347*, 63-71.

27. Chen, C.; Wu, A.; Yan, H.; Xiao, Y.; Tian, C.; Fu, H., Trapping $[PMo_{12}O_{40}]^{3-}$ clusters into pre-synthesized ZIF-67 toward Mo_xCo_xC particles confined in uniform carbon polyhedrons for efficient overall water splitting. *Chem. Sci.* **2018,** *9* (21), 4746-4755.

28. Yan, H.; Tian, C.; Wang, L.; Wu, A.; Meng, M.; Zhao, L.; Fu, H., Phosphorus-Modified Tungsten Nitride/Reduced Graphene Oxide as a High-Performance, Non-Noble-Metal Electrocatalyst for the Hydrogen Evolution Reaction. *Angew. Chem. Int. Ed.* **2015,** *54* (21), 6325-6329.

29. Wu, H.; Geng, J.; Ge, H.; Guo, Z.; Wang, Y.; Zheng, G., Egg-Derived Mesoporous Carbon Microspheres as Bifunctional Oxygen Evolution and Oxygen Reduction Electrocatalysts. *Adv. Energy Mater.* **2016,** *6* (20), 1600794.

30. Liu, T.; Liu, H.; Wu, X.; Niu, Y.; Feng, B.; Li, W.; Hu, W.; Li, C. M., Molybdenum carbide/phosphide hybrid nanoparticles embedded P, N co-doped carbon nanofibers for highly efficient hydrogen production in acidic, alkaline solution and seawater. *Electrochim. Acta* **2018,** *281*, 710-716.

31. Zaman, S. F.; Smith, K. J., Synthesis gas conversion over MoP catalysts. *Catal. Commun.* **2009,** *10* (5), 468-471.

32. Song, X.; Ding, Y.; Chen, W.; Dong, W.; Pei, Y.; Zang, J.; Yan, L.; Lu, Y., Synthesis and Characterization of Silica-Supported Cobalt Phosphide Catalysts for CO Hydrogenation. *Energy Fuels* **2012,** *26* (11), 6559-6566.

33. Qiu, B.; Yang, C.; Guo, W.; Xu, Y.; Liang, Z.; Ma, D.; Zou, R., Highly dispersed Co-based Fischer–Tropsch synthesis catalysts from metal–organic frameworks. *J. Mater. Chem. A* **2017,** *5* (17), 8081-8086.

34. Pei, Y.-P.; Liu, J.-X.; Zhao, Y.-H.; Ding, Y.-J.; Liu, T.; Dong, W.-D.; Zhu, H.-J.; Su, H.-Y.; Yan, L.; Li, J.-L., High alcohols synthesis via Fischer–Tropsch reaction at cobalt metal/carbide interface. *ACS Catal.* **2015,** *5* (6), 3620-3624.

35. Levy, R. B.; Boudart, M., Platinum-Like Behavior of Tungsten Carbide in Surface Catalysis. *Science* **1973,** *181* (4099), 547.

36. Lin, T.; Qi, X.; Wang, X.; Xia, L.; Wang, C.; Yu, F.; Wang, H.; Li, S.; Zhong, L.; Sun, Y., Direct Production of Higher Oxygenates by Syngas Conversion over a Multifunctional Catalyst. *Angew. Chem. Int. Ed.* **2019,** *58* (14), 4627-4631.

37. Nagai, M.; Matsuda, K., Low-temperature water–gas shift reaction over cobalt–molybdenum carbide catalyst. *J. Catal.* **2006,** *238* (2), 489-496.

38. Schweitzer, N. M.; Schaidle, J. A.; Ezekoye, O. K.; Pan, X.; Linic, S.; Thompson, L. T., High Activity Carbide Supported Catalysts for Water Gas Shift. *J. Am. Chem. Soc.* **2011,** *133* (8), 2378-2381.

39. Bao, J.; Sun, Z.-H.; Fu, Y.-L.; Bian, G.-Z.; Zhang, Y.; Tsubaki, N., Mixed Alcohol Synthesis from Syngas on K–Co–Mo/C Catalyst Prepared by a Sol–Gel Method. *Top. Catal.*

2009, *52* (6), 789-794.

40. Feng, W.; Wang, Q.; Jiang, B.; Ji, P., Carbon Nanotubes Coated on Silica Gels as a Support of Cu–Co Catalyst for the Synthesis of Higher Alcohols from Syngas. *Ind. Eng. Chem. Res.* **2011,** *50* (19), 11067-11072.

41. Surisetty, V. R.; Eswaramoorthi, I.; Dalai, A. K., Comparative study of higher alcohols synthesis over alumina and activated carbon-supported alkali-modified MoS_2 catalysts promoted with group VIII metals. *Fuel* **2012,** *96*, 77-84.

42. Surisetty, V. R.; Dalai, A. K.; Kozinski, J., Synthesis of higher alcohols from synthesis gas over Co-promoted alkali-modified MoS_2 catalysts supported on MWCNTs. *Appl. Catal. A-Gen.* **2010,** *385* (1), 153-162.

43. Prieto, G.; Beijer, S.; Smith, M. L.; He, M.; Au, Y.; Wang, Z.; Bruce, D. A.; de Jong, K. P.; Spivey, J. J.; de Jongh, P. E., Design and Synthesis of Copper–Cobalt Catalysts for the Selective Conversion of Synthesis Gas to Ethanol and Higher Alcohols. *Angew. Chem. Int. Ed.* **2014,** *53* (25), 6397-6401.

44. Su, Y.; Wang, Y.; Liu, Z., Preparation and characterization of ultrafine Fe-Cu-based catalysts for CO hydrogenation. *J. Nat. Gas Chem.* **2008,** *17* (4), 327-331.

45. Liu, G.; Geng, Y.; Pan, D.; Zhang, Y.; Niu, T.; Liu, Y., Bi-metal Cu–Co from $LaCo_{1-x}Cu_xO_3$ perovskite supported on zirconia for the synthesis of higher alcohols. *Fuel Process. Technol.* **2014,** *128*, 289-296.

46. Watson, P.; Somorjai, G., The formation of oxygen-containing organic molecules by the hydrogenation of carbon monoxide using a lanthanum rhodate catalyst. *J. Catal.* **1982,** *74* (2), 282-295.

47. Wang, J.; Chernavskii, P. A.; Khodakov, A. Y.; Wang, Y., Structure and catalytic performance of alumina-supported copper–cobalt catalysts for carbon monoxide hydrogenation. *J. Catal.* **2012,** *286*, 51-61.

48. Ma, X.; Lin, G.; Zhang, H., Co-Mo-K Sulfide-Based Catalyst Promoted by Multiwalled Carbon Nanotubes for Higher Alcohol Synthesis from Syngas. *Chinese J. Catal.* **2006,** *27* (11), 1019-1027.

49. Wang, Z.; Laddha, G.; Kanitkar, S.; Spivey, J. J., Metal organic framework-mediated synthesis of potassium-promoted cobalt-based catalysts for higher oxygenates synthesis. *Catal.*

Today **2017,** *298*, 209-215.

Every reasonable effort has been made to acknowledge the owners of copyright material. I would be pleased to hear from any copyright owner who has been omitted or incorrectly acknowledged.

Chapter 7 Conclusions and Recommendations

7.1 Conclusions

The direct synthesis of organic oxygenates from syngas has been widely reported during the past decade. However, the rational design of efficient catalyst for this process remains a challenge. As a rising star material, metal-organic frameworks (MOFs) are porous, crystalline materials that can trap compounds within their molecular cavities, have a wide range of applications such as gas storage, separation, gas capture and catalysis of chemical reactions. In this thesis, MOFs have been used as the precursor or templates to derive novel structured catalysts to be applied for Fischer-Tropsch (F-T) synthesis to covert gas to more valuable chemicals. From this perspective, we conducted fundamental investigations of MOFs-derived catalysts to selectively convert syngas to organic oxygenates. Three different architectures of MOFs-derived catalysts were employed: Cu/STA-UiO composite, Cu/ZnO catalyst derived from CuZn bimetallic MOF and Co/Co_6Mo_6C embedded in carbon matrix prepared from direct carbonization of ZIF-67 composite. The synergistic effect between active components and the influence of calcination procedure and temperature on catalytic performance were explored. The reaction mechanism of Co/Co_6Mo_6C catalyst on higher alcohols synthesis was also explored in this thesis. Several general conclusions can be made from the observations during the research involving the topic "MOFs derived catalyst for efficient syngas conversion to organic oxygenates".

7.1.1 Fabrication of A Novel UiO-66 Encapsulated Silicotungstic Acid Catalyst for DME Synthesis from Syngas

- A bifunctional Cu/STA-UiO composite for DME synthesis was successfully prepared through accommodation of silicotungstic acid (STA) in the UiO-66

framework and followed by deposition of Cu on the external surface. Such a modification method didn't cause framework destruction or STA aggregation.

- The intimate contact of Cu and Zr oxide secondary building blocks (SBU) in UiO-66 evokes strong SMSI effect, which facilitates methanol synthesis.
- Due to the close affinity of Cu component and STA component in the MOF structure, methanol molecules formed on Cu/ZrO_x interfacial areas can be converted quickly on STA site. As a result, the prepared Cu/STA-UiO exhibited highest DME selectivity among all measured catalysts.

7.1.2 Cu/ZnO catalysts derived from bimetallic metal-organic framework for dimethyl ether synthesis from syngas with enhanced selectivity and stability

- CuZn-BTC MOFs were fabricated using trimesic acid as the organic linker.
- Consecutive pyrolysis of CuZn-BTC in N_2 and air is essential to generate Cu/ZnO catalyst with original morphology of MOF.
- The homogeneous distribution of Cu and Zn in the unique octahedron morphology significantly reduced the aggregation and migration of Cu^0 nanoparticles, leading to superior activity and stability for DME production.
- Partial reduction of ZnO in the activated CZ-350 prompts the formation of Cu^+-O-Zn which is more active for methanol production.

7.1.3 Co/Co_6Mo_6C@C nanoreactors derived from ZIF-67 composite for Higher Alcohols Synthesis

- Novel $CoMo_x$@C catalysts consisting of Co and Co_6Mo_6C embedded in the carbon matrix were developed for catalyst component confinement and in situ carbonization of the ZIF-67 composites consisting of ZIF-67 host and PMA ($H_3PMo_{12}O_{40}$) guest resided in the nanopores. This strategy enables desirable contact between C, Co and Mo source and facilitates the simultaneous formation of cobalt molybdenum carbide (Co_6Mo_6C) and metal Co (Co^0)

nanoparticles embedded in the N doped carbon matrix after pyrolysis in N_2 atmosphere.

- A strong synergism between Co and Co_6Mo_6C species in the catalyst is well recognised, where Co^0 is mainly for CO dissociation and carbon chain growth, and Co_6Mo_6C is responsible for CO nondissocative adsorption and subsequent CO insertion to produce HA.
- The relative content of Co and Co_6Mo_6C in the nanoreactors plays a crucial role for higher alcohols production. The appropriate Co/Co_6Mo_6C ratio can boost the higher alcohols synthesis, whereas further increase of Co or Co_6Mo_6C will result in enhanced by-products selectivity.
- The resultant N-doped carbon scaffold can protect the active sites from aggregation, and thus improves the catalyst stability.

7.2 Recommendations

Using MOFs as the template or precursors to develop novel catalysts has not been systematically studied, leaving a completely open field for future research. Our work is at the beginning and there are many challenges for researchers to overcome. Based on the theoretical analysis and experimental results, suggestions for future work include the following five aspects.

- Despite the high selectivity to DME, the Cu/STA-UiO composite exhibited a low CO conversion, due to limited amount of Cu sites. Therefore, future work on the modifications of Cu/STA ratio with uniform dispersion should be conducted to improve the CO conversion.
- Limited by the time frame, this study has not completed the investigation of reaction conditions for DME synthesis. The effect of reduction temperature and period should be evaluated to obtain optimized reaction conditions.
- The encapsulation strategy causes some morphology defects for the prepared

MOF composites, which may damage their catalytic activity. Thus, alternative trapping method should be considered to develop catalysts with more ordered structure.

- In Chapter 6, we demonstrate that Co_6Mo_6C sites are responsible for CO nondissociative adsorption and CO insertion step. Further Density Functional Theory (DFT) calculations should be supplemented to explain the essence of CO molecular adsorption and following insertion on Co_6Mo_6C.
- Since Ni or Fe can also form bimetallic carbide with Mo, the trapping method can be expanded to Ni-MOF or Fe-MOF to investigate the effect of the corresponding Ni_xMo_xC or Fe_xMo_xC bimetallic carbide on higher alcohols synthesis.

APPENDIX Ⅰ: ATTRIBUTION TABLES

Paper "**A novel UiO-66 encapsulated 12-silicotungstic acid catalyst for dimethyl ether synthesis from syngas**". Catalysis Today, 2020, 355.

Min Ao, Gia Hung Pham*, Yun Jin, Minh Hoang Nguyen, Nabil Majd Alawi, Moses O. Tade, Shaomin Liu*

Name	conception and design	Acquisition of data & method	Data conditioning & manipulation	Analysis & statistical method	Interpretation & discussion	Final approval
Min Ao	☐	☒	☒	☐	☒	☐
I acknowledge that these represent my contribution to the above research output. Sign:						
Gia Hung Pham	☒	☐	☒	☐	☒	☒
I acknowledge that these represent my contribution to the above research output. Sign:						
Yun Jin	☐	☒	☐	☐	☒	☒
I acknowledge that these represent my contribution to the above research output. Sign:						
Minh Hoang Nguyen	☐	☒	☐	☐	☐	☐
I acknowledge that these represent my contribution to the above research output. Sign:						
Nabil Majd Alawi	☐	☒	☐	☐	☐	☐
I acknowledge that these represent my contribution to the above research output. Sign:						
Moses O. Tade	☒	☒	☒	☒	☒	☒
I acknowledge that these represent my contribution to the above research output. Sign:						
Shaomin Liu	☒	☒	☒	☐	☒	☒
I acknowledge that these represent my contribution to the above research output. Sign:						

Paper "**Cu/ZnO Catalysts Derived from Bimetallic Metal–Organic Framework for Dimethyl Ether Synthesis from Syngas with Enhanced Selectivity and Stability**". Small, 2020, 16(14).

Min Ao, Gia Hung Pham, Jaka Sunarso, Yanping Chen, Jian Liu*, Kai Wang, Shaomin Liu*

Name	conception and design	Acquisition of data & method	Data conditioning & manipulation	Analysis & statistical method	Interpretation & discussion	Final approval
Min Ao	☒	☒	☒	☐	☒	☐
I acknowledge that these represent my contribution to the above research output. Sign:						
Gia Hung Pham	☒	☐	☐	☐	☒	☒
I acknowledge that these represent my contribution to the above research output. Sign:						
Jaka Sunarso	☐	☐	☐	☐	☒	☒
I acknowledge that these represent my contribution to the above research output. Sign:						
Yanping Chen	☐	☐	☐	☒	☐	☐
I acknowledge that these represent my contribution to the above research output. Sign:						
Jian Liu	☒	☐	☐	☒	☒	☒
I acknowledge that these represent my contribution to the above research output. Sign:						
Kai Wang	☐	☐	☒	☒	☐	☐
I acknowledge that these represent my contribution to the above research output. Sign:						
Shaomin Liu	☒	☒	☒	☒	☒	☒
I acknowledge that these represent my contribution to the above research output. Sign:						

APPENDIX II: Copyright Permission Statements

A. Chapter 4, reprinted with permission from "Fuping Li, Min Ao, Gia Hung Pham, Yun Jin, Minh Hoang Nguyen, Nabil Majd Alawi, Moses O. Tade, Shaomin Liu, A novel UiO-66 encapsulated 12-silicotungstic acid catalyst for dimethyl ether synthesis from syngas. *Catalysis Today*, 2019."

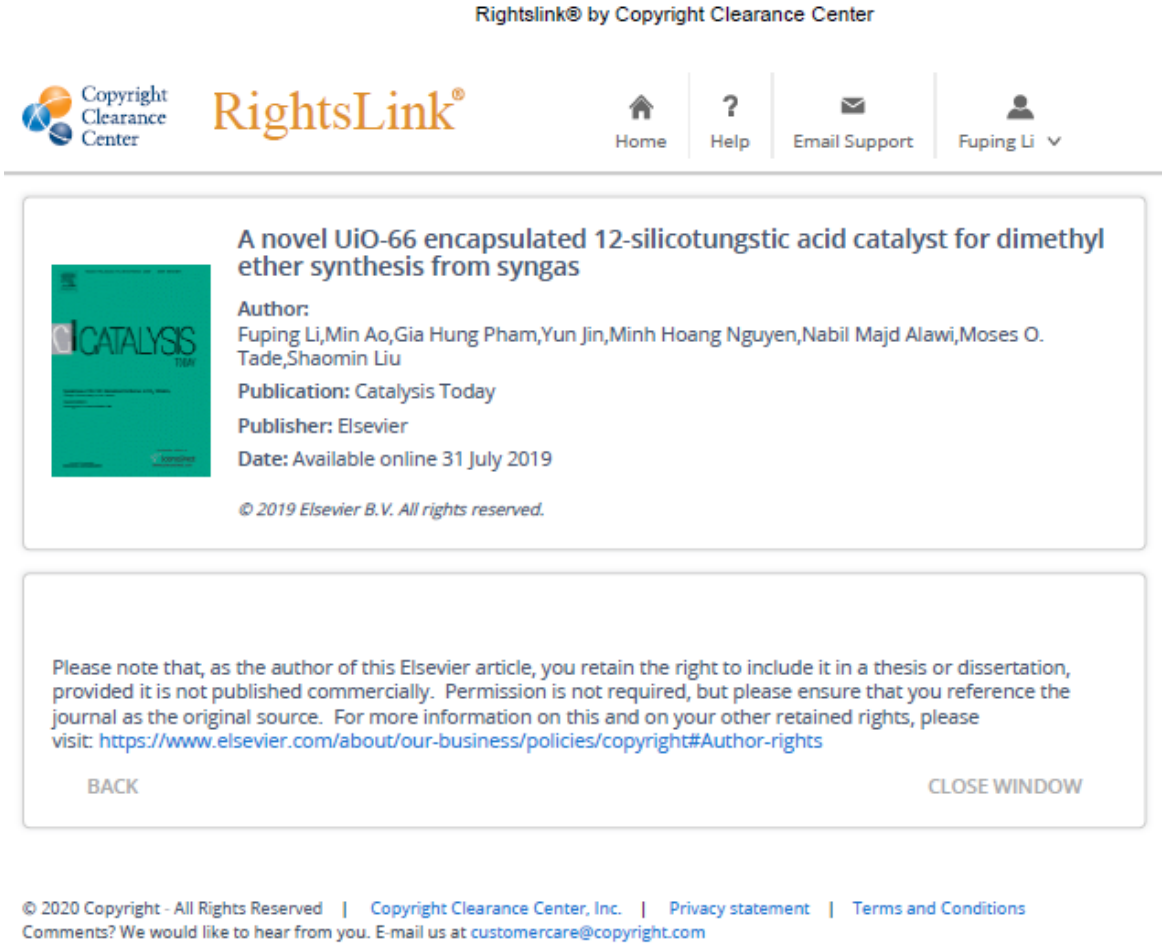

B. Chapter 5, reprinted with permission from "Min Ao, Gia Hung Pham, Jaka Sunarso, Yanping Chen, Jian Liu*, Kai Wang, Shaomin Liu, Cu/ZnO Catalysts Derived from Bimetallic Metal–Organic Framework for Dimethyl Ether Synthesis from Syngas with Enhanced Selectivity and Stability. *Small*, 2020.

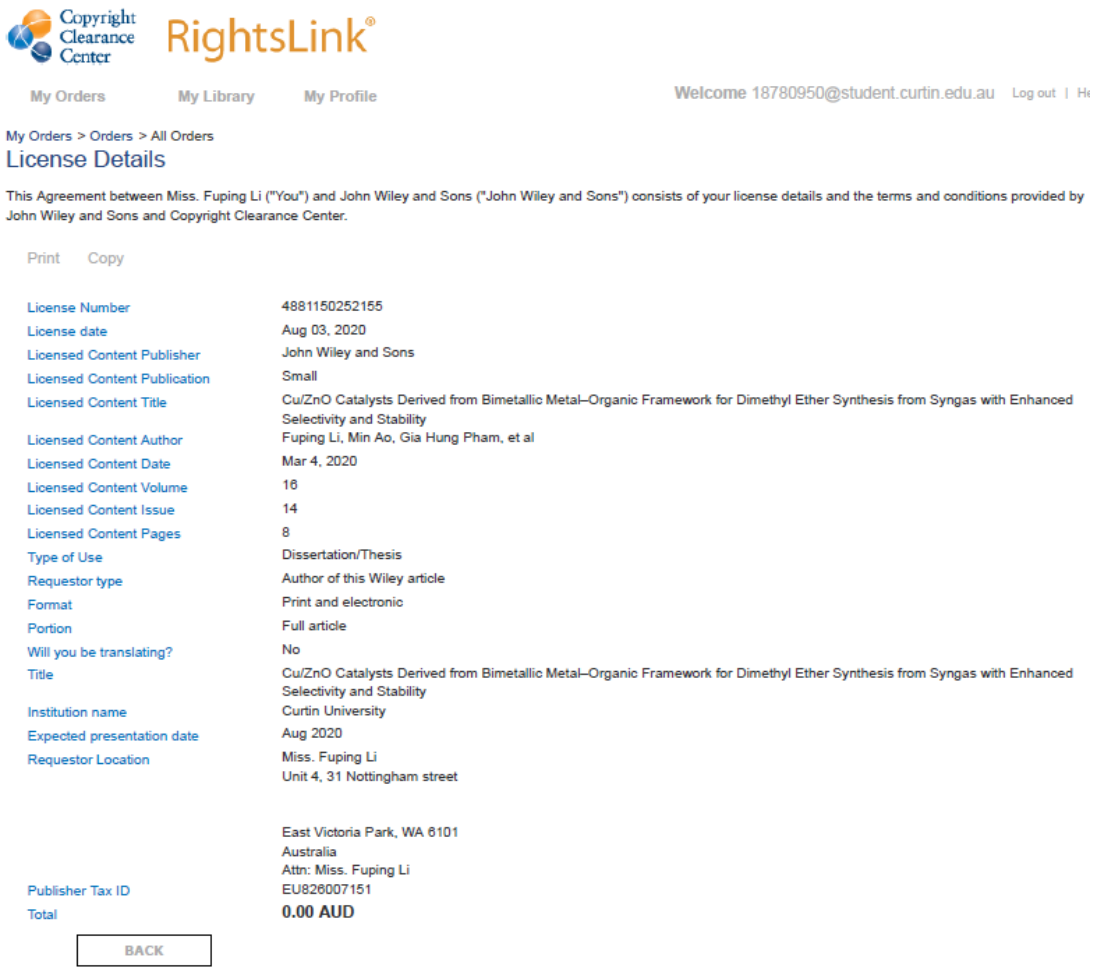

Copyright Clearance Center RightsLink®

My Orders My Library My Profile Welcome 18780950@student.curtin.edu.au Log out | He

My Orders > Orders > All Orders

License Details

This Agreement between Miss. Fuping Li ("You") and John Wiley and Sons ("John Wiley and Sons") consists of your license details and the terms and conditions provided by John Wiley and Sons and Copyright Clearance Center.

Print Copy

License Number	4881150252155
License date	Aug 03, 2020
Licensed Content Publisher	John Wiley and Sons
Licensed Content Publication	Small
Licensed Content Title	Cu/ZnO Catalysts Derived from Bimetallic Metal–Organic Framework for Dimethyl Ether Synthesis from Syngas with Enhanced Selectivity and Stability
Licensed Content Author	Fuping Li, Min Ao, Gia Hung Pham, et al
Licensed Content Date	Mar 4, 2020
Licensed Content Volume	16
Licensed Content Issue	14
Licensed Content Pages	8
Type of Use	Dissertation/Thesis
Requestor type	Author of this Wiley article
Format	Print and electronic
Portion	Full article
Will you be translating?	No
Title	Cu/ZnO Catalysts Derived from Bimetallic Metal–Organic Framework for Dimethyl Ether Synthesis from Syngas with Enhanced Selectivity and Stability
Institution name	Curtin University
Expected presentation date	Aug 2020
Requestor Location	Miss. Fuping Li Unit 4, 31 Nottingham street East Victoria Park, WA 6101 Australia Attn: Miss. Fuping Li
Publisher Tax ID	EU826007151
Total	**0.00 AUD**

BACK

C. Permission of Reproduction from the Copyright Owner in Chapter 2.

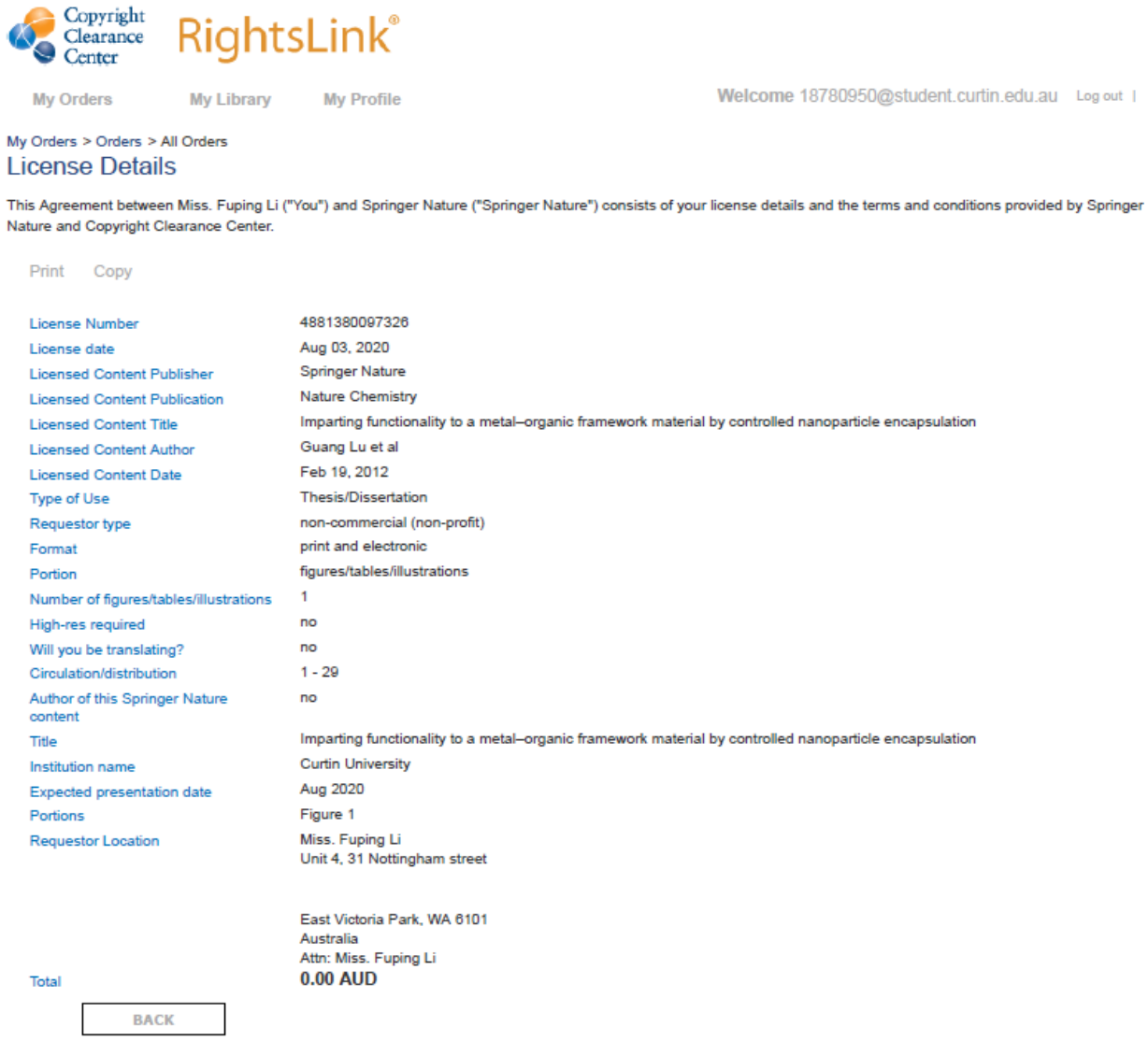

Copyright Clearance Center RightsLink®

My Orders My Library My Profile Welcome 18780950@student.curtin.edu.au Log out |

My Orders > Orders > All Orders

License Details

This Agreement between Miss. Fuping Li ("You") and Springer Nature ("Springer Nature") consists of your license details and the terms and conditions provided by Springer Nature and Copyright Clearance Center.

Print Copy

License Number	4881380097326
License date	Aug 03, 2020
Licensed Content Publisher	Springer Nature
Licensed Content Publication	Nature Chemistry
Licensed Content Title	Imparting functionality to a metal–organic framework material by controlled nanoparticle encapsulation
Licensed Content Author	Guang Lu et al
Licensed Content Date	Feb 19, 2012
Type of Use	Thesis/Dissertation
Requestor type	non-commercial (non-profit)
Format	print and electronic
Portion	figures/tables/illustrations
Number of figures/tables/illustrations	1
High-res required	no
Will you be translating?	no
Circulation/distribution	1 - 29
Author of this Springer Nature content	no
Title	Imparting functionality to a metal–organic framework material by controlled nanoparticle encapsulation
Institution name	Curtin University
Expected presentation date	Aug 2020
Portions	Figure 1
Requestor Location	Miss. Fuping Li Unit 4, 31 Nottingham street East Victoria Park, WA 6101 Australia Attn: Miss. Fuping Li
Total	**0.00 AUD**

BACK

Copyright Clearance Center RightsLink®

Help | Email Support

SPRINGER NATURE

Manufacture of highly loaded silica-supported cobalt Fischer–Tropsch catalysts from a metal organic framework

Author: Xiaohui Sun et al

Publication: Nature Communications

Publisher: Springer Nature

Date: Nov 22, 2017

Copyright © 2017, Springer Nature

Creative Commons

This is an open access article distributed under the terms of the Creative Commons CC BY license, which permits unrestricted use, distribution, and reproduction in any medium, provided the original work is properly cited.

You are not required to obtain permission to reuse this article.

To request permission for a type of use not listed, please contact Springer Nature

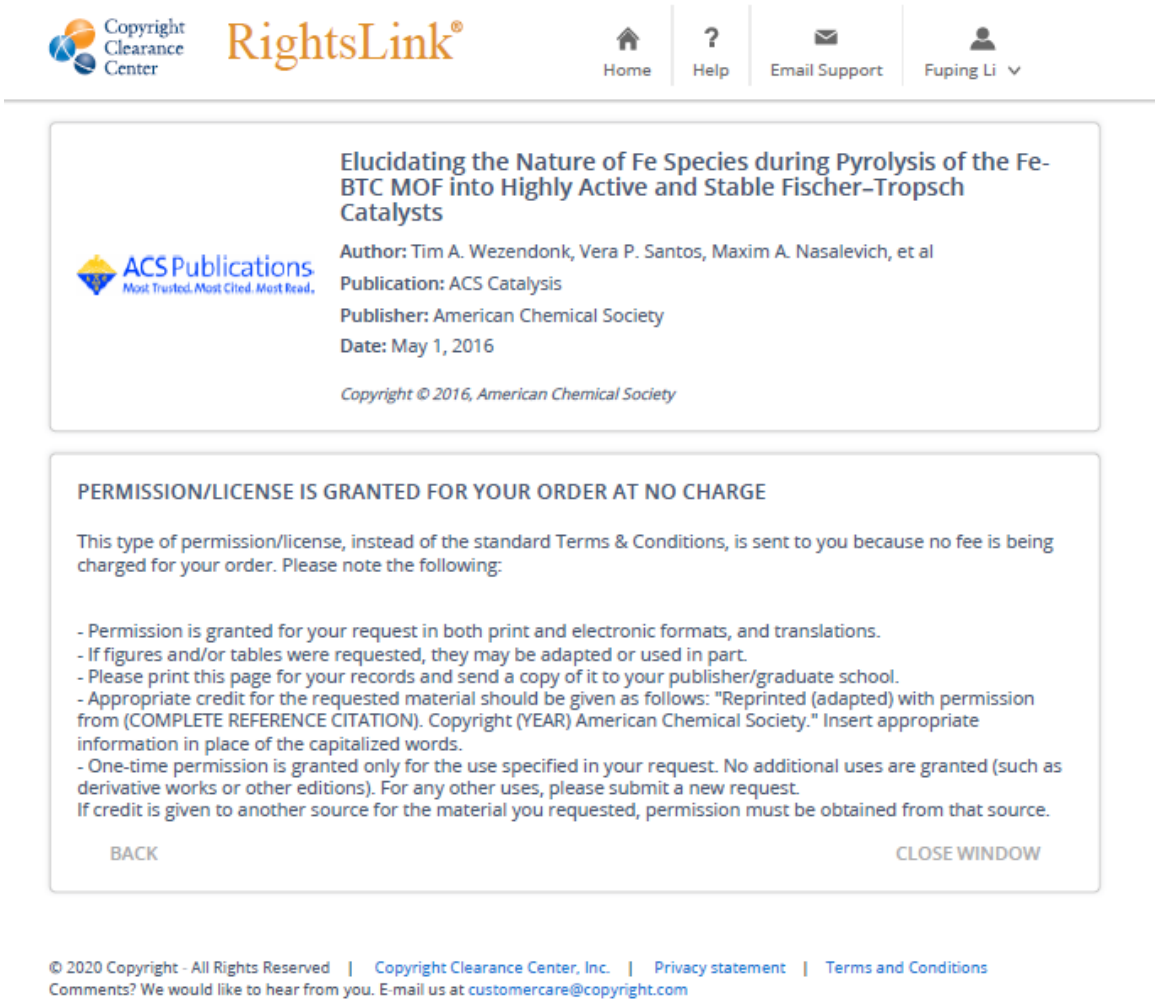

Copyright Clearance Center RightsLink®

Home | Help | Email Support | Fuping Li

ACS Publications
Most Trusted. Most Cited. Most Read.

Elucidating the Nature of Fe Species during Pyrolysis of the Fe-BTC MOF into Highly Active and Stable Fischer–Tropsch Catalysts

Author: Tim A. Wezendonk, Vera P. Santos, Maxim A. Nasalevich, et al
Publication: ACS Catalysis
Publisher: American Chemical Society
Date: May 1, 2016

Copyright © 2016, American Chemical Society

PERMISSION/LICENSE IS GRANTED FOR YOUR ORDER AT NO CHARGE

This type of permission/license, instead of the standard Terms & Conditions, is sent to you because no fee is being charged for your order. Please note the following:

- Permission is granted for your request in both print and electronic formats, and translations.
- If figures and/or tables were requested, they may be adapted or used in part.
- Please print this page for your records and send a copy of it to your publisher/graduate school.
- Appropriate credit for the requested material should be given as follows: "Reprinted (adapted) with permission from (COMPLETE REFERENCE CITATION). Copyright (YEAR) American Chemical Society." Insert appropriate information in place of the capitalized words.
- One-time permission is granted only for the use specified in your request. No additional uses are granted (such as derivative works or other editions). For any other uses, please submit a new request.

If credit is given to another source for the material you requested, permission must be obtained from that source.

BACK CLOSE WINDOW

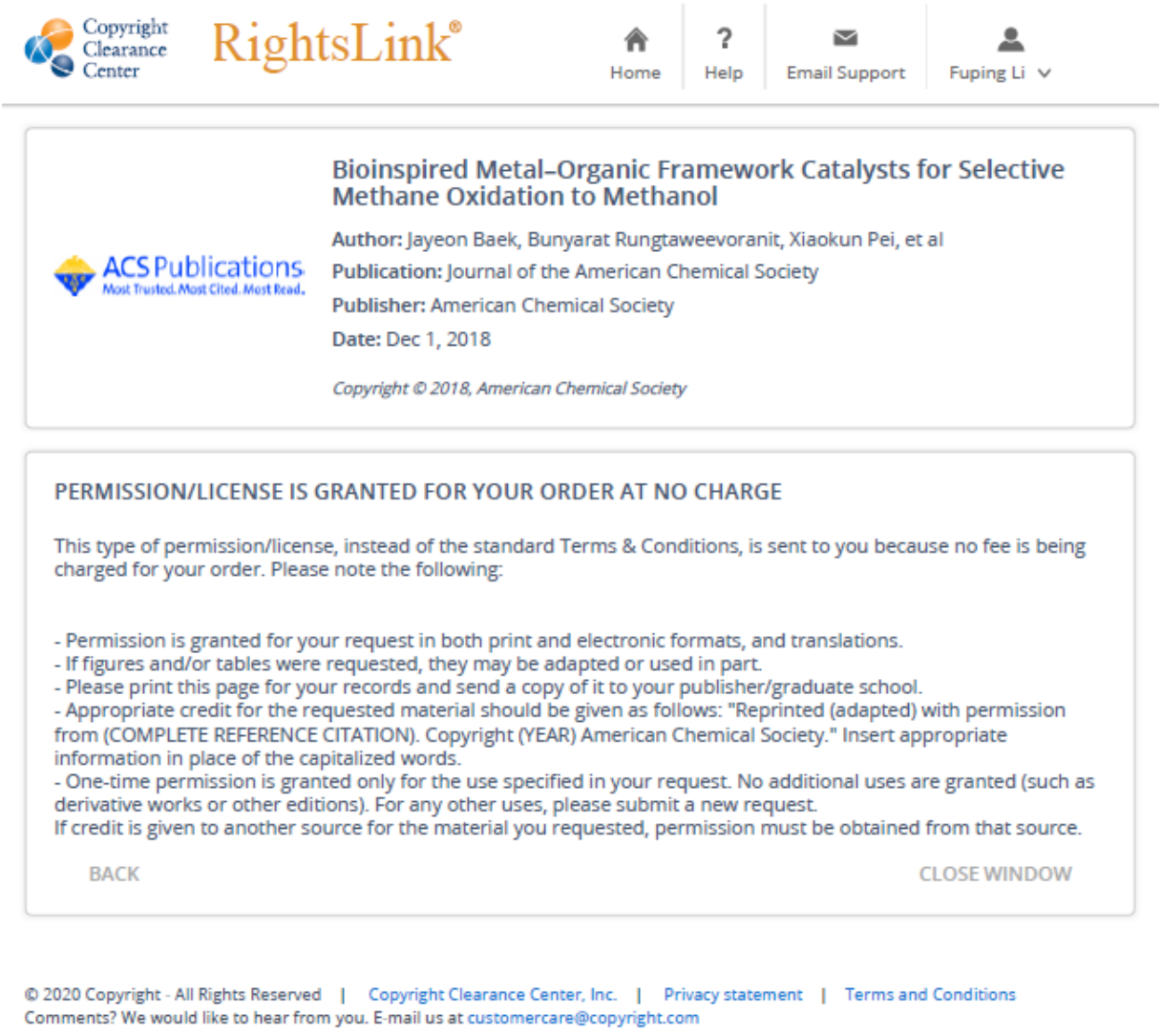

Copyright Clearance Center RightsLink®

Home | Help | Email Support | Fuping Li

ACS Publications
Most Trusted. Most Cited. Most Read.

Bioinspired Metal–Organic Framework Catalysts for Selective Methane Oxidation to Methanol

Author: Jayeon Baek, Bunyarat Rungtaweevoranit, Xiaokun Pei, et al
Publication: Journal of the American Chemical Society
Publisher: American Chemical Society
Date: Dec 1, 2018

Copyright © 2018, American Chemical Society

PERMISSION/LICENSE IS GRANTED FOR YOUR ORDER AT NO CHARGE

This type of permission/license, instead of the standard Terms & Conditions, is sent to you because no fee is being charged for your order. Please note the following:

- Permission is granted for your request in both print and electronic formats, and translations.
- If figures and/or tables were requested, they may be adapted or used in part.
- Please print this page for your records and send a copy of it to your publisher/graduate school.
- Appropriate credit for the requested material should be given as follows: "Reprinted (adapted) with permission from (COMPLETE REFERENCE CITATION). Copyright (YEAR) American Chemical Society." Insert appropriate information in place of the capitalized words.
- One-time permission is granted only for the use specified in your request. No additional uses are granted (such as derivative works or other editions). For any other uses, please submit a new request.

If credit is given to another source for the material you requested, permission must be obtained from that source.

BACK CLOSE WINDOW

© 2020 Copyright - All Rights Reserved | Copyright Clearance Center, Inc. | Privacy statement | Terms and Conditions
Comments? We would like to hear from you. E-mail us at customercare@copyright.com